Impacts of Temporal and Spatial Variation of Submarine Groundwater Discharge on Nutrient Fluxes to Texas Coastal Embayments, Phase III (Baffin Bay)

Final Report

GLO Contract No. 16-060-000-9104
April 10, 2018

Prepared by:
Cody V. Lopez, Graduate Research Assistant

Dorina Murgulet, Principal Investigator

With assistance from:

Audrey Douglas, Graduate Research Assistant

Valeriu Murgulet, Co-Principal Investigator

Texas A&M University-Corpus Christi
6300 Ocean Dr., Unit 5850
Corpus Christi, Texas 78412
Phone: 361-825-2309
Email: Dorina.murgulet@tamucc.edu

Submitted to:
Texas General Land Office
1700 Congress Ave.
Austin, TX 78701-1495

A report submitted to the Texas Land Commissioner pursuant to National Oceanic and Atmospheric Administration Award No. is NA15NOS4190162

CONTENTS

ABBREVIATIONS

ft	feet
cm	centimeter
m	meter
km	kilometer
hr	hour
d	day
s	second
$cm \cdot d^{-1}$	centimeter per day
$m \cdot s^{-1}$	meters per second
$m^3 \cdot s^{-1}$	cubic meters per second
$km^3 \cdot d^{-1}$	cubic kilometers per day
$mg \cdot L^{-1}$	milligrams per liter
$\mu g \cdot L^{-1}$	microgram per liter
µL	microliters
mL	milliliter
µM	micro Molar
$mol \cdot L^{-1}$	mole per liter
$\mu mol \cdot L^{-1}$	micromoles per liter
$\mu mol \cdot d^{-1}$	micromoles per day
DO	dissolved oxygen
SGD	submarine groundwater discharge
^{222}Rn	radon-222
^{223}Ra	radium-223
^{224}Ra	radium-224
^{226}Ra	radium-226
$Bq \cdot m^{-3}$	Becquerels per cubic meter
ERT	electrical resistivity
CRP	continuous resistivity profile
Ω-m	ohm-meter
TA	total alkalinity
DIC	dissolved inorganic carbon
DOC	dissolved organic carbon
N	nitrogen
TDN	total dissolved nitrogen
DIN	dissolved inorganic nitrogen
DON	dissolved organic nitrogen
NO_3^-	nitrate
NO_2^-	nitrite
NOx	nitrate + nitrite
NH_4^+	ammonium
HPO_4^{2-}	phosphate
$HSiO_3$	silica
chl-α	chlorophyll-α

FIGURE LEGEND

TABLE LEGEND

EXECUTIVE SUMMARY

A key goal of this studywas to understand the role of submarine groundwater discharge (SGD) and nutrient transport to Baffin Bay in order to improve environmental flow recommendations and nutrient criteria in Texas estuaries. Groundwater contribution for Baffin Bay estimated as part of this study is representative of mostly dry conditions during January, July, and November 2016. Groundwater discharge rates vary spatially and by season at different locations. However, the average of all SGD rates derived from continuous mobile ^{222}Rn surveys across the entire bay system exhibited little change between July (35.8 $cm \cdot d^{-1}$) and November (22.7 $cm \cdot d^{-1}$). Similarly, SGD rates estimated from the ^{226}Ra inventory across the bay reveal very small changes from July (6.5 $cm \cdot d^{-1}$) to November (1.6 $cm \cdot d^{-1}$). Nutrient concentrations measured in the interstitial porewater vary spatially and temporally. In particular, ammonium concentrations were found to be largely elevated (by one or two orders of magnitude) when compared to other estuaries in South Texas, with the largest measured concentrations in porewater in July (5,531 $\mu mol \cdot L^{-1}$) and a minimum in January (38.6 $\mu mol \cdot L^{-1}$).

In the Baffin Bay system, SGD-derived nutrient fluxes are not so much a function of changes in hydrologic conditions across seasons (i.e. changes in SGD rates) and are more dependent on spatial and temporal nutrient concentrations in the porewater. Bay-wide seasonal average SGD rates indicate that a DIN contribution from the subsurface of $1{,}029.4 \times 10^{11}$ $\mu mol \cdot d^{-1}$ is expected in July, while an over four times lower rate of 235.1×10^{11} $\mu mol \cdot d^{-1}$, may occur in November. Similarly, orthophosphate (HPO_4^{2-}) and hydrogen silicate ($HSiO_3^-$) are larger bay-wide in July (21.3×10^{11} and 284.1×10^{11} $\mu mol \cdot d^{-1}$, respectively) than in November (2.5×10^{11} and 117.4×10^{11} $\mu mol \cdot d^{-1}$, respectively), but with overall lower magnitudes than DIN. Average bay-

wide DOC fluxes from SGD are larger in July ($598.7x10^{11}$ $\mu mol \cdot d^{-1}$) than November ($480.1x10^{11}$ $\mu mol \cdot d^{-1}$).

Surface inflow fluxes, assuming a constant creek solute concentration across seasons, show that a DIN of $39.4x10^{8}$ $\mu mol \cdot d^{-1}$ is expected in January, $7.5x10^{8}$ $\mu mol \cdot d^{-1}$ in July and $4.7x10^{8}$ $\mu mol \cdot d^{-1}$ in November. Orthophosphate (HPO_4^{2-}) and hydrogen silicate ($HSiO_3^{-}$) are also larger in January with flux rates of ($8.9x10^{8}$ and $394x10^{8}$ $\mu mol \cdot d^{-1}$) followed by July ($5.4x10^{8}$ and $253x10^{8}$ $\mu mol \cdot d^{-1}$) and November ($3.8x10^{8}$ and $206x10^{8}$ $\mu mol \cdot d^{-1}$). Average DOC fluxes from surface runoff are larger January ($2,367x10^{8}$ $\mu mol \cdot d^{-1}$), followed by July ($270x10^{8}$ $\mu mol \cdot d^{-1}$) and November ($204x10^{8}$ $\mu mol \cdot d^{-1}$).

A comparison of bay-wide solute fluxes indicates that DIN inputs, mainly in the form of ammonium, are almost five orders of magnitude higher in the SGD component than the surface runoff. DOC inputs are also larger in the SGD component in July and November. Inorganic nitrogen in the form of nitrate is likely to enter Baffin Bay from surface inputs while SGD may have larger contributions of nitrite. SGD-derived orthophosphate and silicate (in the form of hydrogen silicate ion) are very similar in magnitudes and three orders of magnitude larger than the surface runoff. Therefore, the nutrient input associated with SGD, regardless of its nature (i.e. fresh or saline; groundwater or recirculated saline), is likely significant in this shallow bay system. Persistent winds are likely the dominant driver of seawater recirculation, while episodic rain events may enhance the fresher SGD input to the bay. Both scenarios can lead to diffusion of porewater solutes into the water column.

BACKGROUND AND RELEVANCE

In many arid/semi-arid regions, wetlands and estuaries experience seasonal changes in salinity. Many of these environments now experience prolonged periods of high salinity due to human impacts (i.e. limited freshwater inflows due to stream impairments) (Jolly et al., 2008; Murgulet et al., 2016). Prolonged hypersaline conditions could hinder the ability of estuaries to cycle nutrients (e.g. slowing the rate of nitrogen fixation by phytoplankton) leading to eutrophication (Conley et al., 2009; Folk and Siedlecka, 1974; Jolly et al., 2008). Some nutrient cycling processes are expected to decrease as salinities change from below (fresh or brackish) to above (hypersaline) the average salinity of seawater (salinities in this paper referred to in practical salinity units with global ocean seawater having an average salinity of 35 (Millero, 1993)) (Conley et al., 2009; Loáiciga, 2006). For instance, apart from some rare cases, planktonic nitrogen (N) fixation is reported to be insignificant in coastal estuaries with salinities above 10 (Conley et al., 2009) and salinities above 10 can reduce nitrification/denitrification in sediments by 50% compared to salinities of 0 (Rysgaard et al., 1999). However, during removal of N from wastewater, denitrification has been found to occur at 40°C and a salinity of approximately 54, (Glass and Silverstein, 1999; Kristensen and Jepsen, 1991) conditions that may occur naturally in semi-arid estuaries. For instance, near Baffin Bay, Texas, historic climate data for the past decade shows that the temperature exceeded 40°C multiple times (NAAS, 2017). In addition, bay salinity ranges from monthly averages of 40 to 50 to as high as 85 during a historic drought, with flood events bringing salinity to as low as 1.4 (Behrens, 1966; Buzas-Stephens et al., 2014; Folk and Siedlecka, 1974).

Submarine Groundwater Discharge

In the estuarine and coastal ocean setting, groundwater can be a significant source of inorganic N to local ecosystems and may provide up to 30% of the non-recycled N in the nutrient budget (Chaillou et al., 2014; Matson, 1993; Paerl, 1997). Giblin and Gaines (1990) found that N inputs from groundwater were similar in magnitude to riverine inputs in a river-dominated estuary. In bays with limited freshwater inflows and poor connection to a larger body of water, or rainfall that is significantly less than the local evaporation rate, submarine groundwater discharge (SGD) could influence the salinity of the local environment (Jolly et al., 2008) in addition to being an important source of nutrients. SGD, as described by (Moore, 2010), is "any and all flow of water on continental margins from the seabed to the coastal ocean, with scale lengths of meters to kilometers, regardless of fluid composition or driving force." Thus, SGD includes terrestrial groundwater and recirculated seawater (Santos et al., 2012).

Semi-arid estuarine systems are in general characterized by longer residence times, due to limited riverine inflows, and are known to cycle N for prolonged periods of time. In the absence of nutrient inputs from surface runoff, SGD could control primary productivity and lead to excessive algal growth or harmful algal blooms, especially in systems with long residence times (Hu et al., 2006; Jolly et al., 2008; Kroeger et al., 2007). In addition, even under low magnitudes of groundwater input, recirculated seawater can be a significant source of nutrients and anoxic waters to the water column (Santos et al., 2012). Development of anoxic conditions in the porewater could lead to the buildup of ammonium (NH_4) (Prokopenko et al., 2011; Schulz et al., 1994) that, later, can be released to the water column through SGD (including both groundwater and recirculated seawater) (Brock, 2001; Moore, 1996). Increasing salinity levels in porewater is also very common in semi-arid estuaries (Bighash and Murgulet, 2015). Previous studies indicate

that salinity levels affect the N cycle of estuaries (Conley et al., 2009; Giblin and Gaines, 1990; Holmes et al., 2000). For instance, NH_4^+ release from sediment is dependent on salinity with lower salinities effectively storing NH_4^+ in sediments and higher salinities releasing NH_4^+, which may enhance summertime primary production (Giblin et al., 2010; Holmes et al., 2000). The extent of SGD input is not fully known, but given the high enrichment of porewater and groundwater in nutrients, it is recognized to play a significant role in coastal ocean chemistry, even when volumetric inputs are low (Krest et al., 2000; Santos et al., 2012).

Nitrogen Cycling and Salinity

Nitrogen nutrients have a number of different forms, such as nitrite (NO_2^-), nitrate (NO_3^-), ammonia (NH_3), and ammonium (NH_4^+). Nitrogen enters estuarine systems through a variety of pathways including: atmospheric deposition, surface runoff (land and riverine), biological fixation, remineralization of decaying organic matter, and SGD (**Figure 1**) (Fowler et al., 2013; Paerl, 1997; Santos et al., 2012; WSDE, 2017).

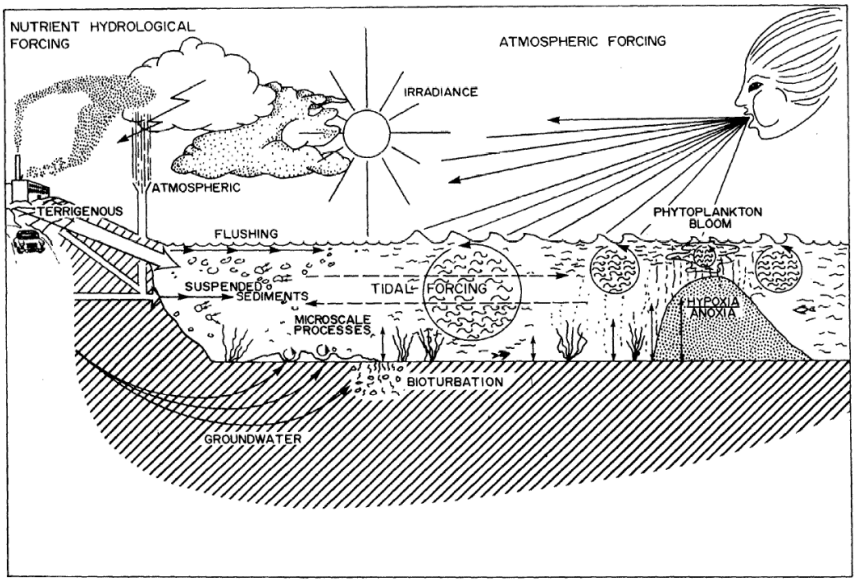

Figure 1: Diagram showing the various sources of nutrient forcing in a coastal setting. The significance of groundwater input is poorly understood (Paerl, 1997).

In marine environments, processes that control the fate of bioavailable N can be affected by many factors including salinity, as previously mentioned (Conley et al., 2009). Nitrogen cycling mechanisms are interrupted in estuaries that can change from fresh to saline conditions (Conley et al., 2009; Jolly et al., 2008). As discussed by Jolly et al. (2008), many bays and estuaries in semi-arid regions are beginning to become hypersaline, reverse estuaries for some parts of the year. This change from a normal salinity, less than average ocean water (i.e., 35), to a hypersaline environment will influence the ecology of the bay or estuary as described above, including its ability to cycle nutrients (Conley et al., 2009). Such conditions occur in south Texas estuaries, like Baffin Bay, where drought conditions contribute to depletion of freshwater inflows from riverine sources leading to increased salinity surface waters (Schmidt and Garland 2012). Baffin Bay is often considered a reverse estuary (i.e. more saline than the bay it drains into) due to limited freshwater inflows from surface runoff, high evaporation rates, and limited connection with the Gulf of Mexico, which result in long residence times, greater than 1 year, and extreme salinities, up to 75-85 (Behrens, 1966; Folk and Siedlecka, 1974; Wetz et al., 2017). The bay is considered a schizohaline environment in that it changes from freshwater salinities to hypersaline conditions repeatedly over time (Folk and Siedlecka, 1974).

This study shows that given Baffin Bay's long residence times and fluctuations from fresh to hypersaline conditions, it is an environment in which the changes salinity forces on nutrient cycling and the effects of SGD can be observed at a large scale. The effects that hypersalinity has in this environment are applicable to other semi-arid or schizohaline environments where salinity is likely to be high for prolonged periods due to limited freshwater inflows or the lack of precipitation from their arid climates (Jolly et al., 2008). Baffin Bay has

previously experienced a harmful algal bloom that lasted eight years, making it an area where understanding sources and cycling of nutrients is very important (Buskey et al., 2001).

Purpose

The extent of groundwater input and its role in releasing nutrients of terrestrial or remineralized origin is not fully understood in estuaries experiencing limited surface runoff, high evaporation rates and hypersaline conditions for most of the year. Since nutrient cycling rates and bioavailability are highly influenced by flushing rates and salinity levels, among other factors, it is important to understand the role SGD plays as a source of nutrients of terrestrial or remineralized origin. This study evaluates the effects of water residence time and SGD magnitudes (both quality (i.e. saline versus fresh) and quantity) on nutrient sources to a hypersaline, semi-enclosed estuary. The relative abundances of different nutrients in the bay and porewater, such as different forms of nitrogen, phosphorus, and silicon, were examined to evaluate forms of inputs, such as terrestrial versus remineralized.

The main objectives are: 1) to characterize the spatial-temporal variation of SGD and nutrient discharge rates; 2) to evaluate the role of subsurface heterogeneity in SGD and nutrient discharge in system-wide nutrient budgets (i.e., inputs-outputs); and 3) understand the main sources of freshwater inflow and nutrients to Baffin Bay. Estimates of seasonal groundwater discharge and nutrients that may contribute to water quality degradation were conducted. This work is critically important for understanding nutrient dynamics in Texas estuaries and helps in setting nutrient criteria by Texas Commission on Environmental Quality (TCEQ) and the US Environmental Protection Agency (USEPA) and helps improve calibration of groundwater availability models (GAMs) by TWDB.

Study Area

Baffin Bay is a shallow, well-mixed, semi-enclosed estuary located in southern Texas, bordered by Kleberg County to the north and Kennedy County to the south, on the Texas coastal plain in the northwestern Gulf of Mexico (**Figure 2**) (Dalrymple, 1964; Simms et al., 2010). The bay has a dendritic shape with three small arms branching off: Alazan Bay to the northeast, Cayo del Grullo in the northwest, and Laguna Salada in the southwest. The estuary provides essential habitat for numerous commercially and recreationally important marine species. The predominantly undeveloped land use surrounding Baffin Bay results in more pristine conditions compared to the Nueces Estuary system. However, there are emerging concerns that the ecological health of this vital habitat is threatened by water quality degradation, specifically pertaining to persistent brown tides (Wetz et al., 2017).

The Coastal Plain gradient is very gentle, approximately 0.8 $m \cdot km^{-1}$ in the area of Baffin Bay (Simms et al., 2010), leading to low land runoff and likely high infiltration rates into soils and recharge to the water table aquifer (Fetter, 2001). The shoreline in the upper reaches of Baffin Bay consists of bluffs 2 to 4m high that grade down to tidal flats along the lower portion of the shoreline (Simms et al., 2010). Baffin Bay is isolated from the Gulf of Mexico by the 180 km long Padre Island and is further insulated from the contiguous Laguna Madre System by shallow reefs at the mouth of the bay (Simms et al., 2010). The nearest inlets that allow for exchange between Baffin Bay and the Gulf of Mexico are Packery Channel and Aransas Pass (~41 km and ~70 km north of Baffin Bay, respectively) and Port Mansfield (~80 km south) (Wetz et al., 2017). Three creeks feed Baffin Bay: the San Fernando flowing into Cayo del Grullo, the Petronila flowing into Alazan Bay, and the Los Olmos into Laguna Salada. These

creeks are believed to have carved the valley that now forms Baffin Bay in response to the last sea level drop at 20 ka (Behrens, 1963; Fisk, 1959; Simms et al., 2010).

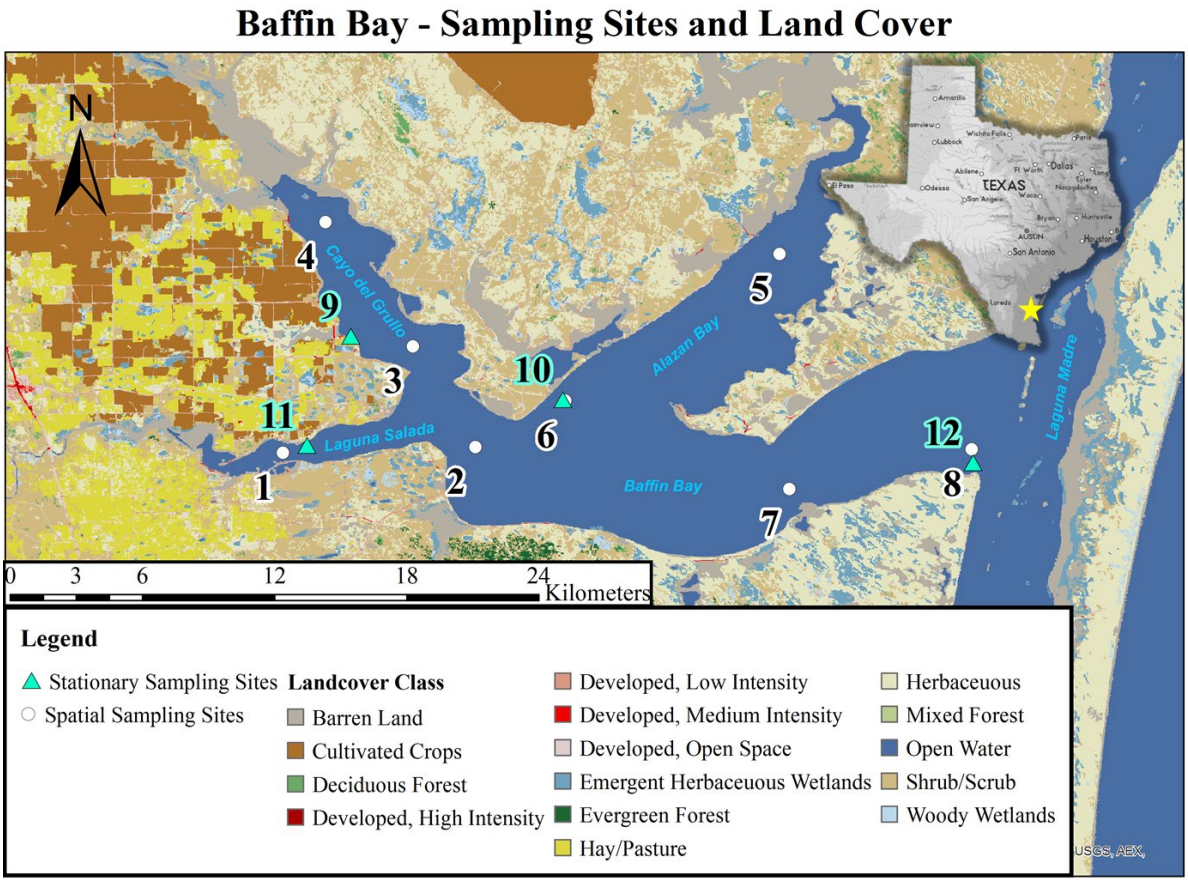

Figure 2: Study area location map including: the land use and land cover data for the Baffin Bay surroundings and the spatial (stations 1-8) and time series (9-12) sampling stations.

The semi-arid area of south Texas is characterized by high evaporation rates that exceed precipitation (60-80 $cm \cdot yr^{-1}$) by 60 cm annually (Behrens, 1966). This leads to average salinities of 40-50 and extremes as high as 85 during droughts and as low as 2 during large precipitation events (Behrens, 1966; Simms et al., 2010). Streamflow discharge data to Baffin Bay from its tributaries is limited; however, the freshwater inflow to and from the creeks is infrequent, thus contributing to the generally high salinities and long residence times (**Figure 3**). Data from 1967-2017 (collected approximately 40km inland from the bay) indicates that the Los Olmos Creek discharges on average 0.13 $m \cdot s^{-1}$ (min: 0 $m \cdot s^{-1}$, max: 3.40 $m \cdot s^{-1}$) (USGS, 2017b). From

1965 to 2017 (collected from a stream gauge approximately 60 km inland from the bay), there was an average discharge of 0.55 $m \cdot s^{-1}$ (min: 0.05 $m \cdot s^{-1}$, max: 15.83 $m \cdot s^{-1}$) from the San Fernando Creek (USGS, 2017a). No data were found for Pentronila Creek.

The major sediment types found in Baffin Bay are black-mud, ooids, quartz-mollusc sands, and coated grains (Alaniz and Goodwin, 1974; Dalrymple, 1964). There are five major depositional environments found in Baffin Bay that differentiate it from other northern Gulf of Mexico bays: well-laminated carbonate and siliciclastic open-bay muds, ooid beaches, shelly internal spits and barrier islands, serpulid worm tube reefs, and prograding upper-bay mudflats (Simms et al., 2010). Sediment transport to Baffin Bay is limited to intense precipitation events by modern aeolian dunes, especially along the south shore (Simms et al., 2010). The dry climate caused an increase in $CaCO_3$ deposition in the soil in this area when compared to that northeast of Baffin Bay. Calcite formation around the shoreline acts as a shoreline stabilizer (Behrens, 1963; Driese et al., 2005; Price, 1936) that allows Baffin Bay to retain its dendritic shape (Behrens, 1963).

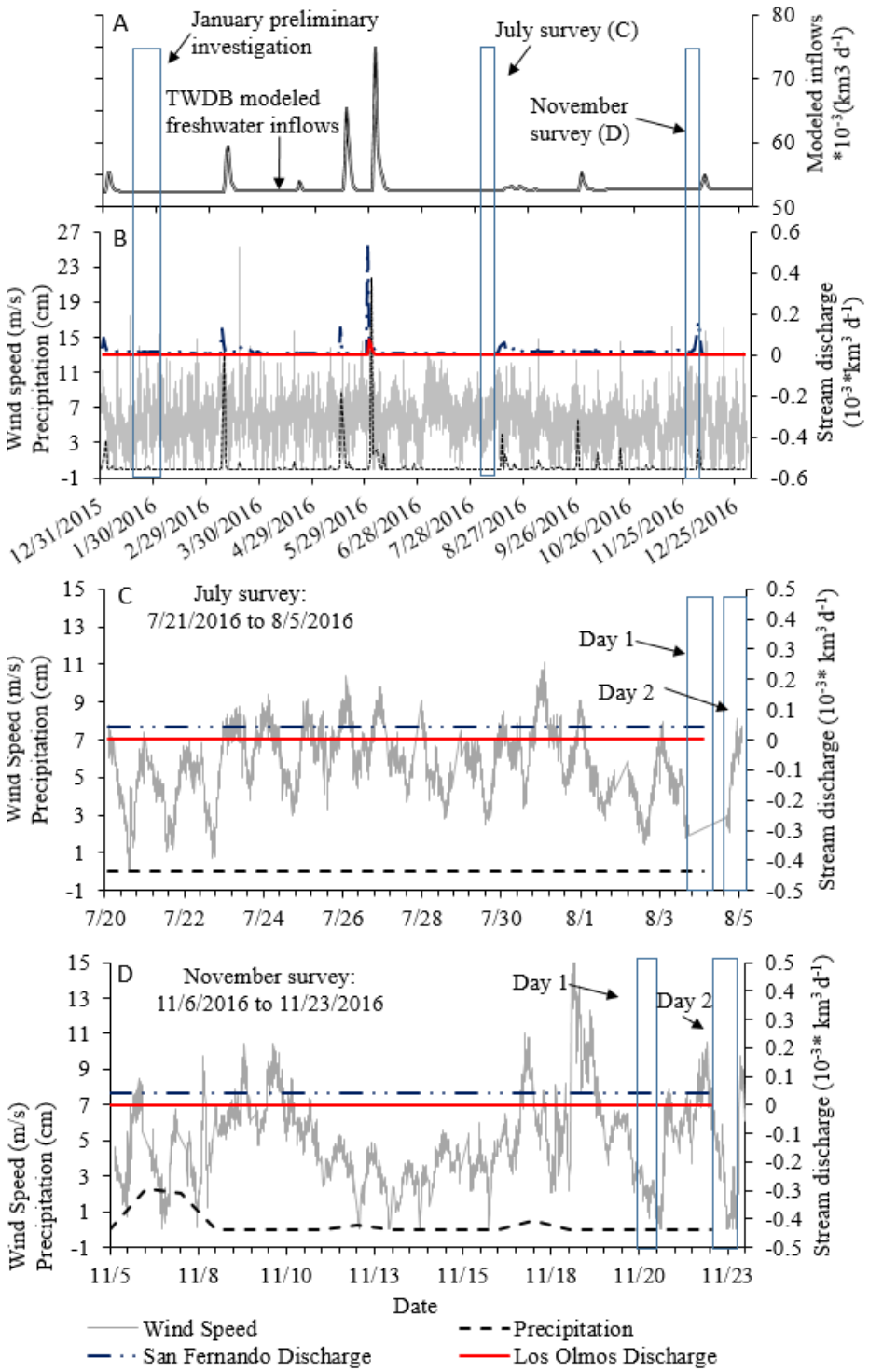

Figure 3: A) (Top Graph) Wind speed ($m \cdot s^{-1}$), precipitation (mm), discharge from San Fernando Creek ($km^3 \cdot d^{-1}$), and discharge from Los Olmos Creek all plotted against the date for the full year of 2016 during which this study took place. B) (In top graph) A box highlighting the first day of the study during which the CRP took place. C) (Top and middle graph) The two weeks leading up to and including the days of the July sampling event were dry and had steadily rising winds. D) (Top and middle graph) The two weeks leading up to and including the days of the November sampling event were not as dry as July and were performed during days of lower wind speed.

Previous studies in the south Texas area (Breier et al., 2010; Nyquist et al., 2008; Service), 2012; Waterstone and Parsons, 2003) as well as the hydraulic conditions indicate that groundwater flows toward the coast, eventually discharging into the bays and estuaries; however, Baffin Bay receives significantly less precipitation than systems further north and there is a significant drawdown around Kingsville that may inhibit groundwater flow toward the coast. The Gulf Coast Aquifer (GCA) is a leaky artesian aquifer comprised of a complex of clays, silts, sands, and gravels (Ashworth and Hopkins, 1995) that form the Chicot, Evangeline, and Jasper aquifers (Waterstone and Parsons, 2003). The Baffin Bay estuary and the surrounding systems are generally in direct contact with the Chicot aquifer, which is the shallowest of the mentioned aquifers. The stratigraphic units of the Chicot aquifer consist of an overlying alluvial formation preceded by Beaumont and Lissie formations (Ashworth and Hopkins, 1995), which are generally composed of clays and clayey silts with intermittent sand and gravel lenses that continue out into the Gulf of Mexico (Waterstone and Parsons, 2003). The maximum total sand thickness of the GCA ranges from 700 ft in the south to 1,300 ft in the north with an average freshwater saturated thickness of about 1,000 ft (George et al., 2011). Brackish groundwater is more common than fresh groundwater in the southern GCA where water quality declines and total dissolved solids of 1,000 $mg \cdot L^{-1}$ or more are common (George et al., 2011).

Previous studies in the south Texas area (Breier et al., 2010; Nyquist et al., 2008; Service), 2012; Waterstone and Parsons, 2003) as well as the hydraulic conditions indicate that groundwater flows toward the coast, eventually discharging into the bays and estuaries; however, Baffin Bay receives significantly less precipitation than systems further north and there is a significant drawdown around Kingsville that may inhibit groundwater flow toward the coast. The Gulf Coast Aquifer (GCA) is a leaky artesian aquifer comprised of a complex of clays, silts,

sands, and gravels (Ashworth and Hopkins, 1995) that form the Chicot, Evangeline, and Jasper aquifers (Waterstone and Parsons, 2003). The Baffin Bay estuary and the surrounding systems are generally in direct contact with the Chicot aquifer, which is the shallowest of the mentioned aquifers. The stratigraphic units of the Chicot aquifer consist of an overlying alluvial formation preceded by Beaumont and Lissie formations (Ashworth and Hopkins, 1995), which are generally composed of clays and clayey silts with intermittent sand and gravel lenses that continue out into the Gulf of Mexico (Waterstone and Parsons, 2003). The maximum total sand thickness of the GCA ranges from 700 ft in the south to 1,300 ft in the north with an average freshwater saturated thickness of about 1,000 ft (George et al., 2011). Brackish groundwater is more common than fresh groundwater in the southern GCA where water quality declines and total dissolved solids of 1,000 $mg \cdot L^{-1}$ or more are common (George et al., 2011).

Strong southeast winds of 16 to 32 km per hour ($km \cdot h^{-1}$) are dominant from February to August (Dalrymple, 1964; Rusnak, 1960); however, from September to February, the dominant wind direction shifts to the northwest with an average speed of 18.35 $km \cdot h^{-1}$ (Lohse, 1955; Network, 2016). Baffin Bay is a shallow estuary with an average depth of 2 m (max: 3 m) (Simms et al., 2010) that experiences only small astronomical tides (<0.1 m) (Simms et al., 2010). With the strong, persistent winds and shallow depths, the tides are mainly controlled by wind and precipitation events (Breuer, 1957; Militello, 1998). Consequently, the bay is generally well-mixed with little stratification under normal conditions.

A previous study in Baffin Bay ranked, from largest to smallest, the sources of external N to the system as: 1) atmospheric deposition, 2) fertilizer, 3) manure from livestock, 4) urban runoff from developed land, and 5) industrial and municipal point sources (Rebich et al., 2011). This study did not account for groundwater although it has been shown to be a likely contributor

of external N to the bay (Breier et al., 2010; Santos et al., 2012; Uddameri et al., 2013). The relative contributions of each source are dependent on hydroclimatic conditions and thus are expected to shift with changes in precipitation and return flows. For instance, during drought conditions some of the tributaries often run dry while others, such as the San Fernando Creek, which has 12 permitted wastewater facilities and likely is dominated by point source N (Wetz et al., 2017), flow perpetually and could contribute a continuous source of N and other forms of nutrients. The typical concentrations of NOx (NO_2+NO_3) in Baffin Bay range from <0.3 µM to 35 µM with an average concentration of <1-4 µM, and NH_4^+ concentrations ranged from 7 µM to 91.7 µM in surface water over the years 2013-2015 (Wetz, 2015). According to Wetz (2015), surface water DON regularly exceeded 35 µM.

METHODS

Preliminary Investigation

The project started with a reconnaissance survey of the study area in which water-based continuous electrical resistivity profiling (CRP) to locate possible groundwater upwelling zones (or SGD). For a detailed description of the CRP methodology see Douglas et al. (2017) and Murgulet et al. (2016). In brief, we used the Advanced Geosciences, Inc. SuperStingR8 Marine system with patented graphite electrodes and EarthImager software with induced polarization imaging system and geophysical interpretive tools to differentiate between types of lithology and water with differing resistivity/electrical conductivity to map out groundwater seepage face and to differentiate between shallow/recirculated seawater and deeper/terrestrial groundwater SGD pathways. The system used is equipped with a 112m cable consisting of 56 graphite electrodes spaced 2m apart with the ability to accurately image to a depth of approximately 20% the length of the cable (i.e. ~20 m into the sediment subsurface). CRPs were collected along three transects: 1) Laguna Madre to the head of Laguna Salada through the southern half of the bay, 2) the length of Alazan Bay, and 3) the length of Cayo del Grullo. These images help determine the location and possible extents of discharge zones and aid in selecting sampling and SGD monitoring sites. Based on these initial assessments eight locations were selected for spatial surface water and groundwater sampling.

To further assist in determining areas of likely SGD, continuous ^{222}Rn measurements were taken during the July spatial sampling following the methods described by (Burnett and Dulaiova, 2003). In brief, water from ~0.3m above the sediment-water interface was pumped via a peristaltic pump to a RAD AQUA air-water exchanger and air was then pumped from the exchanger to three Durridge RAD-7 Radon-in-air detectors connected in sequence. The RAD-7s

were set to 30 minute integrations and were offset by 10 minutes to allow for high temporal resolution with moderate uncertainty. The water sample inlet was placed on the side of a boat, moving at a speed less than 4.0 km hr^{-1}, to continuously sample and measure ^{222}Rn along the path traveled. The measured ^{222}Rn activity was used to determine an excess ^{222}Rn in water inventory as described by Burnett and Dulaiova (2003), whereby ^{222}Rn in water was: 1) corrected for decay and ^{226}Ra supported, 2) converted to an inventory by multiplying by the water depth, 3) corrected for sediment supported ^{222}Rn (measured by sediment equilibration experiment as described by Corbett et al. (2000)), 4) corrected for atmospheric evasion losses, and 5) corrected for mixing loss (i.e. maximum negative difference between corrected inventories). The total flux produced was then divided by the average ^{222}Rn activity of the local groundwater wells to calculate a flux of water (i.e. SGD). A Yellow Springs Instruments (YSI) Pro Plus® was used and placed at the same depth as the water inlet for the ^{222}Rn sampler. The YSI probe measured water quality parameters every 30 seconds along the path. The probe measured parameters including temperature, pressure, pH, DO, oxidation-reduction potential (NBBEST, 2011), salinity, and electrical resistivity. ^{222}Rn and YSI data were plotted for interpretation using ArcGIS. Stations for spatial analysis of nutrients in surface water, porewater, and SGD time-series measurements were selected using these preliminary data. The locations with the highest ^{222}Rn and/or with subsurface anomalies in the CRP were chosen as sites for further investigation. In total an additional four stations selected for time-lapse resistivity imaging and continuous ^{222}Rn measurements in July/August and November/December, 2016, as described below.

Water Sample Collection

Aqueous samples were collected from both surface water and porewater, whenever possible, during spatial and time series sampling events. Water samples were collected at eight stations during three events (winter – January, summer – July/August, and fall – November/December) to capture groundwater discharge rates and nutrient and biomass distribution and concentrations under different environmental conditions. Water samples were collected in compliance with standard sampling techniques (Brown et al., 1970; RCRA SOP, 2009; Wood, 1976). The water depth was measured at each location using a pre-labeled line attached to a weight. Samples from the water column were collected from the surface (0.2m below air-water interface) and bottom (0.2m above sediment-water interface). Field parameters were measured before sample collection using an YSI multiparameter water quality meter. The YSI meter was placed at each sampling depth within the water column for several minutes to allow proper circulation of sample and instrument stability before parameters were recorded.

Surface water samples were collected with a Van Dorn bottle deployed to the desired depth and given a few minutes to allow water to circulate through the cartridge, according to the standard operating procedure (TCEQ, 2012). All sampling bottles were rinsed three times and then overfilled, capped, and placed on ice, depending on the required procedure for each analyte. For dissolved gas samples (i.e. ^{222}Rn, DIC, TA) a rubber tube was used to transfer the sample with minimal air exposure. Porewater was collected at each site by inserting a push-tip piezometer (AMS Retract-a-Tip) connected through silicone tubing to a peristaltic pump about 07 to 3.2 m below the sediment-water interface (i.e. deep enough to prevent bottom waters from contaminating porewater sample (RCRA SOP, 2009)). Before sample collection the tubing was

flushed until the sample was clear (or a minimum amount of sediment was present in the sample) and the field parameters (i.e. salinity, temperature, pH) stabilized.

Stable Isotopes

Samples for measurements of stable isotope ratios of oxygen ($\delta^{18}O$), hydrogen (δD), dissolved inorganic carbon (Dickson et al., 2007), and carbon stable isotope ratio ($\delta^{13}C$) were also collected using the above procedure. Samples were filtered with 0.7 µm GF/F filters in field and $\delta^{13}C$/DIC samples were preserved with 0.1 mL of saturated mercuric chloride ($HgCl_2$) Abundances of oxygen, hydrogen and carbon isotopes were measured (with an uncertainty of ±1per mil (‰) for δD, ± 0.1 for $\delta^{18}O$, and ± 0.2 for $\delta^{13}C$) relative to accepted international standards, which are the Vienna Standard Mean Oceanic Water (VSMOW) (for oxygen and hydrogen) and the Vienna Pee Dee Belemnite (VPDB) (for carbon).

Major Ions

Major ion measurements were determined using a Dionex High Performance Ion Chromatograph (Model DX600) equipped with an autosampler, an anion-exchange column (7 mm; 4 x 250 mm; Dionex AS14A), and a conductivity detector (Dionex CD25). The detection limit of the method ranged between 0.05 and 0.1 mg/L, depending on the background signal of constituents in the samples. Iron (Fe) can also be a limiting nutrient in coastal systems and could have significant impact on GPP as it has a strong affinity for scavenging dissolved phosphate (Testa et al., 2002). Samples for these major ions as well as sodium (Na^+), magnesium (Mg^{2+}), total manganese (Khan and Kumar, 2012), and calcium (Ca^{2+}) were acidified to 2% ultra-high purity nitric acid (end pH <2), filtered at 0.2µm nominal pore size and analyzed using Inductively Coupled Plasma - Mass Spectrometry (ICP-MS) (Method: EPA 200.8). Detection

limits vary by element and are available at http://www.chemtest.co.uk/downloads/metalsmrls-jun10.pdf.

Total Alkalinity and Dissolved Inorganic Carbon

Alkalinity and dissolved inorganic carbon (Dickson et al., 2007) samples were collected in 250 mL borosilicate bottles with no head space and preserved using 100 µL of saturated $HgCl_2$ (Kattner, 1999). Total alkalinity was measured using a Titrando automatic titrator (Metrohm, Switzerland) with a pH electrode. Hydrochloric acid (HCl) was used as the titrant with a concentration of approximately 0.1 $mol \cdot L^{-1}$. Alkalinity samples were run multiple times to reach a precision of 0.1% (Cyronak et al., 2013). DIC was measured by an Apollo SciTech DIC Analyzer, the samples are brought to a temperature of 22°C by a water bath and the concentration was calculated using standard of certified reference material, sample salinity, density and theoretical DIC.

Nutrient and Chlorophyll-α Sampling

Water samples were collected in acid-washed amber polycarbonate bottles using the techniques mentioned above. Bottles were stored on ice until return to a shore-based facility where processing of samples occurred and analyses were conducted for chlorophyll-α (surface water) and nutrients and organic matter (surface water and porewater). Chlorophyll-*α* was determined from samples collected on, and extracted from Whatman GF/F filters (nominal pore size 0.7 µm). Chlorophyll was extracted using methanol and analyzed fluorometrically. All nutrient samples were filtered with Whatman nuclepore track-etched hydrophilic polycarbonate membranes (nominal pore size 0.2 µm) and kept frozen until analysis.

Inorganic nutrients (nitrate (NO_3^-), nitrite (NO_2^-), ammonium (NH_4^+), orthophosphate (HPO_4^{2-}), silicate ($HSiO_3^-$)) were determined from the filtrate using a Seal QuAAtro

autoanalyzer. The method detection limit was determined for each analyte and matrix by the EPA method detailed in 40 CFR Part 136, Appendix B. The method detection limit (MDL) is defined as the Student's t for 99% confidence level times the standard deviation of seven replicate measurements of the same low level sample or spiked sample. The applicable concentration ranges of this method are defined by the concentration range of the calibration solution adjusted by the estimated sample concentrations. If the sample concentration exceeds the linear range, the sample was diluted and reanalyzed. The method detection limit (MDL) in µM for the nutrients are: 0.11for NO_3^-, 0.012 for NO_2^-, 0.057 for NH_4^+, 0.025 for HPO_4^{2-}, 0.14 for $HSiO_3^-$.

Dissolved organic carbon (Boyd et al., 2000) and total dissolved nitrogen (TDN) were determined from the filtrate using a Shimadzu TOC-V analyzer with nitrogen module. Dissolved organic nitrogen (DON) was estimated as the difference between TDN and inorganic nitrogen. The method detection limit is aproximately 1 mg· L^{-1}. Samples with N content of ≥0.07 mg/L as N were sent for stable isotopes of nitrate ($\delta^{15}N$ and $\delta^{18}O_{nitrate}$) measurement, though not many reached this threshold and thus results are not included herein.

Radiogenic Isotopes

Samples for radium (radium-223 (^{223}Ra), radium-224 (^{224}Ra), radium-226 (^{226}Ra)) analysis were collected in three-20L jugs (approximately 45 to 60 L total volume) at each of the spatial sampling sites using a sump pump positioned ~0.2 m above the sediment-water interface. The radium was extracted by processing the samples through ~15g manganese dioxide, MnO_2, impregnated acrylic fibers two times at a flow rate <1 L·min^{-1} (Dimova et al., 2007; Kim et al., 2001). The Mn-fibers were then rinsed thoroughly with Ra-free water to eliminate any salts or particulates and then pressed to a water to fiber ration of 0.3-1g (i.e. 20-30g wet weight) (Sun

and Torgersen, 1998). The fibers were tested for ^{223}Ra (half-life: 11.4 days) and ^{224}Ra (half-life: 3.6 days) on a Radium Delayed Coincidence Counter (RaDeCC). Activities of ^{224}Ra were measured within three days of collection given the short half-life (Moore, 2006). After the short-lived isotope measurements, the fibers were flushed with nitrogen gas and sealed for >21 days to reach secular equilibrium before measuring the ^{226}Ra (half-life: 1,600 years) on a RAD-7 with measurements corrected to a calibration curve determined from 5 standards (Moore, 1996). Measurements of radon (^{222}Rn) from 2L grab samples (surface water) and 250mL grab samples (porewater and terrestrial groundwater) were conducted using a Durridge RAD7 radon-in-air monitor with the soda bottle and WAT250 accessories and protocols, respectively (Lee and Kim, 2006). The accessories are used to sparge the gas from the water bringing it into a closed air loop and to the detector.

Sediment Core Collection and Processing

Sediment cores (ranging from 21cm to 62cm deep) were collected at each time series station for analysis of bulk density porosity and sediment-supported ^{222}Rn activities. During sediment core collection the core tube was manually pressed into the sediment and the top of the tube is sealed with a valve head to create suction so that the core tube can be extracted with the core inside remaining intact. Sediment cores are processed by: 1) carefully, so as not to disturb the top sediments, removing any overlying water from the core tube, and 2) extruding the core directly from the tube while sectioning off samples with a stainless-steel spatula. For every 10cm increment of the upper 50 cm and then every 25cm increment for the remainder of the core, the first 2cm were used in sediment supported ^{222}Rn equilibration experiments as described by Corbett et al. (2000) and the next 5cm were used for bulk density porosity measurements as described by (Fetter, 2001). The remaining sample from each increment was dried and kept for

reference. For sediment-supported ^{222}Rn, sediment samples (i.e. 2cm collected from every 10cm of the cores) were placed into a 500ml Erlenmeyer flask, equilibrated with 400mL of Ra-free bay water, sealed, and after agitation on a shaker table for >21days, were analyzed for the amount of ^{222}Rn that escaped into the fluid phase. This provides the sediment equilibrated ^{222}Rn concentration (or sediment-supported ^{222}Rn) for each SGD site.

Radium Ages

The laboratory experiments conducted using sediment cores show that fluxes from bottom sediment alone are negligible for this study (see section ^{222}Rn-derived Submarine Groundwater Discharge). Therefore, we can assume that the major input of radium comes from groundwater rather than from sediment diffusion or resuspension. Relative radium age of the surface water, or the relative time that has passed since the radium first entered the system in a well-mixed estuary, was calculated using the ratio of the short-lived (^{224}Ra) to the long-lived (^{226}Ra) isotopes using equation 1 from (Knee et al., 2011b):

$$T = \frac{AR_{GW} - AR_{CO}}{AR_{CO} \times \lambda_{224}} \quad (1)$$

where AR_{GW} is the initial activity ratio of discharging groundwater, AR_{CO} is the measured activity ratio at the station of interest, and λ_{224} is the decay constant (d^{-1}) for the short-lived radium-224 isotope (Knee et al., 2011b).

This equation assumes radium activities and activity radios are greatest in the Ra source (i.e. groundwater and sediment containing Ra) and also elevated in receiving nearshore water relative to waters further offshore due to SGD and desorption from sediments. Consequently, radium activities and ARs should be decreasing as the water mass is moving away from the discharge point. This could occur due to two factors: radioactive decay and mixing with more dilute offshore waters. This equation also assumes Ra additions are occurring continuously over a

wide area, in this case the Baffin Bay estuary with multiple groundwater discharge locations. The short-lived isotope is normalized to the long-lived isotope (i.e. ^{226}Ra) with activities that are expected to only decrease due to dilution. Because the half-life of ^{226}Ra is much longer ($T_{1/2}$ = 1600 yr) with respect to mixing time, its decay rate may be neglected. Using the groundwater activity ratios as the source of radium (i.e. water source), an estimate of the time since SGD occurred was provided. It should be noted that water mass ages and residence times are different ways to quantify mixing within a water body and they may not yield the same results as residence times calculate the amount of time it takes a parcel of water to leave the water body whereas water mass ages calculate the length of time since a parcel of water entered the water body.

Submarine Groundwater Discharge Estimates

SGD rates were calculated from time-series ^{222}Rn, continuous ^{222}Rn (see section Preliminary Investigation), ^{226}Ra activities, and time-series ERT, as described below.

^{226}Ra-derived Submarine Groundwater Discharge

To estimate SGD from ^{226}Ra observations in Baffin Bay, an estuarine mass balance is required to determine the excess inventory of ^{226}Ra (due to groundwater flux) in the bay. This includes all sources of radium other than groundwater such as tidal exchange, rivers, desorption from riverine suspended sediments, diffusion from sediments (Moore, 1996). Given the highly saline surface waters in the bay, diffusion from bay bottom sediments may be ignored as Expressed mathematically, excess ^{226}Ra ($^{226}Ra_{ex}$ [Bq·d^{-1}]) in the bay equals:

$$^{226}Ra_{ex} = \left[\frac{(^{226}Ra_{BB} - ^{226}Ra_{sea}) \times V_{bay}}{T_r}\right] - [^{226}Ra_r Q_r] - [^{226}Ra_{des} Q_r] \qquad (2)$$

where $^{226}Ra_{BB}$ is the average measured activity in Baffin Bay; $^{226}Ra_{sea}$ is the average activity in the offshore water body (i.e. Laguna Madre), which exchanges tidally with Baffin Bay; V_{bay} in the volume of Baffin Bay; T_r is the residence time estimated from the apparent radium water

ages (i.e. equation 1); Q_r is the average total discharge rate of the tributaries to the bay; $^{226}R_r$ is the average activity of the tributaries; and $^{226}Ra_{des}$ is the activity of ^{226}Ra desorbed by the sediments in the bay

(Swarzenski, 2007). After accounting for all possible sources of ^{226}Ra, it is assumed that the excess activity from equation (2) is the result of SGD. Thus, using a groundwater endmember activity ($^{226}Ra_{GW}$), SGD is calculated from:

$$SGD_{^{226}Ra} = \frac{^{226}Ra_{ex}}{^{226}Ra_{GW}} \quad (3)$$

Radium desorption experiments were conducted using representative riverine sediment samples (i.e. 0-10cm) from the freshwater portion of each creek. Los Olmos creek had a consistently high salinity (>60), so was ignored for sediment desorption experiments. Low salinity creek water (San Fernando: 2.63 and Petronila: 9.85) samples and high salinity bay water (55) was filtered through Whatman GF/F filters to remove suspended solids and processed through MnO_2 fibers to make radium-free. Solutions of Ra-free creek and bay water were made to match salinities at the time of sample collection (January: 32, July: 37, November: 51). A known mass of dried sediments was added to a known volume of the Ra-free solutions in proportions mimicking naturally occurring total suspended solids (TSS) expected for the study area. Sample solutions were then stirred and placed on a shaker table for 45 minutes before extracting the desorbed radium by passing the solution through MnO_2 fibers and processing as described above. Total ^{226}Ra activity was normalized to the sediment mass and then multiplied by the sediment flux from the creeks.

^{222}*Rn-derived Submarine Groundwater Discharge*

Radon is much more enriched in groundwater when compared to surface waters (typically 1000-fold or greater) (Dimova et al., 2011). Because of its unreactive nature and short half-life

($T_{1/2}$ = 3.83 d) ^{222}Rn is an excellent tracer to identify areas of significant groundwater discharge (Burnett and Dulaiova, 2003). Recent studies demonstrate that continuous radon measurements could provide reasonably high-resolution data to evaluate changes of radon concentration of surface water at one location over time (Burnett and Dulaiova, 2003; Burnett et al., 2001). Continuous time-series measurements of ^{222}Rn were conducted at 4 selected locations where time-lapse ERT profiles were also acquired. The automated radon system (RAD-7 and the RAD AQUA accessories) was placed at the end of each resistivity transect on the deck of the research vessel or pier. The monitoring system measures ^{222}Rn from a constant stream of water (driven by a peristaltic pump) passing through an air-water exchanger. The exchanger distributes radon from a running flow of water to a closed air loop that feeds to the RAD-7 radon-in-air monitor. The continuous time-series ^{222}Rn measurements were used to construct a mass balance to estimate SGD as described in detail by Burnett and Dulaiova (2003); Lambert and Burnett (2003); Smith and Robbins (2012), and references therein. Expressed mathematically, the total ^{222}Rn flux (F_{total}) at the station equals:

$$F_{total} = [z(\lambda A_{Rn} - \lambda A_{Ra})] + F_o - F_i - F_{sed} + F_{atm} \pm F_{mix} \quad (4)$$

where λA_{Rn} is the decay corrected activity of ^{222}Rn in water column, λA_{Ra} is the activity of ^{222}Rn due to production ^{226}Ra in the water column, z is the water depth, F_o is the offshore flux (flood tide), F_i is the inshore/nearshore flux (ebb tide), F_{sed} is the sediment flux, F_{atm} is the losses due to atmospheric evasion, and F_{mix} is the losses due to mixing processes. The main principle behind using continuous radon measurements to quantify groundwater discharge rates to surface waters is based on the inventory of ^{222}Rn over time accounting for losses/gains due to mixing with waters of different radon concentrations (i.e. low activity offshore waters), atmospheric evasion, and sediment inputs. Thus, changes over time, if any, can be converted to radon fluxes. Using the

advective fluid radon activities, ^{222}Rn fluxes are converted to water fluxes (Burnett and Dulaiova, 2003):

$$w\ (m \cdot s^{-1})\ = \frac{F_{total}}{^{222}Rn_{GW}} \quad (5)$$

Monitoring of radon extended over 6 to 10 hours depending on location and weather conditions (e.g., at winds of more than 12 miles per hour bay conditions become very difficult for sampling and data collection). Consequently, tidal effects could not be fully addressed using the presented methods; however, given the microtidal characteristics of this system, tidal effects are expected to be minimal compared to wind-driven circulation (Santos et al., 2012). Nevertheless, changes in water levels of no more than 0.3m are recorded in this area due to tidal fluctuations (NOAA 2014). It is assumed that the lower radon fluxes observed during the monitoring time are due to mixing with offshore waters of lower activity. The maximum absolute values of the observed negative fluxes during each time-series event at each location are used to correct radon fluxes for losses via mixing (Burnett and Dulaiova, 2003; Dulaiova et al., 2006). Sediment-supported radon activities were measured using laboratory equilibration experiments from sediment cores collected at each time-series station following the methods outlined by Corbett et al. (1998), as discussed above.

Electrical Resistivity Time-lapse Measurements

During ERT time series, the cable was laid on the subsurface, at the sediment-water interface, and was used to take detailed measurements of the bulk electrical resistivity of the subsurface. This reading was taken approximately every two hours to allow for the instrument to get an accurate reading as the device automatically reruns any measurement that is considered an error or is different from the last reading by 2 standard deviations. The depth of penetration for this system is about 20% of the total length of the electrode cable or about 22 m deep with a

resolution of 50% of the electrode spacing (i.e. 2m spacing and 1m spatial resolution) (Advanced Geosciences, 2017). The location of the cable was recorded with GPS coordinates at each end of the cable. The data was processed using the AGI's EarthImager software and only results with an RMS error of 10% or lower were used for interpretations. Resistivity inversions were processed into a percent difference in resistivity/conductivity between each time-step which helped to identify potential areas of groundwater upwelling and groundwater-surface water exchange. Any changes in the electrical resistivity of the subsurface was assumed to be caused by changes in the porewater chemistry as the sediment matrix was assumed to remain constant (Nyquist et al., 2008). A salinity mass balance was used to approximate SGD rates (including recirculated and deeper exchange) (Bighash and Murgulet, 2015; Dimova et al., 2012). This calculation includes the assumption that only plumes moving upward are considered and that these plumes discharged into surface water.

To perform the salt balance, the resistivity of the sediment matrix was used to determine the resistivity of the porewater using formulas from Lee and Collett (2006). The formation factor (F) is a value determined by the porosity and clay content of the sediment matrix (Lee and Collett, 2006) as shown below:

$$F = a \times \phi^{-m} \quad (6)$$

Where a and m are constants derived from clay content according to formulas by Lee and Collett (2006) and ϕ is the porosity of the sediment. The resistivity of the porewater was determined by the formation factor using the formula:

$$R_p = {}^{R_f}/_{F} \quad (7)$$

Where R_p is the resistivity of the porewater and R_f is the resistivity of the sediment matrix or formation. The salinity was then calculated from the porewater resistivity using the Manheim et al. (2004) equation:

$$S = 7.042 \times R_p^{-1.0233} \quad (8)$$

Where S is salinity and Rp is the resistivity of the porewater. With the salinity of the beginning and ending porewater of the time-series ERT, the SGD was calculated using the formula:

$$Q_{gwd} = \frac{V_{sal} \times (S_1 - S_2)}{S_2 \times \Delta t} \quad (9)$$

Where Q_{gwd} is the groundwater discharge rate, V_{sal} is the volume of the porewater plume, S_1 is the initial salinity, S_2 the final salinity and Δt the change in time over which the measurements were taken.

The ERT-derived SGD rates will be compared to those derived from the ^{222}Rn and ^{226}Ra method.

RESULTS AND DISCUSSION

Preliminary Investigation

Continuous Resistivity Profiles (CRP)

Continuous resistivity profiles were collected along the northern and southern shorelines of Baffin Bay (**Figure 4**). The inverted profiles were examined in conjunction with local geology to determine locations where SGD was likely to occur. The typical average resistivity for freshwater saturated sediments like clay or sandy loam are 38 Ω-m and 51 Ω-m respectively (Nyquist et al., 2008). Resistivities measured during the CRP ranged from 0.18-1.1 Ω-m, as shown in **Figure 5**, which is indicative of sediments saturated with high salinity water (Murgulet et al., 2016). Areas of higher electrical resistivity located in close proximity to potential lithological connections between the subsurface and surface water were deemed areas of interest, as shown in **Figure 4**. The CRPs were conducted in January, following little to no precipitation (**Figure 3**). A total of eight locations were selected for spatial assessments of groundwater influences and nutrient sources to Baffin Bay (**Figure 2**) extending from the westernmost edge of the southern CRP, into Laguna Salada (station 1), to the center of the bay (station 2), eastward along the southern CRP towards the mouth of Baffin Bay (station 7) and then very near to the mouth of Baffin Bay (station 8). Along the northwestern most point of the northern CRP (station 4), near the mouth of Cayo del Grullo (station 3), where Cayo del Grullo meets Alazan Bay (station 6), and the headwaters of Alazan Bay (station 5).

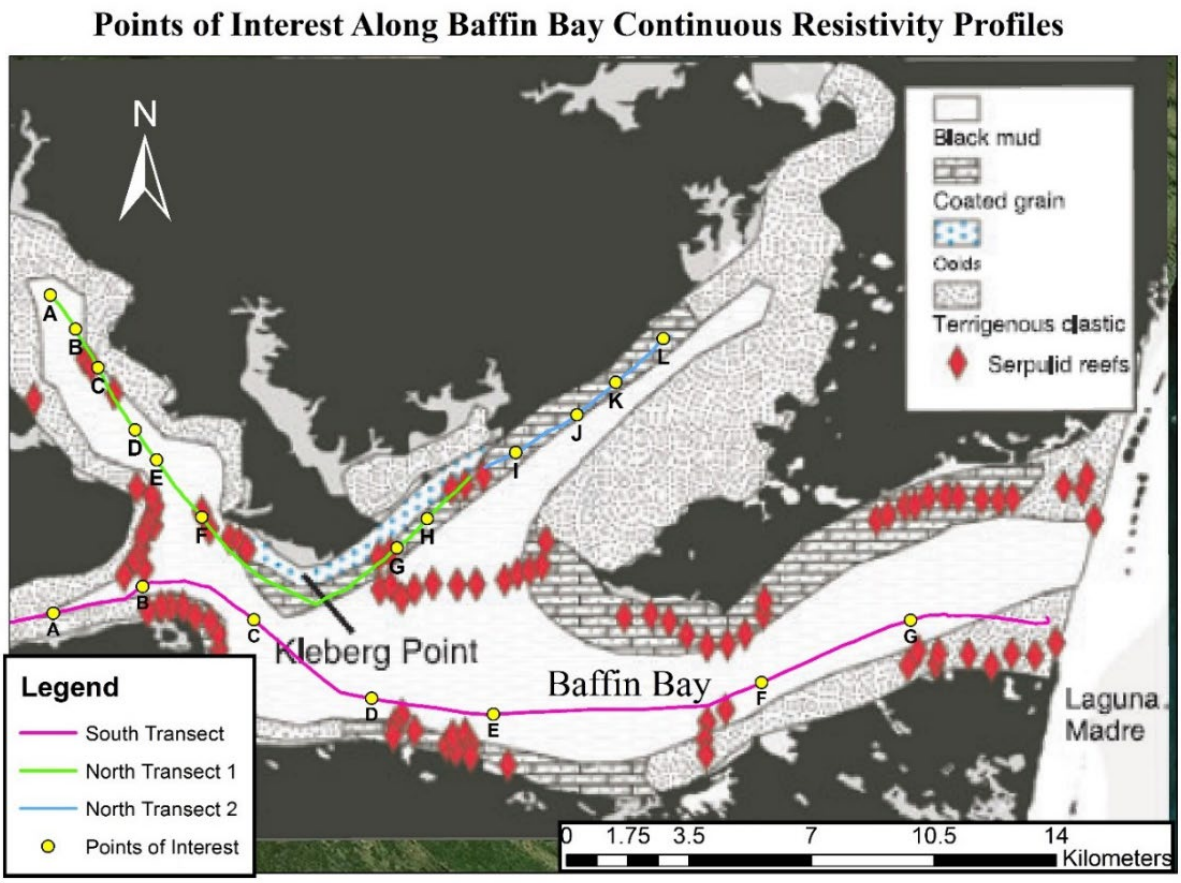

Figure 4: Map of Continuous Resistivity Surveys in Baffin Bay. Areas of interest are marked with letters A-L on the northern shore and A-G on the southern shore.

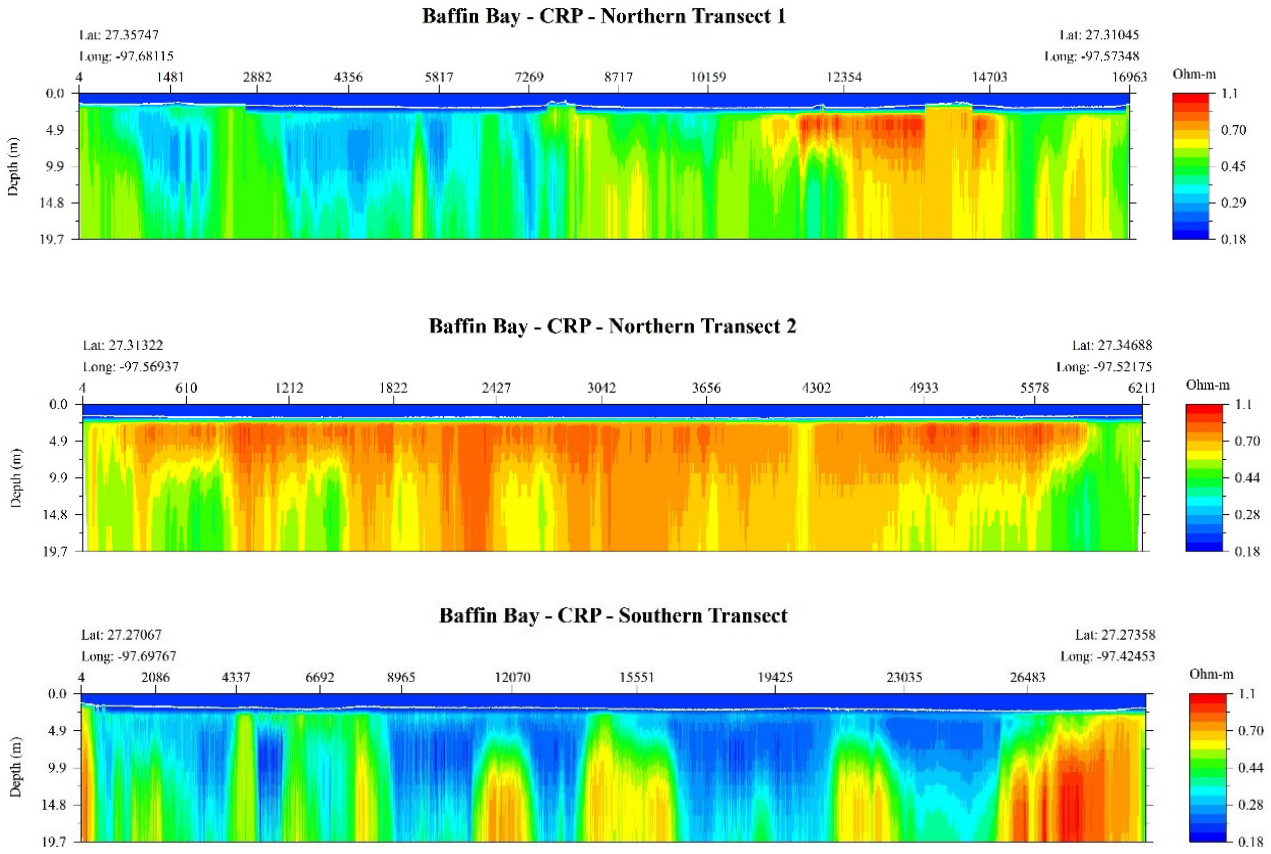

Figure 5: CRP profile images from the northern and southern transects. Images show resistivity in Ohm-m ranging from 0.18 to 1.1. Refer to **Figure 4** for the location of transects.

Spatial and Temporal Data Assessment

Radium

Radium measurements were conducted during all three sampling events, as well as during the July and November time-series events. Activities of ^{226}Ra for each spatial sampling event are included in **Figure 6**. The highest average surface water activity was measured in July (min: 10.6 $Bq \cdot m^{-3}$, max: 22.4 $Bq \cdot m^{-3}$, $\bar{x}$: 18.4 $Bq \cdot m^{-3}$ (n=8)), while the lowest occurred in January (min: 11.9 $Bq \cdot m^{-3}$, max: 15.4 $Bq \cdot m^{-3}$, $\bar{x}$: 14.0 $Bq \cdot m^{-3}$ (n=8)) followed by November (min: 11.1 $Bq \cdot m^{-3}$, max: 18.4 $Bq \cdot m^{-3}$, $\bar{x}$: 15.7 $Bq \cdot m^{-3}$ (n=10)). Average ^{226}Ra activities for each event during the spatial sampling is shown in **Table 1.** The highest activities of all three events were found at station 3, near the mouth of Cayo del Grullo. Three of the highest ^{226}Ra activities for all events

were measured near the heads of Alazan Bay (station 5, 20.6 $Bq \cdot m^{-3}$), Cayo del Grullo (station 4, 20.1 $Bq \cdot m^{-3}$) and Laguna Salada (station 1, 20.6 $Bq \cdot m^{-3}$). The lowest activities were consistently measured in the middle of Baffin Bay (station 7, 11.9-14.9 $Bq \cdot m^{-3}$), and at the mouth of Baffin Bay near Laguna Madre (station 8, 10.5-12.1 $Bq \cdot m^{-3}$) (**Figure 2**). Activities of ^{226}Ra at stations 1 through 6 were greatest in July followed by November and January. Stations 7 and 8 (closest to Laguna Madre) do not follow this pattern (**Figure 6**), likely the result of mixing with Laguna Madre waters. These larger July surface water activities correspond to greater porewater activities (**Figure 7**), which may indicate contribution from SGD (see section **^{222}Rn-derived SGD Estimates**). In addition, salinity levels cannot explain larger activities in July (average salinity of 37.0) because the bay was more saline in the following November event (average salinity of 49.4).

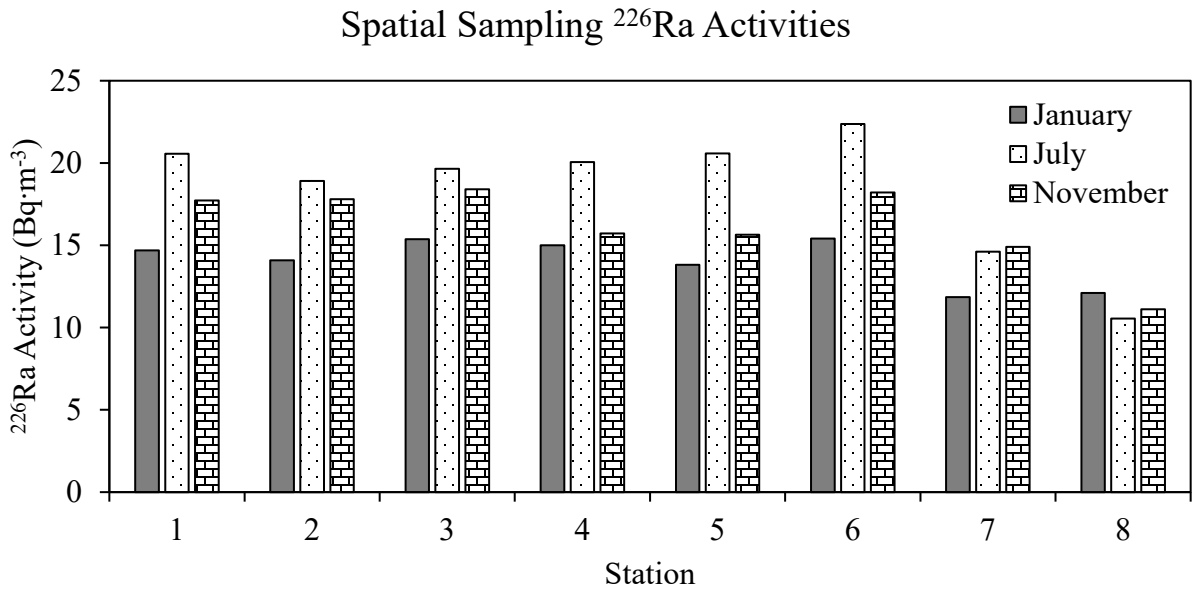

Figure 6: ^{226}Ra activities in $Bq \cdot m^{-3}$ for all seasons of Spatial Sampling. July had the highest concentrations and November the lowest overall.

^{226}Ra by station	1	2	3	4	5	6	7	8
All events max. ^{226}Ra	20.6	18.9	19.6	20.1	20.6	22.4	14.9	12.1
All events average ^{226}Ra	17.7	16.9	17.8	16.9	16.7	18.7	13.8	11.3
All events min. ^{226}Ra	14.7	14.1	15.4	15.0	13.8	15.4	11.9	10.5

Table 1. Mean ^{226}Ra activities (Bq·m^{-3}) for each station over all spatial sampling events. The highest ^{226}Ra activities are found in the westernmost stations, stations 1-4, the lowest activities were found in the easternmost stations, stations 7 and 8.

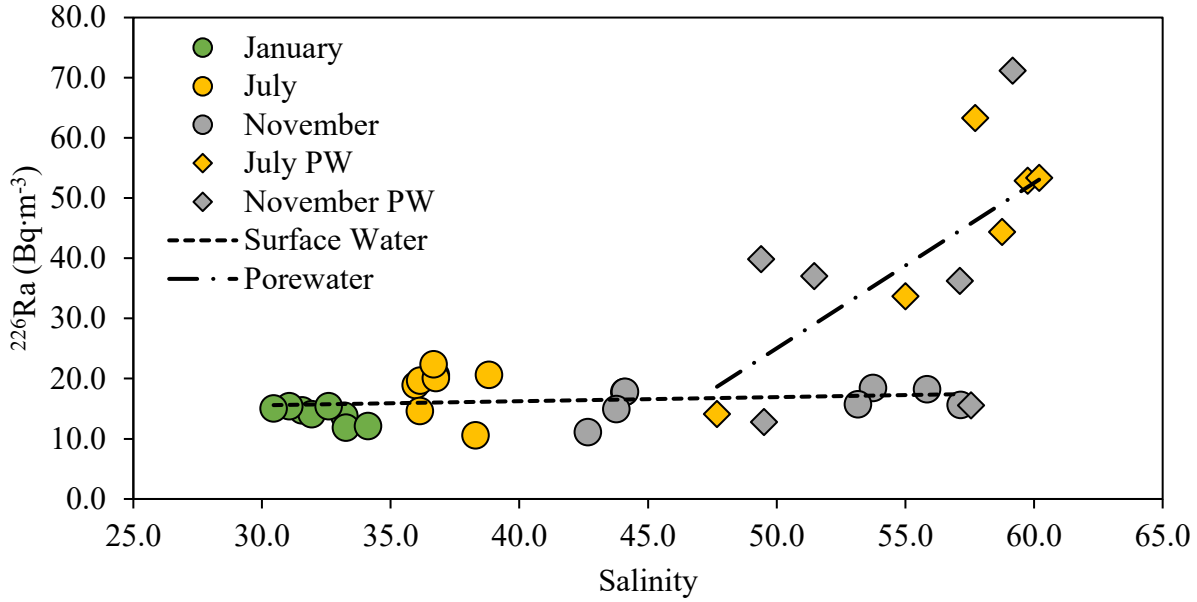

Figure 7: Graph of ^{226}Ra activity (Bq·m^{-3}) for surface and porewater against salinity for all events. No ^{226}Ra measurements were taken in January. There is no clear relationship between salinity and surface water ^{226}Ra (R^2 = 0.02972, p-value =0.4205), though porewater ^{226}Ra and salinity have a positive correlation (R^2 = 0.4328, p-value = 0.02004).

The ^{224}Ra activity exhibited an overall average of 14.9 Bq·m^{-3} (n=23) across all events. The highest mean activity for all events was 21.7 Bq·m^{-3} at station 1 while the lowest of 11.5 Bq·m^{-3} was measured at station 3. Table 2 shows the mean ^{224}Ra activities for each event across all stations. Similar to ^{226}Ra, the event with the highest overall ^{224}Ra activity (Table 3) was July (15.9 - 39.0 Bq·m^{-3}), followed by January (8.7 - 13.5 Bq·m^{-3}) and November (4.5-13.1 Bq·m^{-3}), with some July ^{224}Ra activities more than double the January and November activities (**Figure 8**). This large increase in the shorter-lived ^{224}Ra activities is possibly due to larger SGD inputs in

July (Kelly and Moran, 2002), particularly at stations 1 (Bq·m^{-3} in January and Bq·m^{-3} in July) and 5 (Bq·m^{-3} in January and Bq·m^{-3} in July) (**Figure 8**).

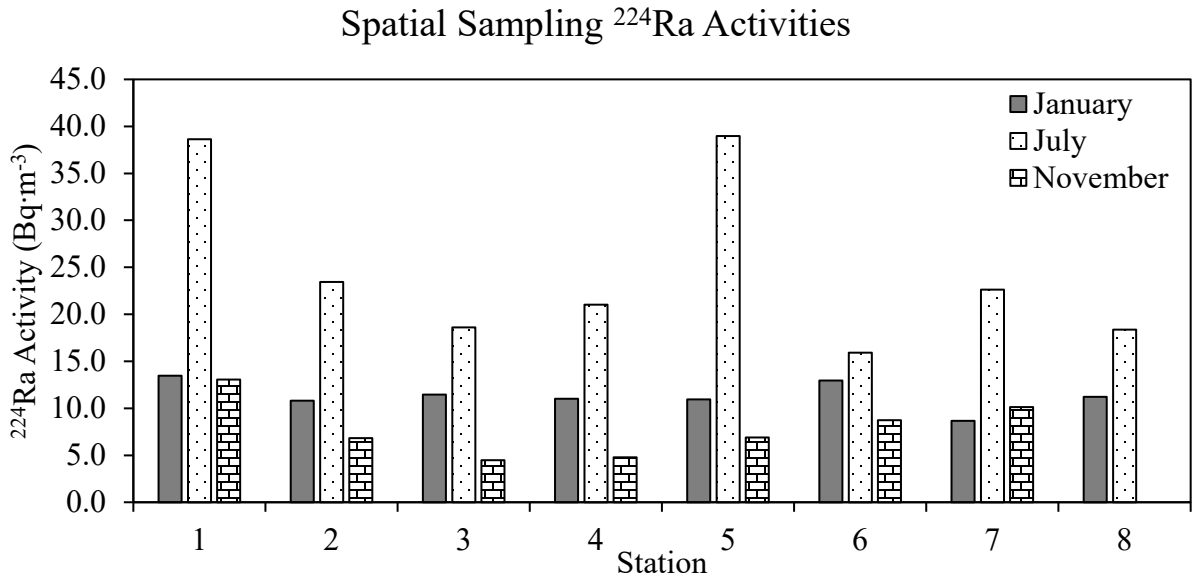

Figure 8: Graph of ^{224}Ra activities in Bq·m^{-3} for each station across all sampling seasons in the Spatial Sampling. Summer has the overall higher activity followed by spring and winter. The numerical values can be found in **Table 2**.

^{224}Ra by station	1	2	3	4	5	6	7	8
All events max. ^{224}Ra activity	38.6	23.4	18.6	21.0	39.0	15.9	22.6	18.4
All events avg. ^{224}Ra activity	21.7	13.7	11.5	12.3	18.9	12.5	13.8	14.8
All events min. ^{224}Ra activity	13.1	6.8	4.5	4.8	6.9	8.7	8.7	11.2

Table 2. Mean ^{224}Ra activities (Bq·m^{-3}) for each station over all events in Spatial Sampling. The highest ^{224}Ra activities can be found at station 1, the lowest at station 3. Station 8 did not have a value for the November event.

Event	January	July	November
All stations ^{224}Ra average activity	11.3, n=8	24.7, n=8	7.8, n=7

Table 3. Mean ^{224}Ra activities (Bq·m^{-3}) for each event using all stations in the surface water Spatial Sampling dataset. July had the highest overall activity and November the lowest with January in between.

Groundwater ^{224}Ra values ranged from 3.5-269.7 Bq·m^{-3} with an average of 50.0 Bq·m^{-3} (**Table 4**). Groundwater ^{226}Ra activities ranged from 1.2-244.7 Bq·m^{-3} with an average of 46.5 Bq·m^{-3} (**Table 4**). Porewater ^{224}Ra activities ranged from 2.0-167.2 Bq·m^{-3} in July with an average of 72.3 Bq·m^{-3} and 5.3-54.5 Bq·m^{-3} in November with an average of 18.8 Bq·m^{-3} (**Table**

5). Porewater ^{226}Ra activities ranged from 14.1-63.3 Bq·m^{-3} in July with an average of 43.6 Bq·m^{-3}, and from 12.8-71.2 Bq·m^{-3} in November with an average of 35.4 Bq·m^{-3} (**Table 6**).

Well ID	8326201	8327501	8329201	8329401	8342508	8334403	Average
^{224}Ra	8.4	3.5	4.3	4.8	9.3	269.7	50.0
^{226}Ra	3.2	4.8	1.2	17.7	7.5	244.7	46.5

Table 4. Groundwater Well Ra activities (Bq·m^{-3}).

PW ^{224}Ra by Station	1	2	3	4	5	6	7	8
July	2.0	30.5	164.4	167.2	--	61.0	--	8.7
November	12.2	--	54.5	9.6	5.3	--	--	12.6
Average	7.1	30.5	109.5	88.4	5.3	61.0	--	10.7

Table 5. Porewater (PW) ^{224}Ra activities (Bq·m^{-3}) for July and November.

PW ^{226}Ra	1	2	3	4	5	6	7	8	average
Jul.	52.9	33.7	63.3	53.4	--	44.4	--	14.1	43.6
Nov.	15.5	37.0	39.9	36.3	71.2	--	--	12.8	35.4

Table 6. Porewater ^{226}Ra (Bq·m^{-3}) for July and November, including average of all stations for each month.

Activity ratios (AR) of $^{224}Ra/^{226}Ra$ measured from local groundwater wells and from station porewater samples were compared to ARs of surface water from the spatial surveys to determine water ages, the time it has been since a particle of water was separated from the radionuclide source (Knee et al., 2011a). With the local groundwater identified as the activity ratio of the advecting fluid, the estimated ages ranged from 5.2 to 7.9 days in January ($\bar{x}$=6.8 days, n=8), 0.7 to 5.6 days in July ($\bar{x}$=3.8 days, n=7), and 12.8 to 40.6 days in November ($\bar{x}$=29.1 days, n=8). A negative age was calculated for station 8 in July, indicating that local groundwater is likely not an appropriate end-member at this location. The negative age is excluded from the July average. In comparison, identifying the porewater activity ratio as the advecting fluid endmember for the calculations provides a new set of ages. In July the porewater based ages range from 1.4 to 2.0 days ($\bar{x}$=1.7 days, n=4), excluding stations 1, 5, 7, and 8, which resulted in

negative ages. The negative ages combined with the lower estimated average ages are two lines of evidence indicating that porewater was not the dominant end-member for the sites (1-8) in July, groundwater is a more plausible source. In November the ages ranged 1.4 to 11.6 days ($\overline{x}$=7.3 days, n=8) indicating that porewater was a plausible important end-member at the time. The lower age range than the groundwater ($\overline{x}$=7.7 for porewater based compared to $\overline{x}$=29.1 for groundwater based) does not rule porewater out as a possible source for ^{224}Ra and ^{226}Ra. For both porewater AR based and groundwater AR based station 8 is always the youngest or negative, it may be closest to a groundwater source or the influence of Laguna Madre Ra is very strong. For Ra based SGD calculations porewater ^{226}Ra will be used with the assumption that its proximity to the bay (shallow depth and locations in the bay) make it more representative of possible SGD.

Major Ions

As another method to constrain SGD estimates, surface and porewater samples were analyzed for major ions such as chloride (Cl^-), bromide (Br^-), sulfate (SO_4^{2-}), sodium (Na^+), potassium (K^+), magnesium (Mg^{2+}), calcium (Ca^{2+}), total iron (Fe), and total manganese (Kahn and Kumar, 2012). A majority of these ions are conservative and the minerals in which these elements commonly occur are highly soluble in seawater (i.e. NaCl, KCl, $MgSO_4$, and $CaSO_4$). Thus, the ratio of each of these elements to chlorinity (Cl^{-1}) should remain constant and similar to that of seawater if only conservative processes are involved. For instance, SO_4^{-2} which is conservative in oxygenated waters, but non-conservative in anoxic conditions may be converted to HS^- or H_2S by sulfur reducing bacteria like *Desulfovibrio vulgaris* in anoxic environments (Heidelberg et al., 2004). Thus, a SO_4^{-2}/Cl^{-1} below that of seawater (0.14) would be indicative of SO_4^{-2} reduction while production would be associated with an increase in the ratio above that of

seawater. The more conservative elements, like Na^{+} and Cl^{-}, have long residence times and they are found to be well mixed in the ocean, very soluble, and in the same ratio to one another throughout the ocean with no correlation to salinity (Millero et al., 2008). Elements, such as Fe, that are relatively reactive or insoluble in seawater (i.e. pH dependent) are easily removed and unevenly distributed throughout the ocean, and therefore have short residence times compared to the more conservative elements (Millero et al., 2008).

The ratios of major elements to chlorinity can be used to analyze sources of water to estuaries. The SO_4^{-2}/Cl^{-1} varied from event to event with the highest ratios in July (min: 0.148; max: 0.154; $\bar{x}$: 0.149 (n=16)). The lowest ratios were measured in January (min: 0.145; max: 0.148; $\bar{x}$: 0.147 (n=16)). In November, ratios were lower than July but greater than January (min: 0.146; max: 0.152; $\bar{x}$: 0.148 (n=16)) (**Figure 9**). In July, when the highest SO_4^{-2}/Cl^{-1} ratios were measured, runoff from the watershed feeding into Baffin Bay was the greatest (TWDB, 2016). Across all events, the SO_4^{2-}/Cl^{-} ratios are lowest at the mouth of Baffin Bay and highest in one of the bay members: the head of Cayo del Grullo in January, the head of Laguna Salada in July, and the head of Cayo del Grullo again in the November. Sulfate concentrations are decreasing seaward, from the head of the bay members to the mouth of Baffin Bay, which could be indicative of dilution due to mixing with Laguna Madre waters. There is a very weak correlation with surface water salinity and surface water SO_4^{2-}/Cl^{-} (R^2: 0.05612, p-value: 0.105), except in January when a strong negative linear correlation is observed (R^2: 0.6959, p-value: 5.881×10^{-5}) (**Figure 10**).

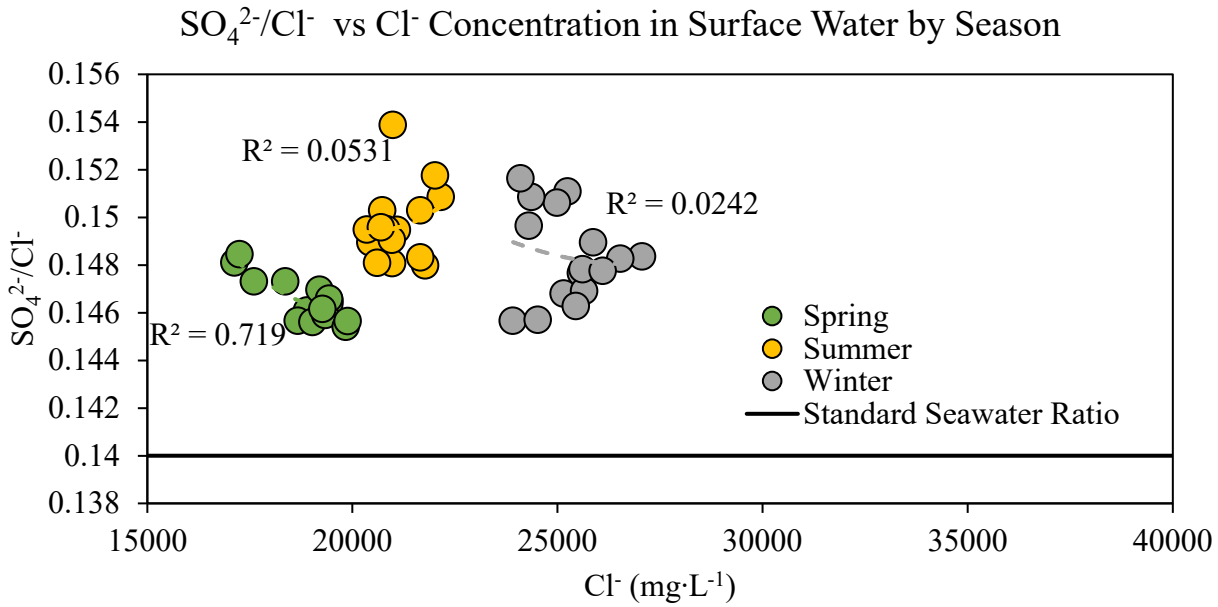

Figure 9: SO_4^{2-}/Cl^- ratios against Cl^- concentration, no clear relationship is evident. All samples had ratios above the standard seawater ratio of 0.14 (Millero et al., 2008).

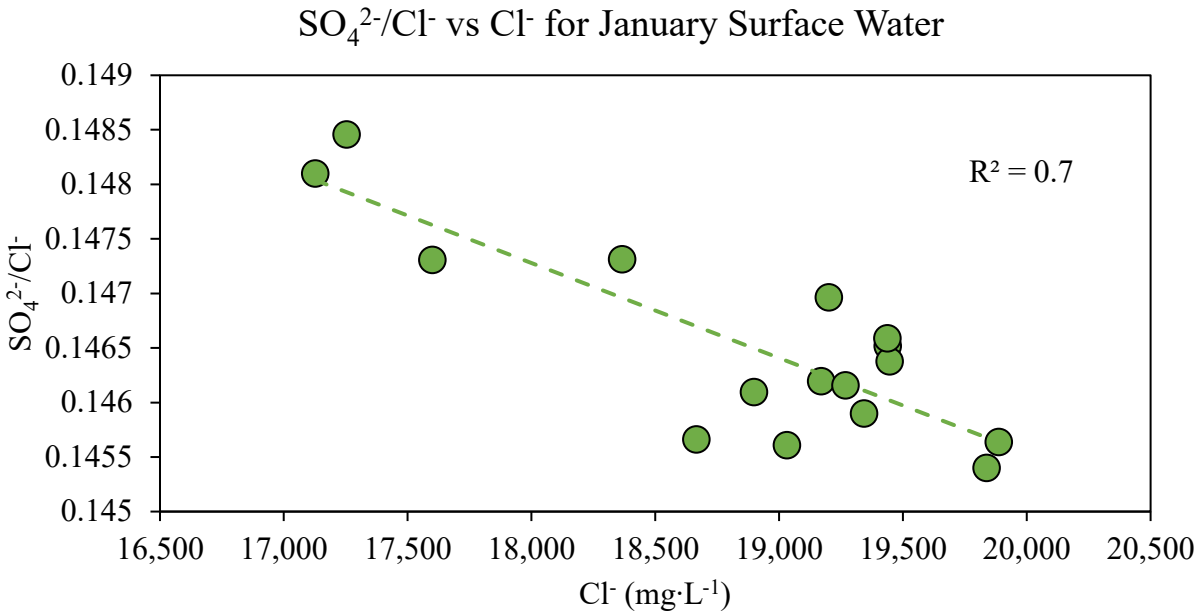

Figure 10: January SO_4^{2-}/Cl^- vs Cl^- with an observable negative relationship (R^2: 0.6959, p-value: 5.881×10^{-5}).

Studies have shown that riverine inputs can increase SO_4^{2-}/Cl^- ratios (Matson and Brinson, 1985). All surface water samples had SO_4^{2-}/Cl^- ratios greater than that of average seawater (Millero et al., 2008). On the other hand, all porewater ratios were lower than seawater,

likely an indication of SO_4^{2-} reduction within the sediment. The linear regression performed failed to reject the null (p-value: 0.68) at the 95% confidence interval, and it indicates that no significant linear correlation exists between Cl^- and SO_4^{2-}/Cl^- ratios. The lack of a linear trend indicates that SO_4^{2-} is affected by non-conservative processes, such as SO_4^{2-} reduction, rather than conservative mixing.

Similar to the SO_4^{2-}/Cl^-, there was no relationship between the surface water Br^-/Cl^- ratio and Cl^- concentration (R^2: 0.0018, p-value:0.8, **Figure 11**). The average Br^-/Cl^- ratio was found to be 0.03435 (min: 0.00311; max: 0.003957; n=48), the Br^-/Cl^- ratio of standard seawater is 0.003473 (Millero et al., 2008). The Br^-/Cl^- ratios are very similar, but again, a linear relationship between Br/Cl^- and Cl^- does not exist. As the concentration of Cl^- increases in surface water, the range of possible Br^-/Cl^- ratios increases as well. The average porewater Br^-/Cl^- ratio is 0.003087 (min: 0.002713; max: 0.003624; n=16), lower than the standard seawater ratio (0.003473). The Br^-/Cl^- and Na^+/Br^- ratios are offering information related to geochemical processes that may be affecting the water chemistry of the bay. For instance, halite precipitation and dissolution could lead to a non-conservative behavior of Na^+ and Cl^-. Halite precipitation can also cause the Br^-/Cl^- ratio to remain above the average seawater ratio (Murgulet et al., 2016). The strong linear relationship between the Na^+/Br^- and Na^+ (R^2: 0.96, p-value: $<2.2x10^{-16}$, **Figure 12**), indicates that Na^+ and Br^- are originating from similar sources and/or affected by similar processes. Therefore, since during the halite precipitation process, very small amounts of Br^- are incorporated in the mineral structure, conditions may be favorable to dissolution, or concentrations are only affected by mixing processes.

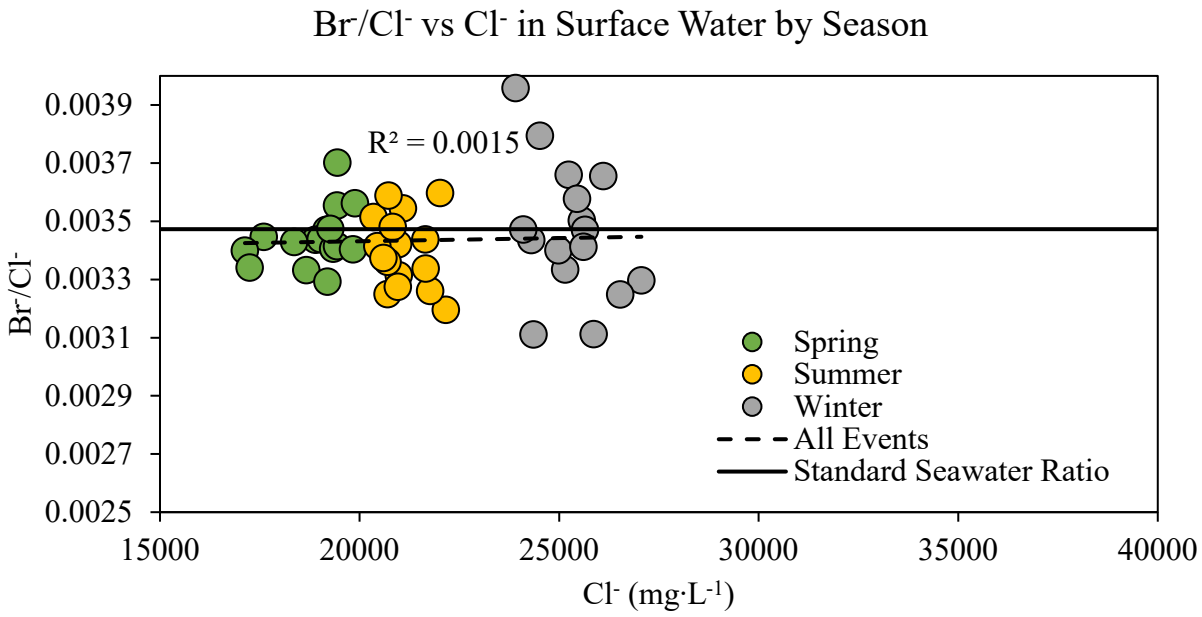

Figure 11: Graph of the Br^-/Cl^- ratio of surface water against the Cl^- concentration of that surface water. There was no relationship between the Br^-/Cl^- ratio and Cl^- (R^2: 0.0018, p-value: 0.8).

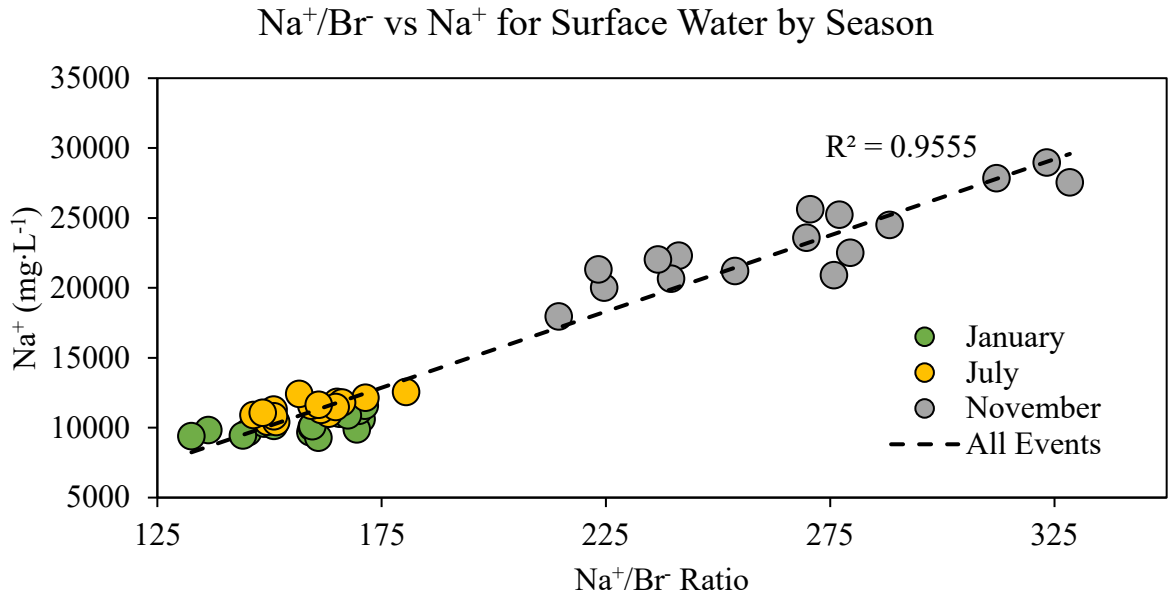

Figure 12: Graph of the relationship between Na^+ and the Na^+/Br^- ratio for surface water showing a significant linear relationship between the two (R^2: 0.9555, p-value: $<2.2x10^{-16}$).

Ratios of Mg^{2+}/Cl^-, Ca^{2+}/Cl^-, and K^+/Cl^- also show no significant evidence of linear relationship (p-values: 0.73, 0.07, 0.26, respectively). The average ratio of surface water

Mg^{2+}/Cl^-, 0.0815 (min: 0.0140; max: 0.1491; n=48) was greater than that of standard seawater (0.0663) showing that the water in Baffin Bay is being altered, more than likely by precipitation of Cl^- due to the hypersalinity of the bay (**Figure 13**). The same is true for K^+, with an average ratio of 0.0212 (min: 0.0062; max: 0.0376; n=40) compared to the standard ratio of seawater (0.0206) is greater as well. Ca^{2+} has an average ratio of 0.0194 (min: 0.0049; max: 0.0305; n=48), which when compared to the average seawater ratio (0.0213) is lower.

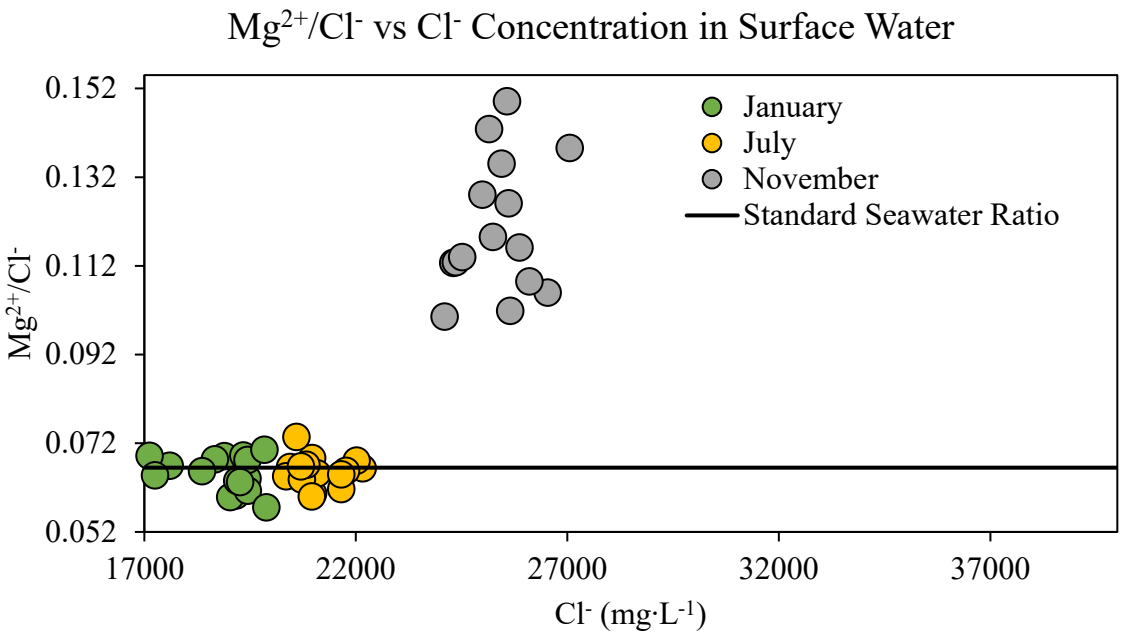

Figure 13: Graph of Cl^- concentration against the ratio of Mg^{2+}/Cl^- for January, July and November. Standard Seawater Ratio for Mg^{2+}/Cl^- is 0.066491 (Millero et al., 2008).

In general, the cation to chlorine ratios are near seawater averages, indicating the limited freshwater input and the large influence from Laguna Madre. The observed variations in the ratios from standard seawater averages are more than likely to be caused by dilution when freshwater inflow occurs, mineralization by flora and fauna, or sediment adsorption (Mitsch and Gosselink, 2015).

An important nutrient for phytoplankton is iron (Fe), iron concentrations can hinder or increase primary production and influence the higher trophic levels. Low iron concentrations can limit biomass even in the presence of high non-iron nutrient concentrations (de Baar et al., 1999). Likely sources of iron for Baffin Bay include aeolian input, surface water inflows, and groundwater input. Iron can also enter into the water column if it is reduced in anoxic sediments and then is released into the overlying water. In the three spatial sampling events, surface- and bottom- water and porewater iron is found to follow a similar pattern. In November, total Fe concentrations were approximately 1 to 2 orders of magnitude greater than concentrations in January and July. The resultant Fe/Cl^- ratios are an average of $1.6x10^{-5}$ (min: $1.9x10^{-6}$; max: $3.4x10^{-5}$; n=14) for January, $9.7x10^{-6}$ (min: $2.0x10^{-6}$; max: $2.0x10^{-5}$; n=16) for July, and 0.00016 (min: 0.00013; max: 0.00035; n=16) for November. The average Fe/Cl^- mass ratio of the porewater samples also indicates that Fe is in larger excess to Cl^- in November (average mass ratio:$1.62x10^{-4}$) when compared to July ($3.03x10^{-6}$) and January ($4.18x10^{-5}$) averages. Accumulation of Fe in the water column in November could be result of limited bioproduction and/or increased SGD rates. Iron concentrations in seawater are on average in the magnitude of 10^{-8} $mg{\cdot}L^{-1}$ (Martin et al., 1994). Iron concentrations in Baffin Bay are therefore much more enriched compared to average seawater.

Stable Isotopes of Oxygen and Hydrogen

The stable isotopes of oxygen ($\delta^{18}O$) and hydrogen (δD) in water are important tracers of the local, regional, and global hydrologic cycle. The importance of these isotopes as tracers is well known by the International Atomic Energy Agency (IAEA) which maintains a Global Network of Isotopes in Precipitation (GNIP) to provide the isotopic signatures of precipitation worldwide since 1961. In Baffin Bay surface water, the $\delta^{18}O$ abundances ranged from 0.3‰ to

4.3‰ ($\bar{x}$: 2.14‰ ± 0.1‰, n=62) and the δD ratio ranged from 4.2‰ to 22.8‰ ($\bar{x}$: 13.3‰ ± 1‰, n=62). In porewater, the $\delta^{18}O$ abundances ranged from 0.3‰ to 2.7‰ ($\bar{x}$: 1.60‰ ± 1‰, n=17) and the δD ratio ranged from 4.21‰ to 14.06‰ ($\bar{x}$: 10.08‰ ± 1‰, n=17). All surface- and bottom- water signatures fall below the global meteoric water line (GMWL) and the Waco meteoric water line (WMWL), but are above the line formed by measurements of local groundwater (**Figure 14**). The $\delta^{18}O$ and δD enrichment, observed mainly in July $\delta^{18}O$ δD (min: 2.2‰, max: 4.3‰, $\bar{x}$: 3.0‰ ± 1‰, n=16, and min: 13.6‰, max: 21.0‰, $\bar{x}$: 17.2‰ ± 1‰, n=16) and November (min: 2.4‰, max: 4.1‰, $\bar{x}$: 3.0‰ ± 1‰, n=16, and min: 15.6‰, max: 22.7‰, $\bar{x}$: 18.3‰ ± 1‰, n=16), is suggestive of evaporation effects caused by persistent winds and warm temperatures (Katz et al., 1997). The most depleted $\delta^{18}O$/δD ratios of all surface water samples were measured in January (min: 0.6‰, max: 1.3‰, $\bar{x}$: 0.8‰ ± 1‰, and min: 6.0‰, max: 8.4‰, $\bar{x}$: 7.2‰ ± 1‰, n=14), when temperatures are much lower. When compared to other bays in south Texas the $\delta^{18}O$ (min: -1.79‰, max: 1.91‰ for $\delta^{18}O$ in Aransas Bay, and min: -2.5‰, max: 2.1‰ for $\delta^{18}O$ in Nueces Bay) and δD (min: -7.22‰, max: 12.9‰ for δD in Aransas Bay, and min: -12.9‰, max: 13.9‰ for δD in Nueces Bay) are more enriched, especially for the July and November months (Murgulet et al., 2018; Murgulet et al., 2015). This could be the result of higher evaporation rates as well as the limited freshwater input from runoff.

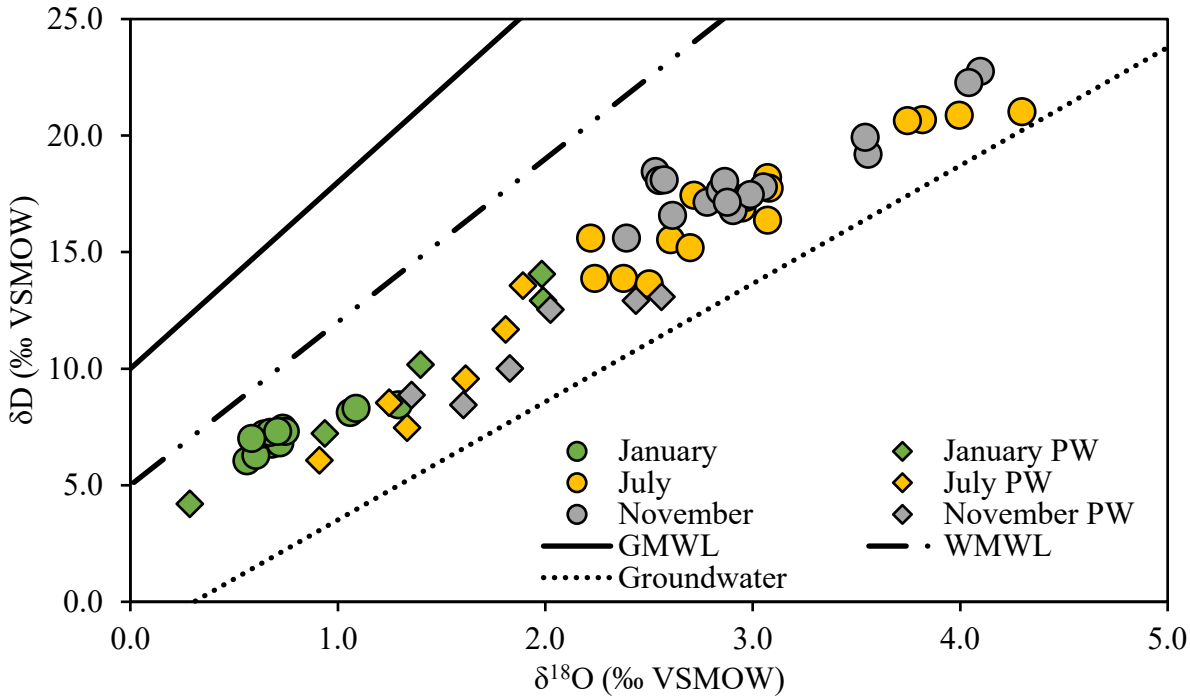

Figure 14: All surface water and porewater $\delta^{18}O$ and δD ratios were found to be greater than those of the local groundwater line, but less than that of the Waco meteoric water line (WMWL).

All porewater samples (min: 0.29‰, max: 2.56‰, $\bar{x}$: 1.60‰ ± 1‰, n=17 for $\delta^{18}O$, and min: 4.21‰, max: 14.26‰, $\bar{x}$: 10.08‰ ± 1‰, n=17 for δD) were more depleted when compared to July and November. The lowest abundance in porewater of both $\delta^{18}O$ and δD (min: 0.29‰, max: 1.99‰, $\bar{x}$: 1.32‰ ± 1‰, n=5) was measured in January. Since porewater was extracted at depths ranging from 1 m to 1.5 m below the sediment-water interface, the more depleted signatures indicate that recirculation is likely not to extending below 1m below the sediment water interface. Nevertheless, porewater and surface water samples fall along a mixing line, indicating that SGD may be occurring. The signature of porewater, as also indicated by elevated salinities (in most instances exceeding seawater, cannot be associated with a freshwater source. Freshwater aquifers in south Texas exhibit negative signatures in relation to VSMOW ($\delta^{18}O$ -4.21‰, δD -22.90 ‰), when compared to the positive ones in Baffin Bay porewaters.

Total Alkalinity and DIC

The average total alkalinity (TA) of Baffin Bay across all events was 6,288.98 $\mu mol \cdot L^{-1}$ (n=48) in the surface water and 6,004.1 $\mu mol \cdot L^{-1}$ in porewater (n=18). The highest surface water TA (33,645.8 $\mu mol \cdot L^{-1}$) was measured at station 3, near the mouth of Cayo del Grullo in November while the lowest (2,201.4 $\mu mol \cdot L^{-1}$) was observed at the mouth of Baffin Bay in July. The highest porewater TA (15,714.6 $\mu mol \cdot L^{-1}$) was measured at station 1, in Laguna Salada, in November while the lowest (2,788.8 $\mu mol \cdot L^{-1}$) was observed at station 3 in July, at the mouth of Cayo del Grullo. The highest alkalinities measured each event occurred in surface water at the mouth of Cayo del Grullo (station 3), with each concentration being more than 2 standard deviations greater than the mean of all the surface water alkalinity samples.

DIC follows a similar trend with TA with the exception for one surface water sample that had much lower TA than DIC (**Figure 15**). The high positive relationship between DIC and TA are an indication of a similar source of carbonate and the potential of limited TA consumption. The average DIC of Baffin Bay across all events was 5,450.4 $\mu mol \cdot L^{-1}$ (n=44) in the surface water and 5,507.6 $\mu mol \cdot L^{-1}$ in porewater (n=18). The highest surface water DIC (30,005.6 $\mu mol \cdot L^{-1}$) was measured at station 3, near the mouth of Cayo del Grullo in July and the lowest (2,092.1 $\mu mol \cdot L^{-1}$) was measured at station 7 in the middle of Baffin Bay in the July. The highest porewater DIC (14,714.9 $\mu mol \cdot L^{-1}$) was measured in Laguna Salada at station 1 in July, while the lowest (2,312.2 $\mu mol \cdot L^{-1}$) was observed at station 2 where Laguna Salada and Cayo del Grullo meet. The highest DIC's measured each event occurred in surface water at the mouth of Cayo del Grullo (station 3), and are more than 2 standard deviations greater than the mean of all the surface water DIC samples.

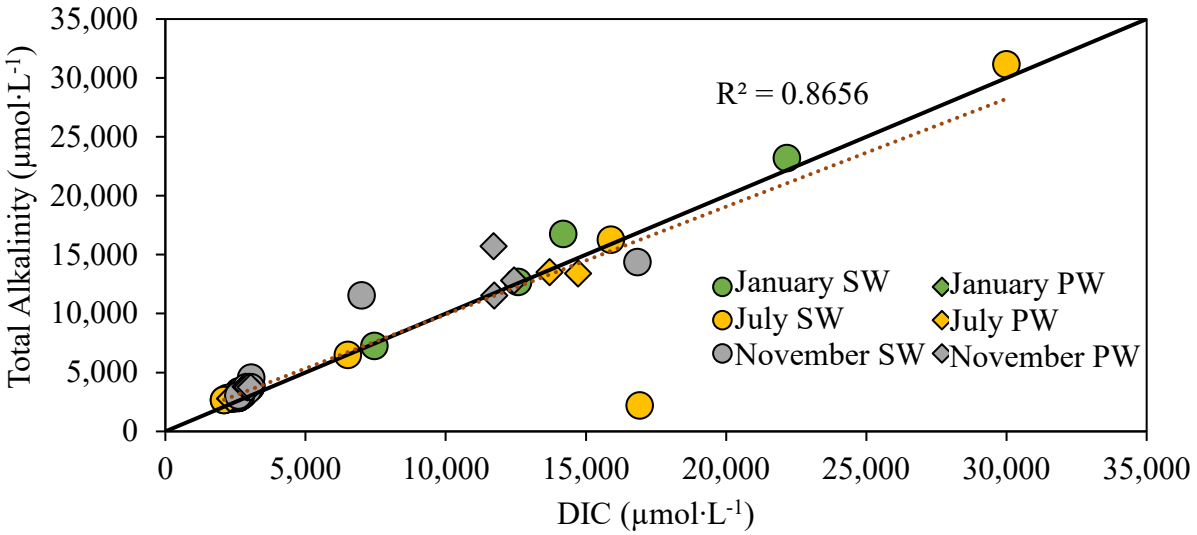

Figure 15: Graph of DIC versus total alkalinity, the relationship between total alkalinity and DIC indicated by the dashed line (R^2 of 0.8656, p-value of $<2.2x10^{-16}$) is nearly 1:1 (indicated by the solid black line), the average DIC:TA ratio for surface water and porewater is 1.02. Only one sample deviates from this relationship (more than 2σ from the mean DIC:TA), station 8, at the mouth of Baffin Bay in July.

Total alkalinity exceeds DIC for 88.7% of the samples, both surface and porewater. DIC only exceeds TA at stations 3 and 8 in the surface water in January, July, and November, and in the porewater at stations 1, 3, and 8 in July and November. Nevertheless, TA and DIC levels in surface water are in general much larger than those of seawater (2322 µmol·L^{-1} for alkalinity (Takahashi et al., 1981) and approximately 2000 µmol·L^{-1} DIC (Winn et al., 1998)), indicative of in-situ production or groundwater input.

Carbon-13

The average $\delta^{13}C$ abundance across all events was -4.40 ‰ (n=34) in the surface water and -5.03 ‰ in the porewater (n=15). The most enriched surface water $\delta^{13}C$ ratio (-0.72 ‰) was measured at station 1 in Laguna Salada in January while the most depleted (-15.37 ‰) was measured at station 8, the mouth of Baffin Bay, in July. The most enriched $\delta^{13}C$ signature in porewater (-1.58 ‰) was measured at station 2, where Laguna Salada and Cayo del Grullo meet, in July, while the most depleted (-12.62 ‰) at station 1 in Laguna Salada in November.

Regardless of the type of sample (i.e. pore- or surface-water), no relationship is observed between $\delta^{13}C$ and salinity, as seen in **Figure 16**, indicating that mixing is not the dominant process controlling the $\delta^{13}C$ signature (Murgulet et al., 2018). In addition, the most depleted surface water signatures were not measured in close proximity to the creek mouths that discharge into the bay. Thus, no significant influence associated with freshwater inflows from surface runoff could be implied due to the lack of mixing trends.

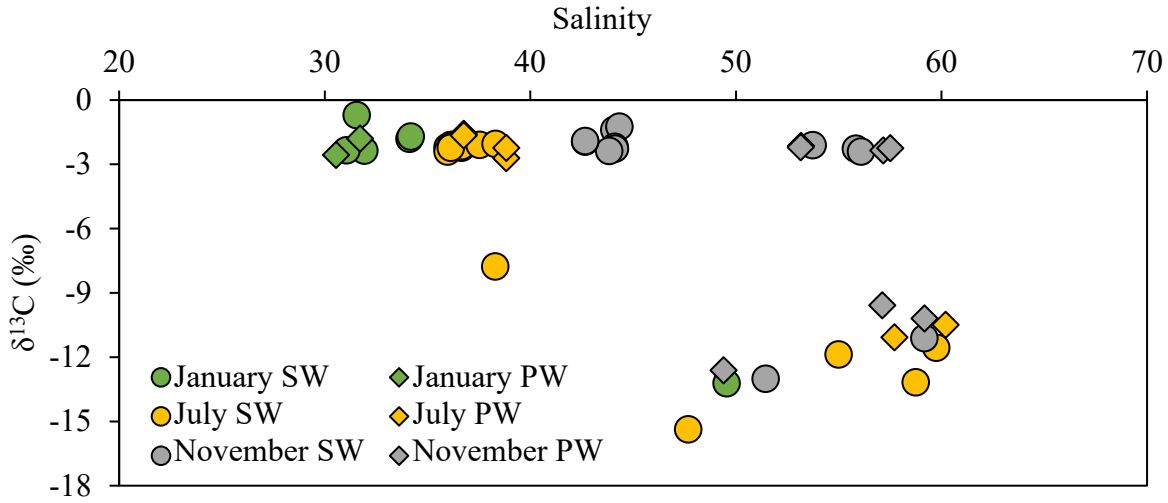

Figure 16: Change in $\delta^{13}C$ with salinity. There is no clear relationship between salinity and $\delta^{13}C$. The most depleted $\delta^{13}C$ samples were from stations 3, 6, and 8 in the surface water and stations 1 and 4 in the porewater.

Although, visually a linear correlation between DIC and $\delta^{13}C$ may be inferred from **Figure 17**, a statistically significant relationship was not found, because of the non-uniform distribution of data. For most samples, the largest DIC concentrations are associated with the most depleted $\delta^{13}C$. Unlike other studies conducted in the south Texas estuaries (Bighash and Murgulet, 2015; Douglas et al., 2017; Murgulet et al., 2015), the largest DIC (and TA) concentrations and most depleted $\delta^{13}C$ were not confined to only porewater. Rather, larger DIC (and TA) concentrations were measured in surface water, especially in July (4 samples). A few

occurrences of higher concentrations and more depleted $\delta^{13}C$ signatures were also observed in November (2 samples) and January (1 sample) (**Figure 17**).

It was suggested that denitrification produces DIC with a heavier isotopic signature (Smith et al., 1991). A two-fold increase in denitrification rates associated with higher DIC efflux was observed during July in other estuaries in Texas (Zimmerman and Benner, 1994) and in other areas, such as the Yangtze Estuary (Wang et al., 2007), among others. Alkalinity is also produced during denitrification processes; thus, in the absence of surface runoff that is expected to introduce higher alkalinity and more depleted $\delta^{13}C$ water, geo-microbiological processes are likely affecting the nitrogen fate and the carbonate chemistry of the bay (Murgulet et al., 2018).

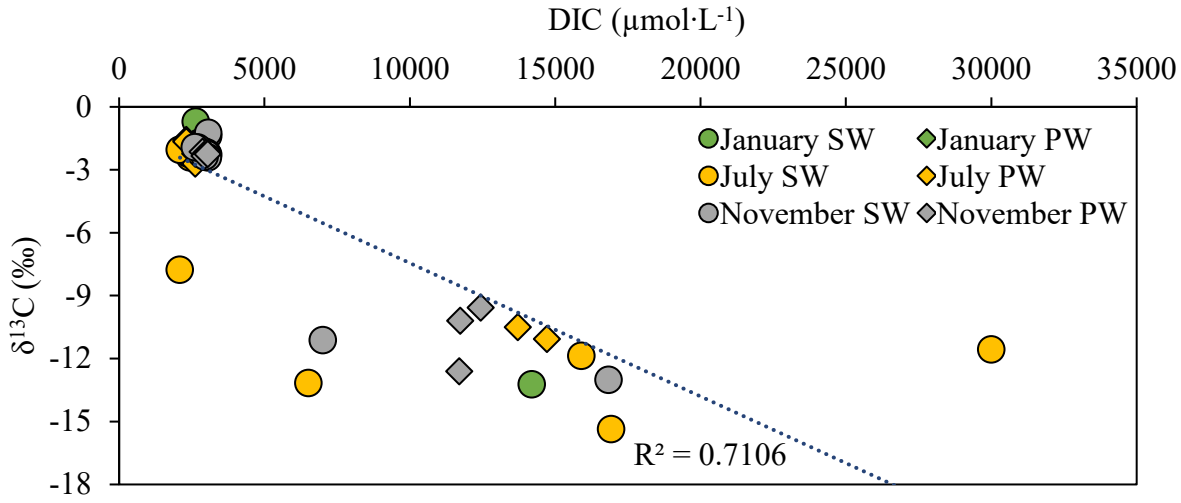

Figure 17: $\delta^{13}C$ signatures versus DIC for surface- and pore-water by event. In general, an inverse relationship between DIC and $\delta^{13}C$, though the correlation is not statistically significant, given the non-uniform distribution of the data.

Phytoplankton and Nutrients

Chlorophyll-a

In the surface of the water column, the highest chl-α concentration in January was measured at station 1 (25.1 µg·L^{-1}) and the lowest at station 5 (7.0 µg·L^{-1}) ($\bar{x}$: 13.0 µg·L^{-1};

standard deviation of 5.3). The highest chl-α measured in August was at station 1(26.0 $\mu g \cdot L^{-1}$) and the lowest was at station 4 (6.6 $\mu g \cdot L^{-1}$) ($\bar{x}$: 15.6 $\mu g \cdot L^{-1}$, standard deviation of 5.7). The highest concentration of chl-α in November was at station 1 (14.9 $\mu g \cdot L^{-1}$) and the lowest was at station 3(7.8 $\mu g \cdot L^{-1}$) ($\bar{x}$: 10.9 $\mu g \cdot L^{-1}$, standard deviation: 2.0). The average concentration of chl-α in the bottom of the water column, in January, was 14.4 $\mu g \cdot L^{-1}$ with a maximum and minimum concentration of 23.8 $\mu g \cdot L^{-1}$ and 6.7 $\mu g \cdot L^{-1}$ (standard deviation: 5.6) at stations 1 and 6, respectively. In July, the average bottom chl-α concentration was 14.4 $\mu g \cdot L^{-1}$ (standard deviation of 5.5), with a maximum and minimum of 28.4 $\mu g \cdot L^{-1}$ and 6.8 $\mu g \cdot L^{-1}$ at stations 1 and 4, respectively (**Figure 18**).

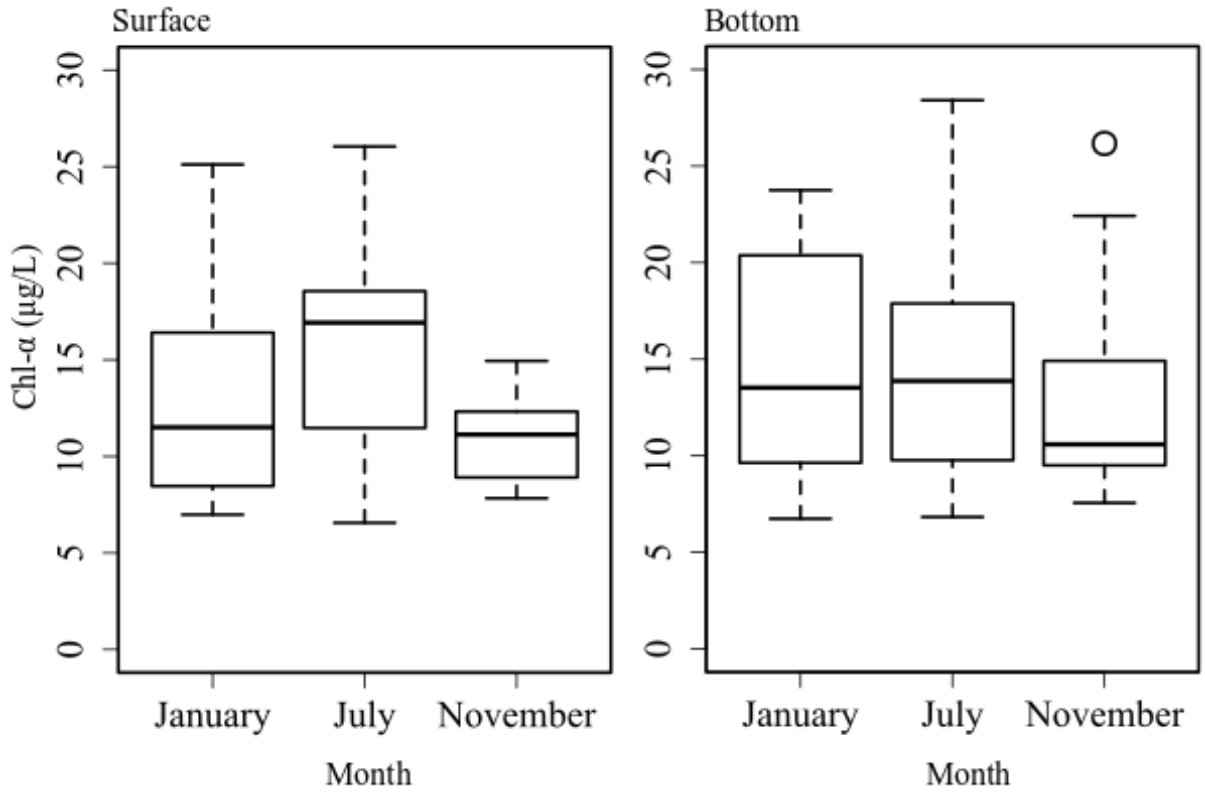

Figure 18: Chl-α concentrations for Surface and Bottom water displayed as boxplots. Chl-α concentrations did not vary much from season to season or between surface and bottom.

The average concentration of chl-α in November bottom waters was 13.1 $\mu g \cdot L^{-1}$ (standard deviation of 5.3), with a maximum and minimum of 26.2 $\mu g \cdot L^{-1}$ and 7.6 $\mu g \cdot L^{-1}$ at

stations 2 and 6, respectively. When compared to other estuaries in South Texas, primary productivity occurs in high levels year-round for the period of study. For instance, in Aransas Bay, chl-α levels are the highest in July and much lower in January and November (Douglas et al., 2017). For this study, maxima of chl-α in Baffin Bay exceed the July Aransas Bay in both, January and July, and closely match in November.

Station 1 had consistently the highest chl-α concentrations each event with the exception of November in bottom waters. Overall, the lowest concentrations were found at several locations throughout Cayo del Grullo and Alazan Bay, including stations 4, 6, 5, and 3, in order of increasing concentration. The consistently high chl-α at station 1, close to the head of the Laguna Salada, coincides with the highest TDN concentrations, consistently measured in porewater at this location: 31.0, 45.9, and 47.6 $mg \cdot L^{-1}$ ($\bar{x}$ for each event of 8.7, 18.0, and 15.1 $mg \cdot L^{-1}$) for January, July and November, respectively.

Nutrients

The average NO_3^- concentration across all events was 2.5 $\mu mol \cdot L^{-1}$ (n=48) in the surface water and 0.2 $\mu mol \cdot L^{-1}$ in porewater (n=18). The highest surface water NO_3^- concentration (14.1 $\mu mol \cdot L^{-1}$) was measured at station 1, in Laguna Salada in July while below detection limit concentrations (0.0 $\mu mol \cdot L^{-1}$) occurred at multiple sites, including 3, 5, and 7 in Cayo del Grullo, the head of Alazan Bay, and mid- Baffin Bay in January, July, and November, respectively (**Figure 19a**). NO_3^- concentrations were consistently below the detection limit at station 7, located midway between the mouth of Baffin Bay and the intersection of the three end-member bays (**Figure 2**). The highest NO_3^- concentrations measured each event occurred in surface water in Laguna Salada (station 1), or the head of Alazan Bay (station 5).

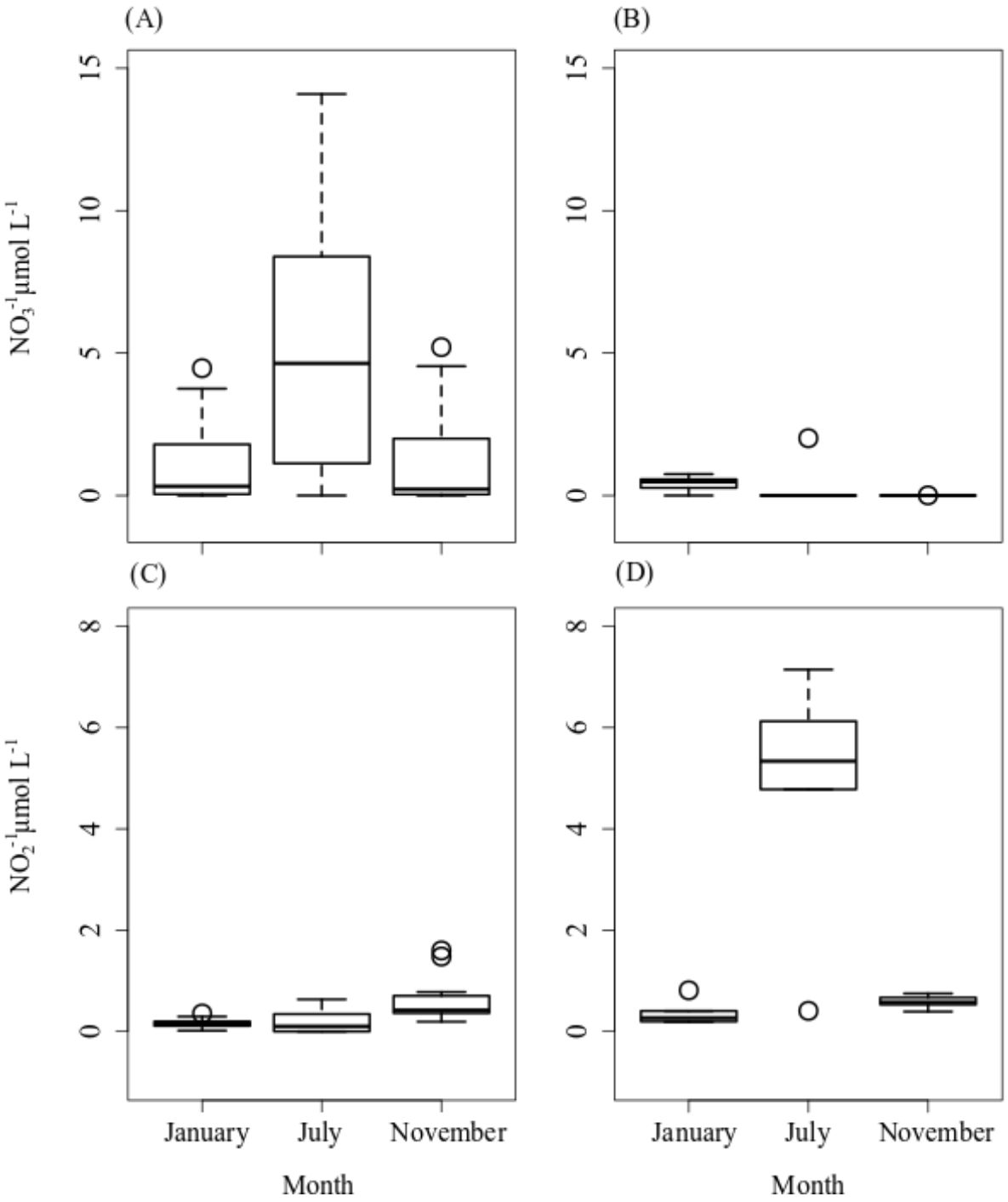

Figure 19: NO_3^- and NO_2^- concentrations for all events in surface and porewater. A) surface water concentrations B) Porewater concentrations.

The highest porewater NO_3^- (2.0 µmol·L^{-1}) was measured at station 8 (**Figure 19b**), at the mouth of Baffin Bay, in July while concentrations below the detection limit were consistent

across events at multiple locations: in January at stations 2, 3, and 7; in July at stations 7 and 8; and in November at stations 2 and 7.

The average NO_2^- concentration across all events was 0.3 µmol·L^{-1} (n=48) in the surface water (which is lower than that of NO_3^-) and 2.0 µmol·L^{-1} in porewater (n=18) (which is higher than that of NO_3^-). The highest surface water NO_2^- concentration (1.6 µmol·L^{-1}) was measured at station 6, near the mouth of Alazan Bay in November while the lowest/or below the detection limit (0.0 µmol·L^{-1}) occurred at multiple sites including stations 1, 3, and 5 at the head of Laguna Saladaand Alazan Bay, and in Cayo del Grullo in July (**Figure 19a**). The highest porewater NO_2^- (7.2 µmol·L^{-1}) was measured at station 1, in Laguna Salada, in July while the lowest (0.2 µmol·L^{-1}) at station 3, in the Cayo del Grullo in January (**Figure 19b**). The highest NO_2^- concentrations measured each event occurred in surface water at the head of Alazan Bay (station 5), the middle of Baffin Bay, or at the mouth of Baffin Bay (**Figure 2**, **Figure 19**).

The average NH_4^+ concentration across all events was 6.2 µmol·L^{-1} (n=48) in surface water and $1.18x10^3$ µmol·L^{-1} in porewater (n=18) (**Figure 20a, Figure 20b**). The highest and lowest surface water NH_4^+ concentrations (18.7 and 0.1 µmol·L^{-1}, respectively) were measured at station 1, in Laguna Salada in July and January, respectively. The highest porewater NH_4^+ ($5.5x10^3$ µmol·L^{-1}) was also measured at station 1 in July (**Figure 2, Figure 20b**) while the lowest (38.6 µmol·L^{-1}) at station 3, at the mouth of Cayo del Grullo in January. The highest NH_4^+ concentrations measured surface water each event occurred in Laguna Salada, near the mouth of Alazan Bay and the mouth of Baffin Bay (stations 1, 6, 8) (**Figure 21, Figure 22, Figure 23**). Ammonium is typically thought to be a preferred nitrogen source for phytoplankton (Dortch, 1990), so the preferential uptake of ammonium may be heightened during times of severe N-limitation.

Similar to NH_4^+concentrations, HPO_4^{2-} is by large more concentrated in porewater (**Figure 20c, Figure 20d**). The average HPO_4^{2-} concentration across all events was 0.7 $\mu mol \cdot L^{-1}$ (n=48) in surface water and 16.0 $\mu mol \cdot L^{-1}$ in porewater (n=18). The highest surface water HPO_4^{2-} concentration (1.5 $\mu mol \cdot L^{-1}$) was measured at station 7, in the mid- Baffin Bay in November while the lowest (0.1 $\mu mol \cdot L^{-1}$) at station 8, in January (**Figure 2, Figure 20c**). The highest porewater HPO_4^{2-} (43.7 $\mu mol \cdot L^{-1}$) was measured at station 1, in Laguna Salada, in July while the lowest (1.6 $\mu mol \cdot L^{-1}$) at station 3, at the mouth of Cayo del Grullo in January (**Figure 2**, **Figure 20d**). The highest HPO_4^{2-} concentrations measured each event in surface water occurred near the head of Cayo del Grullo, in Laguna Salada, and near the middle of Baffin Bay (stations 4, 1, 7). Although HPO_4^{2-}concentrations are in low levels in surface water, the larger porewater concentrations, particularly in July, are an indication that Baffin Bay could receive significant amounts of terrigeneous or anthropogenic nutrients (especially P and N). This is particularly true for the Laguna Salada, where the largest concentrations of the most nutrients were measured which are accompanied by persistently larger chl-a levels (Khalil and Rifaat, 2013).

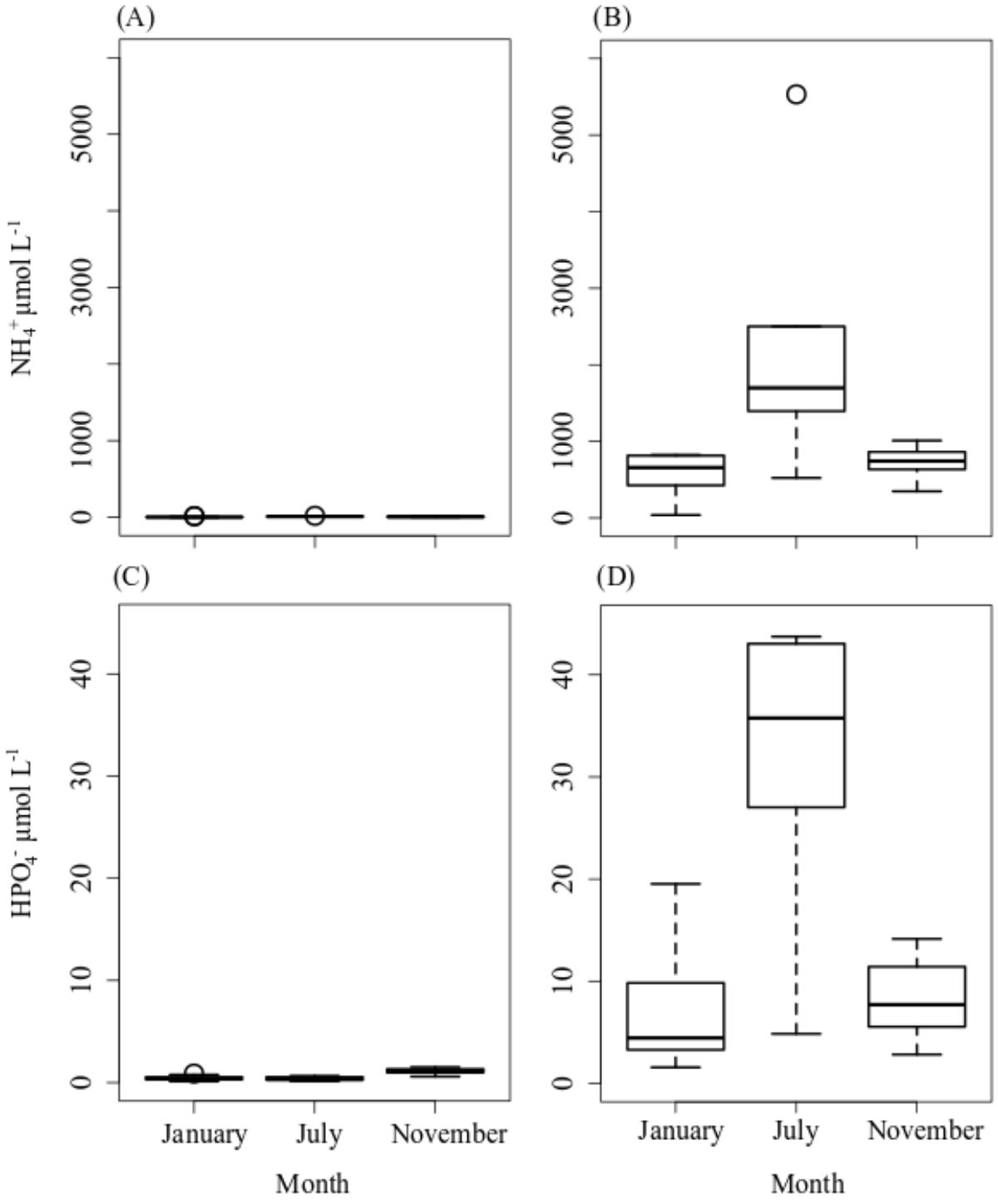

Figure 20: A) NH_4^+ concentrations for surface water spatial sampling B) NH_4^+ concentrations for porewater spatial sampling C) HPO_4^{2-} concentrations for surface water samples D) HPO_4^{2-} concentrations for porewater samples.

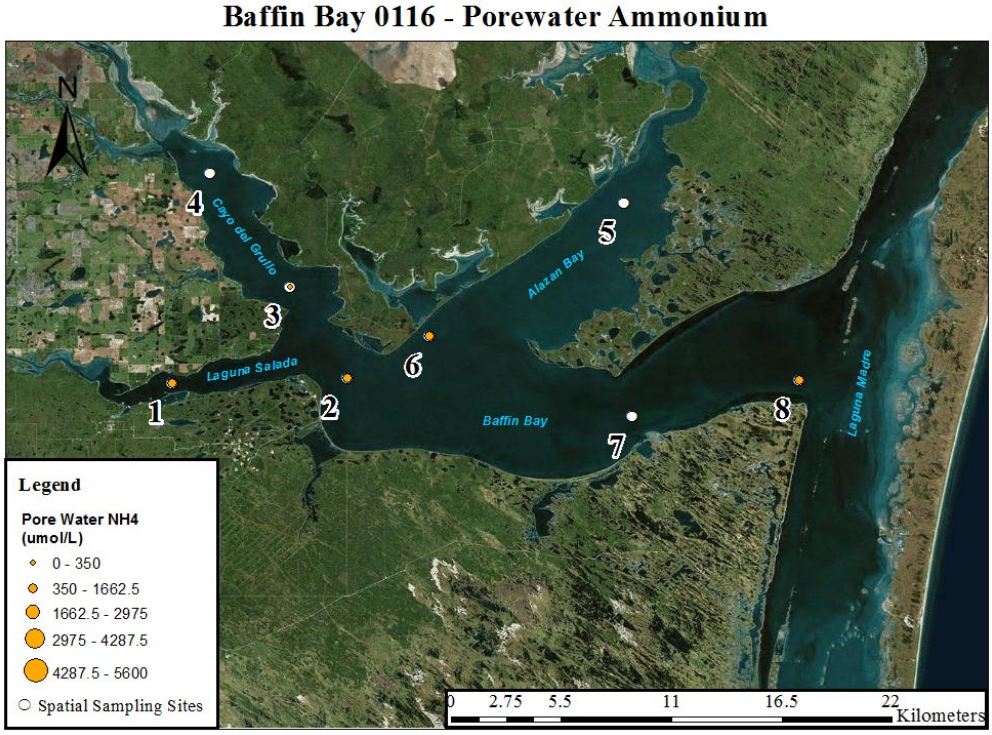

Figure 21: Porewater NH_4^+ in µmol L^{-1} for January, there are no data for stations 4, 5, and 7.

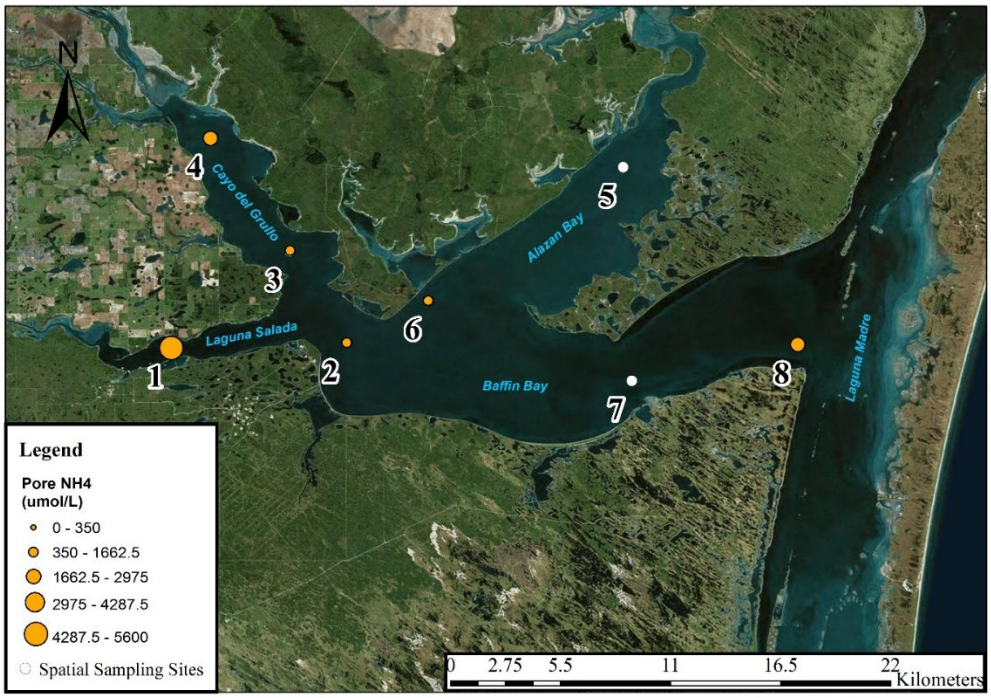

Figure 22: Porewater NH_4^+in µmol L^{-1} for July, there are no data for stations 5 and 7.

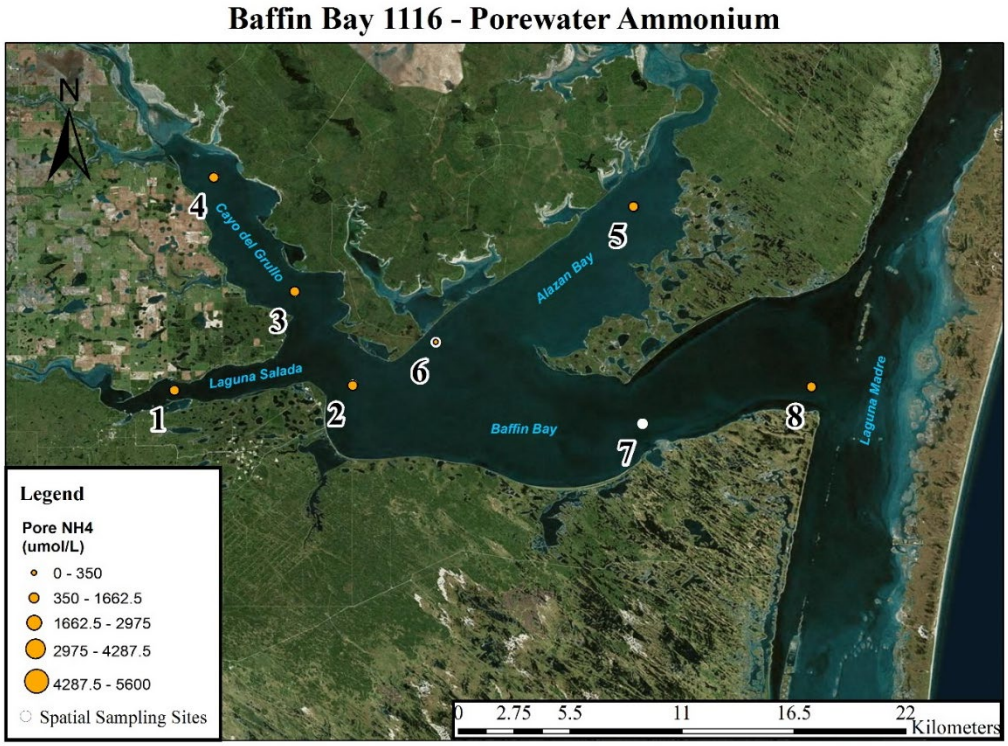

Figure 23: Porewater NH_4^+ in µmol L^{-1} for November, there is no data for station 7.

Larger enrichment of porewaters over surface water is also observed for $HSiO_3^-$ (**Figure 24**). The average $HSiO_3^-$ concentration across all events was 101.4 µmol·L^{-1} (n=48) in surface water and 275.4 µmol·L^{-1} (n=18) in porewater. The highest surface water $HSiO_3^-$ concentration (188.3 µmol·L^{-1}) was measured at station 8, at the mouth of Baffin Bay in November while the lowest (13.0 µmol·L^{-1}) at station 7, in the middle of Baffin Bay in January. The highest porewater $HSiO_3^-$ (559.0 µmol·L^{-1}) was measured at station 1, in Laguna Salada, in July while the lowest (56.7 µmol·L^{-1}) at station 3, at the mouth of Cayo del Grullo in January. The highest $HSiO_3^-$ concentrations measured in surface water during each event occurred near the head of Cayo del Grullo, near the middle of Baffin Bay, and in Laguna Salada (stations 4, 7, 1). Although, average concentrations of $HSiO_3^-$ in surface water increased from January to July to November, the chl-α level does not show a similar pattern, indicating that an increase in available silica did not play an important role on diatomaceous algae growth.

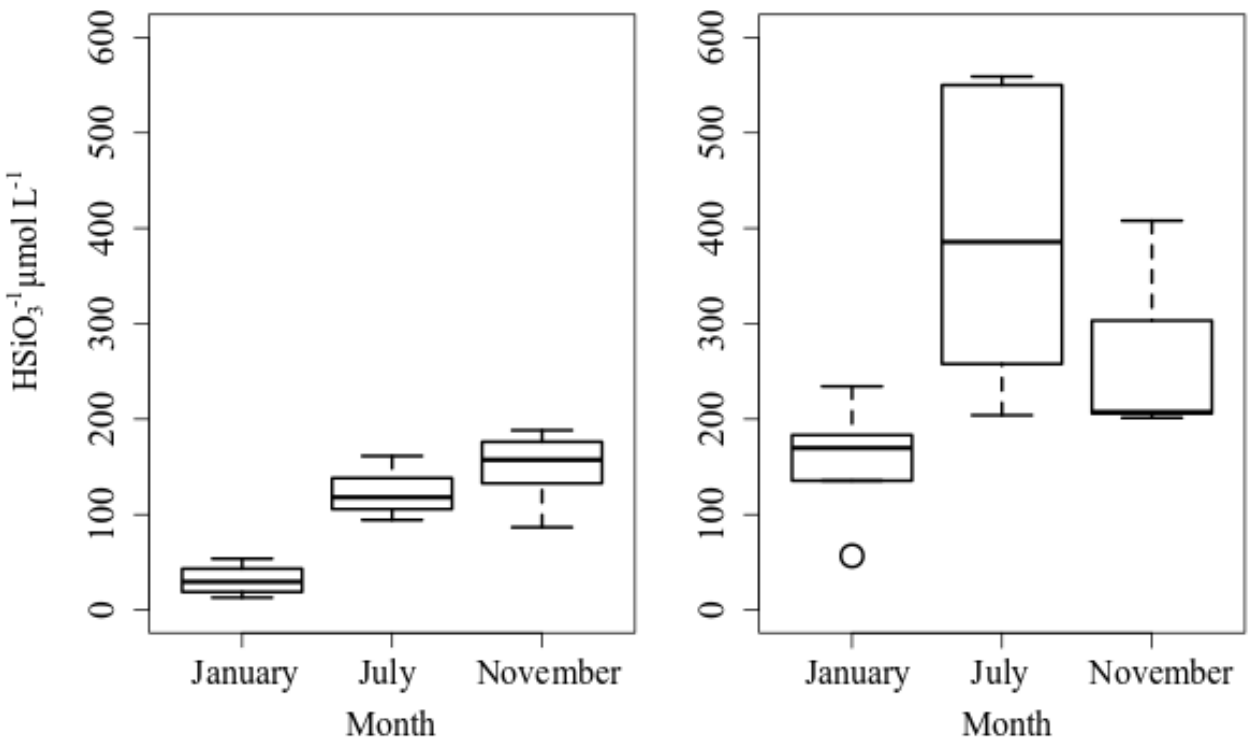

Figure 24: Surface (left) and porewater (right) $HSiO_3^-$ concentrations.

Submarine Groundwater Discharge

Rates of SGD were calculated using three different methods: ^{222}Rn-inventories from both time-series (in-situ) and continuous (spatial) ^{222}Rn data collection, ^{226}Ra mass balance, and from time-lapse (in-situ) ERT.

^{222}Rn-derived SGD Estimates

All, but one radon measurements were conducted during times with no recorded precipitation (Texas Water Development Board, Water Data for Texas website (NAAS, 2017; TWDB, 2016)). Time-series at station 12 in July was performed within 24 hours of a precipitation event (total rainfall: 51 mm (NAAS, 2017)).

Porewater ^{222}Rn activities were measured at a minimum of five locations every sampling event (i.e. January, July, and November). These porewater grab samples do not always exceed

the supported ^{222}Rn activity derived from sediment equilibration experiments (Murgulet et al., 2018) (**Table 7**). This could be an indication that ^{222}Rn is escaping during in-situ sample extraction. ^{222}Rn grab samples equal to 0.0 Bq·m^{-3} were not included in this study. In January and July, porewater ^{222}Rn activities ranged from 1.5 Bq·m^{-3} to 49.10 Bq·m^{-3} ($\bar{x}$=19.2 Bq·m^{-3}, n=4) and 56.0 Bq·m^{-3} to 266.1 Bq·m^{-3} ($\bar{x}$=138.6 Bq·m^{-3}, n=5), respectively (**Table 7**). Porewater ^{222}Rn activities in November ranged from 169.5 Bq·m^{-3} to 1557.5 Bq·m^{-3} ($\bar{x}$=632.7 Bq·m^{-3}, n=6) (**Table 7**). Groundwater samples from local aquifers (ranging 186.8-383.4 m in depth) had ^{222}Rn activities ranging from 1,884 Bq·m^{-3} to 13,136 Bq·m^{-3} ($\bar{x}$=7094.4 Bq·m^{-3}, n=6). (**Table 8**). Measured surface and bottom water ^{222}Rn activities ranged from 4.7 Bq·m^{-3} to 37.5 Bq·m^{-3} ($\bar{x}$=17.5 Bq·m^{-3}, n=16), from 2.9 Bq·m^{-3} to 45.7 Bq·m^{-3} ($\bar{x}$=17.7 Bq·m^{-3}, n=14), and from 5.9 Bq·m^{-3} to 26.9 Bq·m^{-3} ($\bar{x}$=20.4 Bq·m^{-3}, n=8) in January, July, and November, respectively (**Table 7**) excluding all ^{222}Rn measurements of 0.0.

Previous studies have shown that selection of a representative groundwater endmember for estimation of SGD fluxes is challenging (Burnett and Dulaiova, 2003; Cerdà-Domènech et al., 2017; Garcia-Orellana et al., 2013; Lamontagne et al., 2008; Urquidi-Gaume et al., 2016) as it can result in a large range of magnitudes. To account for these possible uncertainties, we used three ^{222}Rn groundwater endmembers to perform a radon mass balance to estimate SGD rates: 1) the greatest porewater ^{222}Rn activity (1,557 Bq·m^{-3}), 2) the average of six select terrestrial well activities ($\bar{x}$ = 7,094 Bq·m^{-3}) and 3) the highest groundwater ^{222}Rn activity (13,136 Bq·m^{-3}). The highest ^{222}Rn in porewater for the duration of the study (1,557 Bq·m^{-3}) was similar to the lowest groundwater activity from close proximity to the bay (1,884 Bq·m^{-3}). The different ^{222}Rn activities in the groundwater endmembers do not result in significantly different SGD rates (**Table 9, Table 10, Table 11**). However, using the largest porewater ^{222}Rn activity, yields SGD

rates that are relatively high when considering the hydroclimatic and hydrologic conditions in this area. We deem the SGD estimates derived with the highest porewater activity as the least conservative and most unrealistic, not only when compared to Uddameri et al. (2013), but given the hydrogeologic (i.e. reverse hydraulic gradients caused by Kingsville cone of depression) and climatic (i.e. semi-arid with low precipitation and recharge rates to the water table aquifer) settings.

Sample type	January				July				November			
	min	max	$\bar{x}$	n	min	max	$\bar{x}$	n	min	max	$\bar{x}$	n
Porewater	1.5	49.1	15.4	4	56.0	266	115	5	169.5	1557	542	6
Surface water	4.7	37.5	17.7	8	4.7	35.4	16.1	8	15.5	26.7	23.5	4
Bottom water	12.5	25.2	17.4	8	2.9	45.7	19.3	7	5.9	26.9	17.2	4
Surface- and bottom-water	4.7	37.5	17.5	16	4.67	45.7	17.7	15	5.9	26.9	20.4	8

Table 7: Minimum, maximum, mean ($\bar{x}$), and number of sample (n) for ^{222}Rn activities ($Bq \cdot m^{-3}$) in porewater, surface water and bottom water for each event. November porewater has the highest ^{222}Rn activity while in January, porewater activities are lowest.

Well ID	Well Depth (m)	^{222}Rn Activity
8326201	264	15,376.4
8327501	244	4,725.8
8329201	358	2,836.7
8329401	383	8,719.2
8342508	222	13,133.6
8334403	187	2,039.9
Average	276	7,805.3

Table 8: ^{222}Rn activities ($Bq \cdot m^{-3}$) in local groundwater aquifers within the Baffin Bay watershed. Shallow wells were not located within the watersheds. Anecdotal evidence indicates that shallow wells are not available in the area given the high salinity content.

Event	Endmember	Cayo del Grullo	Alazan Bay	Laguna Salada	Baffin Bay Mouth	Average
July	Avg. gw	36.9±20.7	42.3±32.7	29.4±24.4	38.4±17.6	36.7
	Max. gw	18.7±10.5	21.5±16.6	14.9±12.4	19.5±8.9	18.6
	Max. pw	185.1±103.6	212.0±164.1	147.3±122.4	192.4±88.3	184.2
November	Avg. gw	31.0±9.0	25.8±17.2	16.8±4.3	7.7±5.5	20.3
	Max. gw	15.7±4.6	13.1±8.7	8.5±2.2	3.9±2.8	10.3
	Max. pw	155.4±45.4	129.3±86.1	84.1±21.6	38.8±27.5	101.9

Table 9: SGD rates (in $cm \cdot d^{-1}$) calculated from continuous ^{222}Rn measurements for July and November sampling events for the Baffin Bay inlets and mouth. Standard deviation of SGD rates is included with each station average. Included are SGD rates calculated using the average groundwater (Avg. gw) ^{222}Rn and the maximum groundwater (Max. gw) ^{222}Rn.

Event	Endmember	Station 9	Station 10	Station 11	Station 12	Average
July	Avg. gw	17.8±9.1	10.7±5.4	28.4±10.4	26.3±13.9	20.8
	Max. gw	9.1±4.6	5.4±2.7	14.4±5.3	13.4±7.1	10.6
	Max. pw	89.4±45.6	53.5±27.1	142.2±52.2	132.1±69.7	104.3
November	Avg. gw	16.5±14.1	14.1±10.0	52.7±29.9	13.3±7.3	24.2
	Max. gw	8.4±7.2	7.1±5.1	26.7±15.2	6.8±3.7	12.3
	Max. pw	82.7±70.7	70.6±50.1	264.1±149.9	66.7±36.7	121.0

Table 10: SGD rates (in $cm \cdot d^{-1}$) calculated from time-series ^{222}Rn measurements for July and November sampling events. Standard deviation of SGD rates is included with each station average. Included are SGD rates calculated using the average groundwater (Avg. gw) ^{222}Rn and the maximum groundwater (Max. gw) ^{222}Rn.

Event	Endmember	Station 9	Station 10	Station 11	Station 12	Average
July	Avg. gw	40.8±5.6	47.4±14.6	20.8±8.4	39.6±0.03	37.1
	Max. gw	20.7±2.9	24.1±7.4	10.5±4.3	20.1±0.02	18.9
	Max. pw	204.5±28.2	237.6±73.1	104.0±42.3	198.7±0.2	186.2
November	Avg. gw	35.2±7.8	24.5±3.2	26.9±1.8	8.2±2.3	23.7
	Max. gw	17.9±4.0	12.4±1.6	13.7±0.9	4.2±1.2	12.0
	Max. pw	176.5±39.2	122.7±16.2	134.9±9.0	41.1±11.6	118.8

Table 11: SGD rates (in $cm \cdot d^{-1}$) calculated from continuous ^{222}Rn measurements for July and November sampling events. Standard deviation of SGD rates is included with each station average. Included are SGD rates calculated using the average groundwater (Avg. gw) ^{222}Rn and the maximum groundwater (Max. gw) ^{222}Rn.

The average groundwater endmember yields more reasonable and comparable SGD estimates for both time-series and continuous assessments. The time-series measurements of ^{222}Rn activity yield SGD rates ranging from 11.7 $cm \cdot d^{-1}$, at station 10 in July, to 58.0 $cm \cdot d^{-1}$, at

station 11 in November (**Table 10**). SGD rates determined from continuous/bay-wide measurements for each corresponding time-series station, ranged from 10.8 $cm \cdot d^{-1}$ at station 12 in November, to 87.7 $cm \cdot d^{-1}$ at station 10 in July (**Table 11**). These rates were estimated using an average ^{222}Rn activity measured during the continuous survey in surface water in close proximity to each of the time-series stations, for comparison purposes. Average SGD rates for each one of the Baffin Bay sub-bays and the Baffin Bay mouth (**Table 9)** follow the same trend and match the in station estimates from continuous measurements (**Table 11, Figure 2**). Average SGD from the time-series and continuous measurements at the time-series stations indicate that rates are similar between July (time-series: 22.9 $cm \cdot d^{-1}$; continuous: 63.8 $cm \cdot d^{-1}$) and November (time-series: 26.6 $cm \cdot d^{-1}$; continuous: 29.7 $cm \cdot d^{-1}$) (**Table 10, Table 11**).

The highest groundwater endmember results in more conservative SGD estimates with rates about half lower than those determined using the average groundwater, but with the same trends as described above. Time-series SGD rates ranged from 6.3 $cm \cdot d^{-1}$ to 31.3 $cm \cdot d^{-1}$ over the course of this study. Continuous SGD rates for each corresponding time-series station ranged from 5.9 $cm \cdot d^{-1}$ to 47.4 $cm \cdot d^{-1}$. Continuous SGD rates for each of the sub-bays ranged from 4.6 $cm \cdot d^{-1}$ to 41.2 $cm \cdot d^{-1}$.

Overall, SGD rates derived from the time-series measurements do not show a trend similar to those from continuous/bay-wide estimates. To note, however, is that the rates are within the same order of magnitude, and, SGD rates are lower than 90 $cm \cdot d^{-1}$ in both instances. Time-series rates are an average of a large number of ^{222}Rn integrations in-situ (n= 16), thus increasing the potential of capturing variations in SGD throughout the day (i.e. higher or lower rates of SGD). Continuous measurements, which are a snapshot of ^{222}Rn activities within a relatively small area, capture larger areas that could include more significant SGD rates, as well as variable wind

conditions. Commonly, in the study area, calm wind conditions occur in the first part of the day while winds start picking up in the afternoon (**Figure 3**). Wind conditions also vary from one day to another. The increased wind speed causes more wave action and degassing of ^{222}Rn from the water column at rates greater than during calm conditions (Wanninkhof, 1992). This variation in wind conditions, throughout one survey or between two survey days, could lead to ^{222}Rn degassing rates captured in some parts of the bays and not in others. In this study, we find that wind speed and ^{222}Rn activity are significantly inversely correlated (R^2=0.4; p-value $1.223x10^{-14}$) (**Figure 25**).

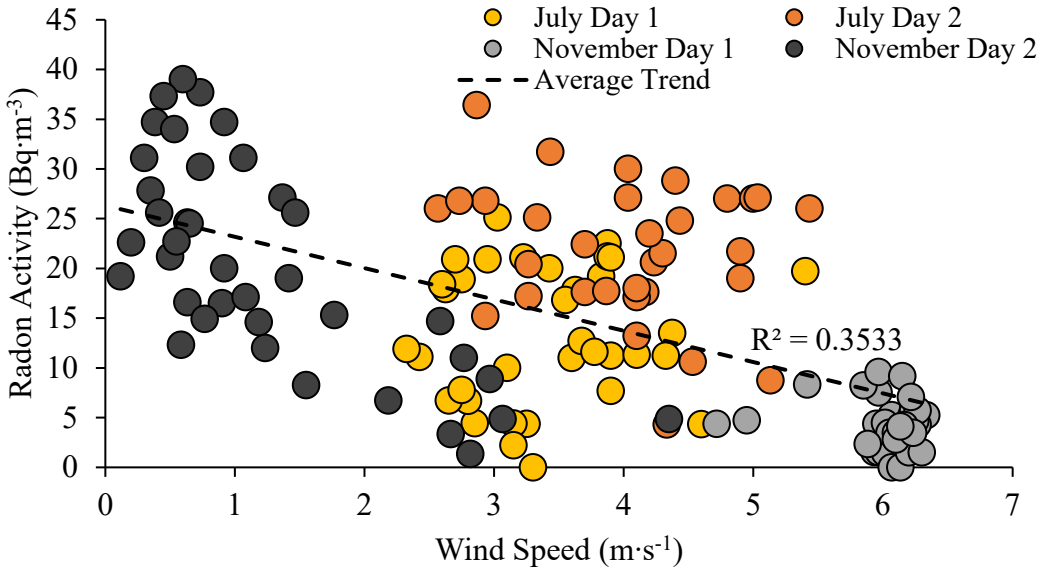

Figure 25. Wind speed ($m \cdot s^{-1}$) versus ^{222}Rn activity ($Bq \cdot m^{-3}$) in the water column during the continuous surveys.

During the first survey day in November, the majority of ^{222}Rn activities (n=51) were below those supported by the ^{226}Ra in the water column (11.1 to 18.5 $Bq \cdot m^{-3}$). These measurements are associated with the maximum wind speeds for all surveys (**Figure 25**). As long-term high winds may lead to degassing of ^{222}Rn and lower activities in the water (Wanninkhof, 1992), beyond those accounted for in the mass-balance, SGD rates will also

decrease. In this study, the lowest ^{222}Rn was measured along the transect going from the Baffin Bay Mouth to the Laguna Salada. Mixing of bay waters with more isotopically lighter water coming from the Laguna Madre is expected to also lead to lower SGD rates if not accurately accounted for in the ^{222}Rn inventory. However, ^{226}Ra was measured at each of the eight sampling stations within the bay (**Figure 2**), and the activity at the mouth of the bay going into Laguna Madre was accounted for. Thus, there is a strong indication that ^{222}Rn degassing due to prolonged high-wind speeds and gusts in the days leading up to sampling is unaccounted for in the atmospheric evasion term of the mass-balance, which leads to lower SGD rates for the season. Consequently, SGD rates for November were calculated using the lowest observed surface water ^{222}Rn activity as an estimate of the expected background ^{222}Rn activity. All ^{222}Rn activities measured during the continuous mobile survey in July were above those supported by the ^{226}Ra in the water column and the wind speeds in the days prior to sampling were several $m \cdot s^{-1}$ lower than in November, thus wind effects were significantly less in July.

The most outstanding difference in SGD was estimated using the continuous ^{222}Rn assessment between July and November at stations 9 (in Cayo del Grullo), 10 (Alazan mouth), and 12 (Baffin Bay mouth). SGD fluxes are lower in November at each station almost by half (**Table 10)**, which could be explained by the observations above related to wind effects and Laguna Madre input. For the other stations, the change in rates is much smaller from July to November, particularly with the time-series method.

^{226}Ra-derived SGD Estimates

The ^{226}Ra-based SGD estimates are representative of the entire bay (Charette et al., 2001). The ^{226}Ra-based water ages, the freshwater inflow estimates (TWDB, 2016), and the porewater ^{226}Ra measurements are used to estimate the SGD of the entire bay (Charette et al.,

2001). The discharge of ^{226}Ra into the bay from its tributaries was determined with data from a model for the local watershed (TWDB, 2016). It is assumed that the data is reasonably accurate, though the model includes surface runoff for all surrounding land and not just the creek discharge and as of the completion of this report the model had yet to include diversions and return flows to and from the creeks (TWDB, 2016). This was necessary to use as there was no other available data for all three tributaries including Petronila Creek which was ungagged. The estimates for average daily discharge in the form of SGD for Baffin Bay averaged 4.1 cm·d^{-1} (n=2) with the average ^{226}Ra activity of porewater used as the groundwater endmember. The average porewater ^{226}Ra activity gave an estimated SGD of 5.6 cm·d^{-1} for January, 6.4 cm·d^{-1} for July, and 1.6 cm·d^{-1} for November. This small variability is mainly related to changes in the porewater endmember as well as surface water activities (**Table 12, Table 13**). The variables underlying most of the calculations are surface and porewater ^{226}Ra activities, the water ages depend on them, the ^{226}Ra inventory depends on them, and the conversion to a final bay wide SGD depends on them (Charette et al., 2001).The average SGD being greater in July corresponds with the overall greater surface water and porewater ^{226}Ra activities, as discussed above.

^{226}Ra by station	1	2	3	4	5	6	7	8
All events max. ^{226}Ra	20.6	18.9	19.6	20.1	20.6	22.4	14.9	12.1
All events average ^{226}Ra	17.7	16.9	17.8	16.9	16.7	18.7	13.8	11.3
All events min. ^{226}Ra	14.7	14.1	15.4	15.0	13.8	15.4	11.9	10.5

Table 12: Mean ^{226}Ra activities (Bq·m^{-3}) for each station over all spatial sampling events. The highest ^{226}Ra activities are found in the westernmost stations, stations 1-4, the lowest activities were found in the easternmost stations, stations 5-8.

PW ^{226}Ra by Station	1	2	3	4	5	6	7	8	Average
July	52.9	33.7	63.3	53.4	--	44.4	--	14.1	43.6
November	15.5	37.0	39.9	36.3	71.2	--	--	12.8	35.5

Table 13: Porewater (PW) ^{226}Ra activities (Bq·m^{-3}) for all three sampling events (January, July and November). Note that, in general, porewater activities in November are lower and the average is higher because of the largest activity measured at station 5, which was not available in

July. The average for stations 1-4 and 8, that were measured both events, is 28.3 $Bq \cdot m^{-3}$ is much lower.

Time-Series Electrical Resistivity Profiling and Resistivity-Derived SGD Estimates

SGD calculated from the ERT depends on differences in the resistivity of any potential groundwater and the subsurface matrix. Discharges calculated from the resultant tomographs are made with the assumption that any plumes of subsurface groundwater will eventually be discharged, this means that the SGD's determined from this method may be overestimates. Electrical resistivity was only performed at the time-series sites (stations 9-12), however some of the data proved to be unrecoverable once downloaded from the system. The data that were usable and their resultant SGDs are reported in **Table 14** in cm d^{-1}. At station 9, in Cayo del Grullo, resistivities ranged from 0.16-1.7 Ω-m in July and 0.16-2.4 Ω-m in November. Station 10 at the mouth of Alazan Bay had resistivity ranges from 0.15-0.78 Ω-m in July and 0.15-1.8 Ω-m in November. The resistivities measured in station 11, Laguna Salada, ranged from 0.16-1.5 Ω-m in July and 0.15-3.2 Ω-m in November. Station 12, near the mouth of Baffin Bay had resistivities ranging from 0.14-1.4 Ω-m in July and 0.16-2.5 Ω-m in November.

Time series	Station/Season	9	10	11	12	Average
ERT	July	--	27.7±0.5	85.5±2.4	--	56.6±1.3
	November	--	45.7±0.9	43.1±1.1	31.1±0.5	40.0±0.8

Table 14: SGD rates ($cm \cdot d^{-1}$) derived from the time-lapse ERT salinity.

Time-series resistivity profiles were collected at four stations in July and November. The average imaging depth of each ERT was 24.5 m below the sediment-water interface and, similar to CRPs, with resistivity ranges between 0.14 to 3.2 Ω-m for both the July and November events. The small range of bulk resistivities is indicative of an overall more conductive media (i.e. green-blue range) (Samouëlian et al., 2005), likely caused by a combination of fine sediments

and high salinity porewater/groundwater. The first time-series ERT were performed in August, following a dry period, with an average of approximately 0.05 mm of precipitation for July (a total of 1.5 mm) and an average of 2.2 mm of rainfall in August (total of 68 mm) (**Figure 3**). The same survey lines were imaged in November, with an average daily rainfall of less than 1 mm per day and a total of less than 25 mm for the month.

Time-lapse inversions were performed on the time-series ERT data for the development of a salinity mass-balance using the percent difference in resistivity between the first and the last time-step ERT images. Possible zones of surface water-groundwater interaction are visible at several monitoring stations. Plumes of possible upwelling groundwater are reoccurring at similar locations in July and November, though of variable extent and magnitude (**Figure 26 - Figure 33**, note the different % difference scales). For most stations changes in resistivity occurred near the sediment-water interface, an indication of shallow transport or deep recirculation.

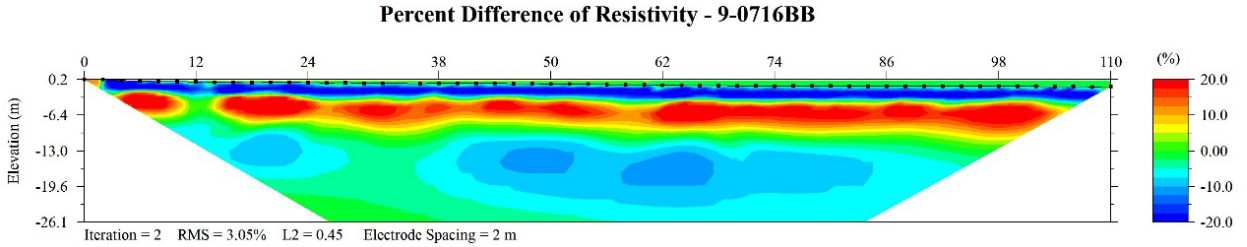

Figure 26: Percent Difference of Resistivity for station 9 ERT in July.

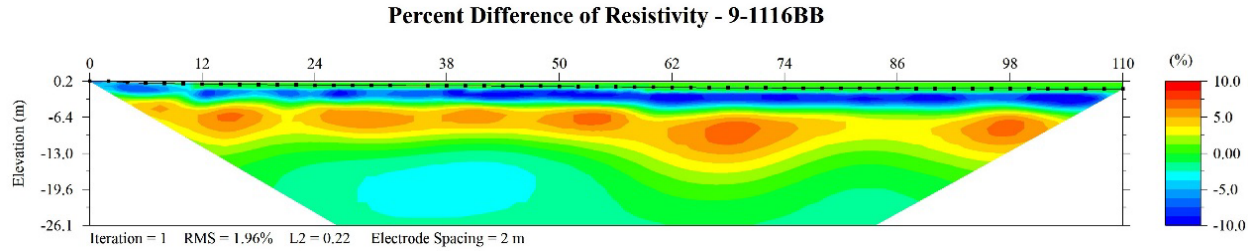

Figure 27: Percent Difference of Resistivity for station 9 ERT in November.

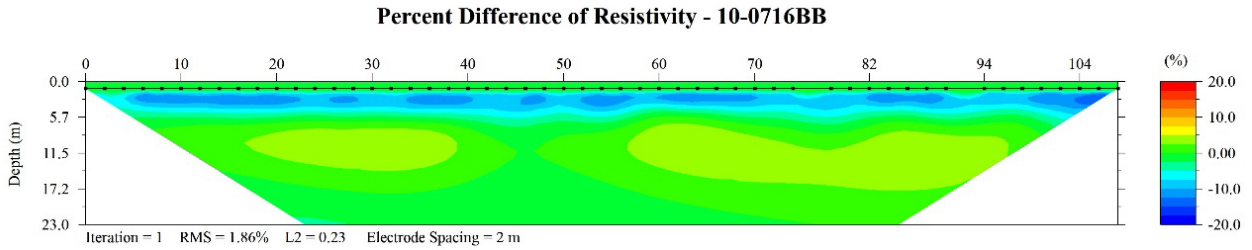

Figure 28: Percent Difference of Resistivity for station 10 ERT in July.

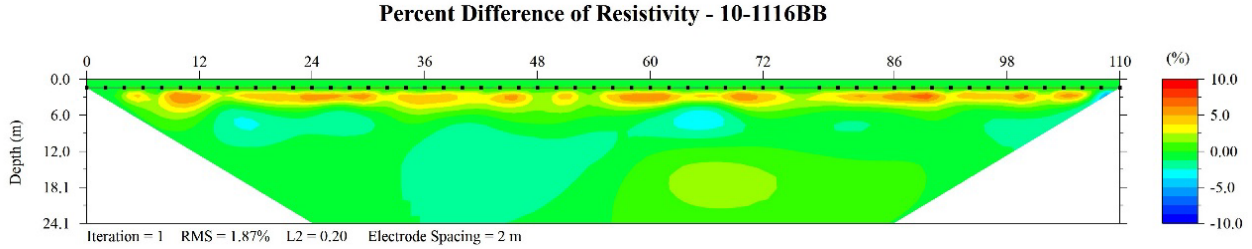

Figure 29: Percent Difference of Resistivity for station 10 ERT in November.

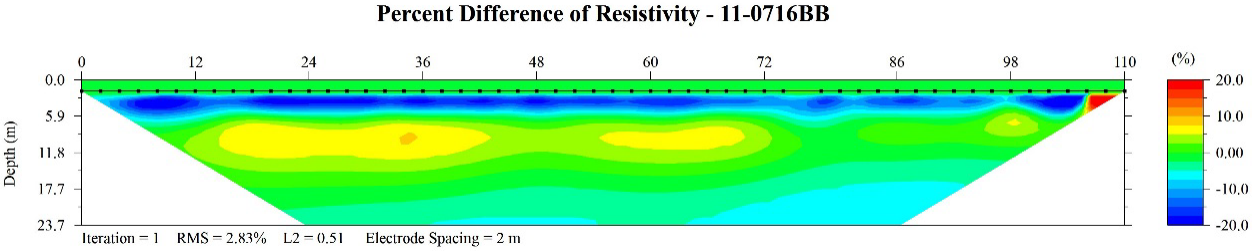

Figure 30: Percent Difference of Resistivity for station 11 ERT in July.

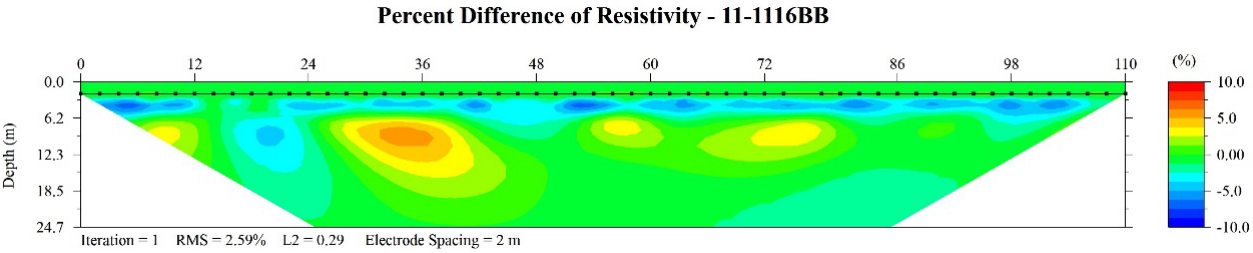

Figure 31: Percent Difference of Resistivity for station 11 ERT in November.

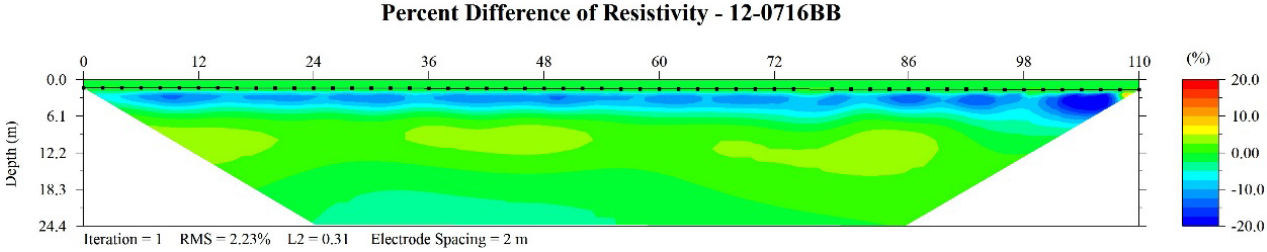

Figure 32: Percent Difference of Resistivity for station 12 ERT in July.

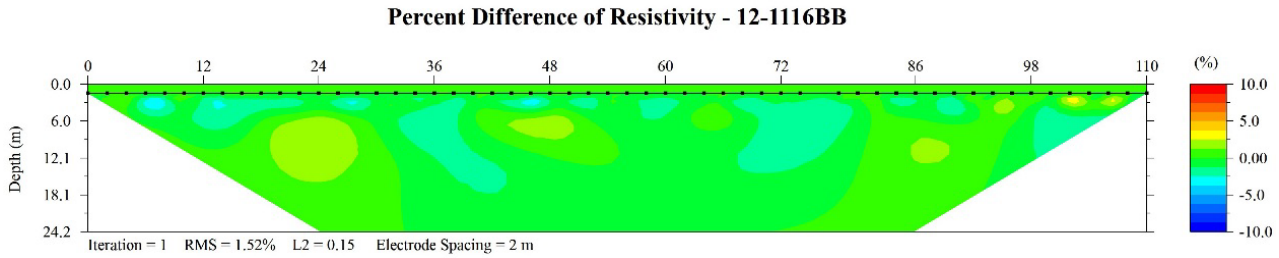

Figure 33: Percent Difference of Resistivity for station 12 ERT in November.

In November, changes in resistivity were much lower than those measured in July (see **Figure 26 - Figure 33**). In November, the percent change in resistivity did not exceed 10%, whereas in July it routinely approached 20%. The highest SGD rate derived from the time-series ERT was 86 ± 2.4 cm·d^{-1} at station 11 in July whereas the lowest was at station 10 in July (28 ± 0.51 cm·d^{-1}), showing again the larger July range compared to the November range (31.1±0.5 cm·d^{-1} to 45.7±0.9 cm·d^{-1}). The average SGD for July was estimated to be 57 ± 1.3 cm·d^{-1}, the average for November was estimated to be 40 ± 0.8 cm·d^{-1}. The average SGD determined from the time-series ERT method for the entire study period was 47 ± 0.74 cm·d^{-1} with a range of 28 ± 0.51 cm·d^{-1} to 86 ± 2.4 cm·d^{-1}.

SGD Comparison

The different methods employed in this study produced SGD rates that were in the same magnitude, however there were some discrepancies. The time-series ^{222}Rn and ^{226}Ra mass balance methods are within the same order of magnitude, but disagree in terms of seasonal intensity, which may reflect changes in climatic (i.e. wind) and/or hydrologic (i.e. precipitation) conditions (see section ***^{222}Rn-derived SGD Estimates***, and ***226Ra-derived SGD Estimates***).

The time-series ^{222}Rn, mobile continuous ^{222}Rn and ERT methods are able to give seasonal averages for the combined locations of stations 9-12. The ERT and mobile continuous ^{222}Rn show July as having larger average SGDs (56.6 cm·d^{-1}and 37.1 cm·d^{-1}, respectively) than

November (40.0 cm·d^{-1} and 23.7 cm·d^{-1}, respectively), while the time-series ^{222}Rn shows no substantial difference between July (20.8 cm·d^{-1}) and November (24.2 cm·d^{-1}) SGD rates. For the entire bay, an SGD rate can most reliably be estimated by the mobile continuous ^{222}Rn and ^{226}Ra methods as they provide greater spatial coverage and a more spatially integrated signal, respectively. Both ^{222}Rn and ^{226}Ra inventories estimate July as having a similar SGD rate (36.7 cm·d^{-1} and 6.4 cm·d^{-1} for mobile continuous ^{222}Rn and ^{226}Ra respectively) to November (20.3 cm·d^{-1} and 1.6 cm·d^{-1} for mobile continuous ^{222}Rn and ^{226}Ra respectively), though July is slightly higher than November. The discrepancy in the calculations may stem from salinity variations, when the salinity varied greatly in the subsurface the time-series electrical resistivity method assumes this is due to groundwater discharge, when it may in fact be due to recirculation of surface water through shallow subsurface sediments. Thus, these measurements are more qualitative in nature, rather than quantitative.

The ^{222}Rn and ^{226}Ra methods face a similar discrepancy, while ^{222}Rn is unreactive and capable of reliably measuring total SGD (including fresh terrestrial groundwater, saline porewater, and recirculating seawater) (Burnett and Dulaiova, 2003), ^{226}Ra requires that the SGD be saline enough to keep the ^{226}Ra in solution and not adsorbed to the sediment. Thus, ^{226}Ra reliably accounts for saline groundwater discharge or seawater recirculation, but likely misses freshwater SGD (Moore, 2006). Consequently, the similarities between the mobile continuous ^{222}Rn (i.e. total SGD) and the ^{226}Ra (i.e. saline SGD input) mass balance discharge rates reflects the relative dominance of saline groundwater discharge in Baffin Bay.

Nutrient Flux Rates

Nutrient fluxes (in µmol m^{-2} d^{-1}) were calculated as the product of porewater nutrient concentrations and SGD rates at specific locations from both the ^{222}Rn inventories. For this

study, the ^{222}Rn-derived SGD (in cm d^{-1}) rates estimated using the average groundwater ^{222}Rn endmember are used to calculate nutrient fluxes and for discussion purposes. Nutrient fluxes were calculated as the product of SGD rates and the porewater nutrient concentrations. Since porewater samples were collected at different range depths, we include nutrient fluxes derived from the average nutrient concentrations of all porewater depths and the deep (approximatively 1 to 2 m below sediment-water interface) and shallow range (approximatively 0.2-0.3 m below sediment-water interface) (**Table 16**). The resulting range of nutrient fluxes is included in the ***Comparison of Subsurface and Surface Fluxes of Solutes*** section.

Nitrate

These different endmembers are useful in identifying processes driving the fate of nutrients in the subsurface from the deeper horizons (i.e. subterranean estuary) to the oxic layer. Because the SGD rates used to estimate the nutrient fluxes were derived from the bay wide continuous surveys, below we include the nutrient fluxes derived from the average deep porewater concentrations which were collected along the SGD transects.

SGD rates derived from the mobile continuous ^{222}Rn inventories at each of the eight sampling stations were calculated to evaluate nutrient fluxes at different locations within the bay (**Figure 2**). The average flux of NO_3^- in Baffin Bay across all events was 72.5 μmol per day (μmol·d^{-1}) (n=11) using the mobile continuous ^{222}Rn method for the spatial sampling sites (1-6, 8). No nutrient fluxes were determined for station 7, as extraction of porewater samples at this location was not successful. The only measurable NO_3^- flux ($8.0x10^2$ μmol·d^{-1}) was at station 8, near the mouth of Baffin Bay, in July. For all other stations there were no measurable nitrate fluxes (0.00 μmol·d^{-1}: stations 1-4, 6)). In November, all porewater NO_3^- concentrations were below the MDL resulting in no measurable fluxes. The absence of measurable NO_3^- in porewater

associated with large amounts of NH_4^+ in July and November, suggests low nitrification activity and rapid consumption or reduction to NH_4^+ (DNRA). Measurable amounts of NO_3^- in January at four out of five stations, accompanied by some of the lowest NH_4^+, could result from lower reduction rates as ambient temperatures are lower. Dong et al. (2011) suggests that, at lower temperature and higher nitrate concentrations, estuaries in temperate environments exhibit proportionately greater levels of anammox (AN) and benthic denitrification (DN).

Nitrite

The average flux of NO_2^- in Baffin Bay across all events was $1.0x10^3$ µmol·d^{-1} (n=11) for the spatial sampling sites. The highest NO_2^- flux ($2.6x10^3$ µmol·d^{-1}) was measured at stations 2 and 6, near the mouth of the three bay inlets and upstream of the mouth of Alazan Bay in July and the lowest (33 µmol·d^{-1}), at station 8 in November (**Figure 2 and Figure 34)**. Lower average NO_2^- fluxes in November are driven mostly by the lower porewater NO_2^- concentration measured at all stations but at 8. In some instances, SGD rates are also lower in November, such as at stations 5, 7 and 8. The larger flux at station 6 is driven mostly by the SGD rate, which is the highest, measured during each event (**Table 15**). At station 2, both larger SGD flux and larger NO_2^- concentrations are leading to one of the largest NO_2^- fluxes in July.

Event	1	2	3	4	5	6	7	8	Average
July	20.8	41.7	44.1	31.0	46.2	47.4	23.2	39.6	36.7
Nov	17.7*	--	31.8	29.2	20.3	31.8	7.0	8.4	20.9

Table 15: SGD rates (cm·d^{-1}) determined from the mobile continuous ^{222}Rn survey.

Ammonium

The average flux of NH_4^+ in Baffin Bay for the July and November events was $4.5x10^5$ µmol·d^{-1} (n=11). The largest NH_4^+ flux ($1.2x10^6$ µmol·d^{-1}) was measured at stations 1, in the Laguna Salada in July (**Figure 2 and Figure 34**). The lowest flux of NH_4^+ ($7.9x10^4$ µmol·d^{-1}) was measured at station 8 in November. The highest porewater NH_4^+ measured each event

occurred at station 1 and station 3. In July, the largest NH_4^+ fluxes measured at stations 1 are a combination of larger SGD fluxes and higher NH_4^+ concentrations while the lower measured SGD rates and porewater NH_4^+ in November lead to lower NH_4^+ fluxes. While average SGD rates are similar between July and November, porewater concentrations of NH_4^+ (as well as NO_2^-, HPO_4^{2-}, and $HSiO_3^-$) are significantly decreasing from July to November (**Table 16**). As a result, the solute flux was lower in November at all stations within the bay (**Figure 2 and Figure 34**).

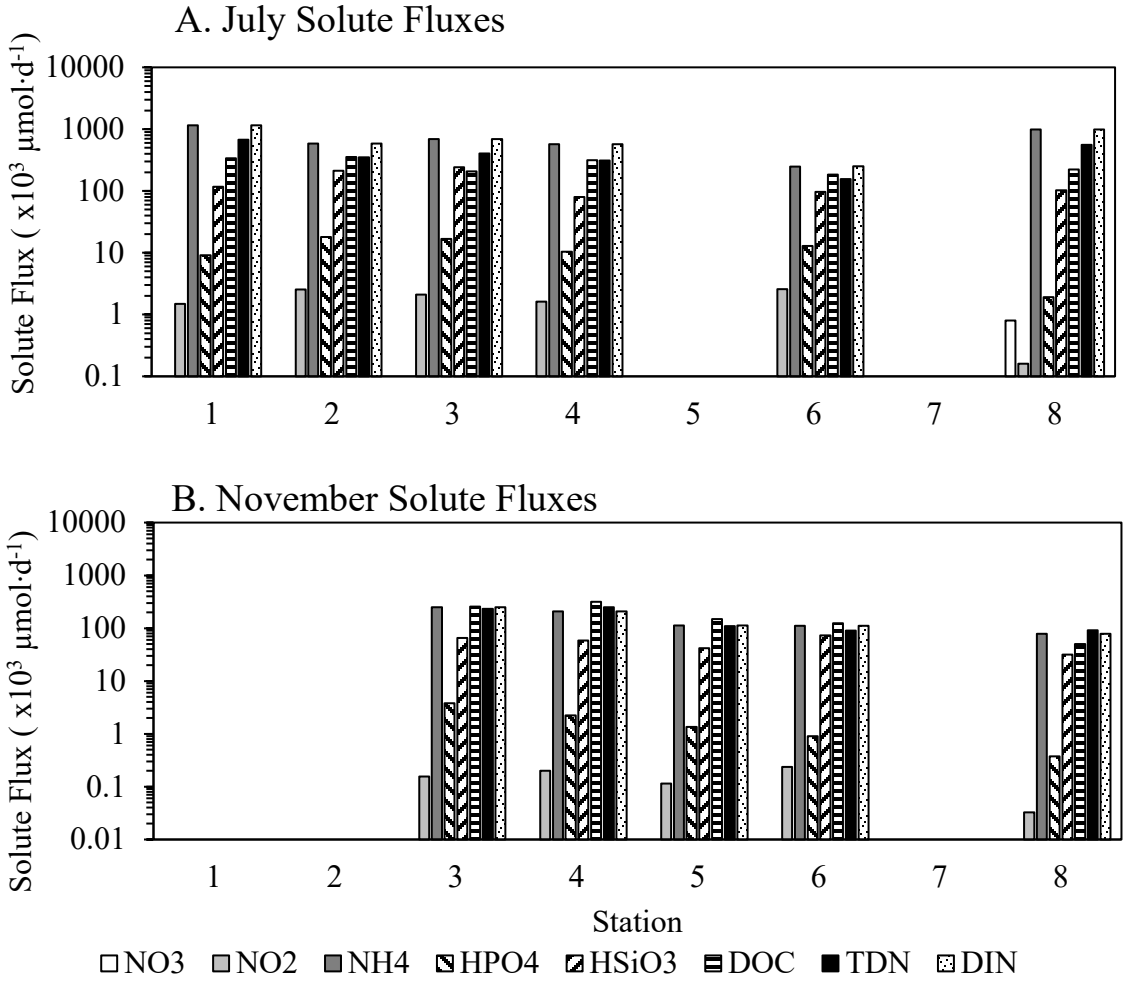

Figure 34: Graphical representation of solute fluxes derived as the product of porewater solute concentrations from the deep porewater samples and SGD rates from the continuous mobile ^{222}Rn surveys.

Station	Event	Depth*	NO_3^-	NO_2^-	NH_4^+	HPO_4^{2-}	$HSiO_3^-$	DOC	TDN	DIN	DON
1	Jan.	1.0	0.0	0.8	816.0	19.5	234.3	1270.5	1860.2	816.8	1043.4
	Jul.	1.6	0.0	7.1	5531.3	43.7	559.0	1630.2	3224.9	5538.5	==
	Nov.	1.70	0.0	0.6	1011.0	14.2	407.9	3126.4	3226.7	1011.6	2215.1
2	Jan.	1.0	0.6	0.3	658.9	9.8	183.4	480.6	420.2	659.7	==
	Jul.	1.8	0.0	6.1	1394.9	43.0	511.6	850.9	841.7	1401.1	==
	Nov.	1.95	0.0	0.7	744.1	11.0	205.9	814.1	818.5	744.8	73.7
3	Jan.	1.0	0.8	0.2	38.6	1.6	56.7	647.4	384.2	39.5	344.7
	Jul.	1.7	0.0	4.8	1563.6	38.0	550.0	469.2	911.3	1568.4	==
	Nov.	1.68	0.0	0.5	788.1	11.9	205.9	810.2	729.2	788.6	==
4	Jan.	--	--	--	--	--	--	--	--	--	--
	Jul.	1.4	0.0	5.2	1833.4	33.5	257.8	1013.7	1007.7	1838.6	==
	Nov.	1.7	0.0	0.7	716.4	7.7	201.3	1085.7	856.7	717.1	139.6
5	Jan	--	--	--	--	--	--	--	--	--	--
	Jul.	--	--	--	--	--	--	--	--	--	--
	Nov.	>1	0.0	0.6	553.6	6.7	207.4	737.1	543.5	554.2	==
6	Jan.	1.5	0.5	0.4	426.3	4.5	169.7	619.5	183.4	427.2	==
	Jul.	1.3	0.0	5.4	523.8	27.0	204.1	387.8	328.1	529.2	==
	Nov.	>1	0.0	0.7	348.8	2.8	230.0	393.1	282.7	349.6	==
7	Jan.	--	--	--	--	--	--	--	--	--	--
	Jul.	--	--	--	--	--	--	--	--	--	--
	Nov.	--	--	--	--	--	--	--	--	--	--
8	Jan.	1.0	0.3	0.2	824.6	3.3	135.5	462.0	241.7	825.1	==
	Jul.	1.9	2.0	0.4	2501.7	4.9	259.7	560.6	1408.6	2504.1	==
	Nov.	0.85	0.006	0.4	937.8	4.4	376.4	596.3	1093.8	938.2	155.6
9	Jul.	0.2	6.30	1.66	447.5	8.61	394.2	564.6	250.3	455.5	==
	Nov.	0.2	12.6	0.40	19.2	2.26	128.0	1155.0	111.4	32.2	79.2
10	Jul.	1.4	0.0	4.71	489.5	29.9	249.4	490.2	323.9	494.2	==
	Nov.	0.8	0.0	0.45	448.5	2.97	238.9	686.6	359.4	449.0	==
11	Jul.	--	0.0	5.31	1908.9	45.0	440.1	1515.3	1245.1	1914.2	==
	Nov.	1.1	0.0	0.74	488.2	6.19	345.2	715.1	456.2	488.9	==
12	Jul.	--	--	--	--	--	--	792.2	52.4	--	==
	Nov.	--	0.0	0.62	12.3	0.65	138.2	--	--	--	==

Table 16. Porewater nutrient concentrations ($\mu mol \cdot L^{-1}$) and depths of retrieval, below the sediment-water interface, for each of the spatial sampling sites (1-8) and time-series (9-12) by season. Samples where no nutrients were measured are denoted by "--" and DON derived from DIN concentrations larger than TDN, leading to negative DON, are denoted by "==". Porewater NO_3^- below the method detection limit (MDL) of <0.11 are reported as "0.0".

Statistically, a positive inverse relationship between porewater NH_4^+ concentrations and SGD in November (**Figure 35**) indicates that NH_4^+ is accumulating in the sediments where SGD rates are lower. Increasing SGD in the form of porewater recirculation may remove NH_4^+ from

porewater sediments (Santos et al., 2012). On the other hand, in November, although a negative relationship is visible, the correlation is statistically insignificant. As discussed in the SGD section, in November, degassing of radon due to high winds, preceding the mobile continuous survey, may have lowered SGD rates, potentially skewing the relationship discussed above.

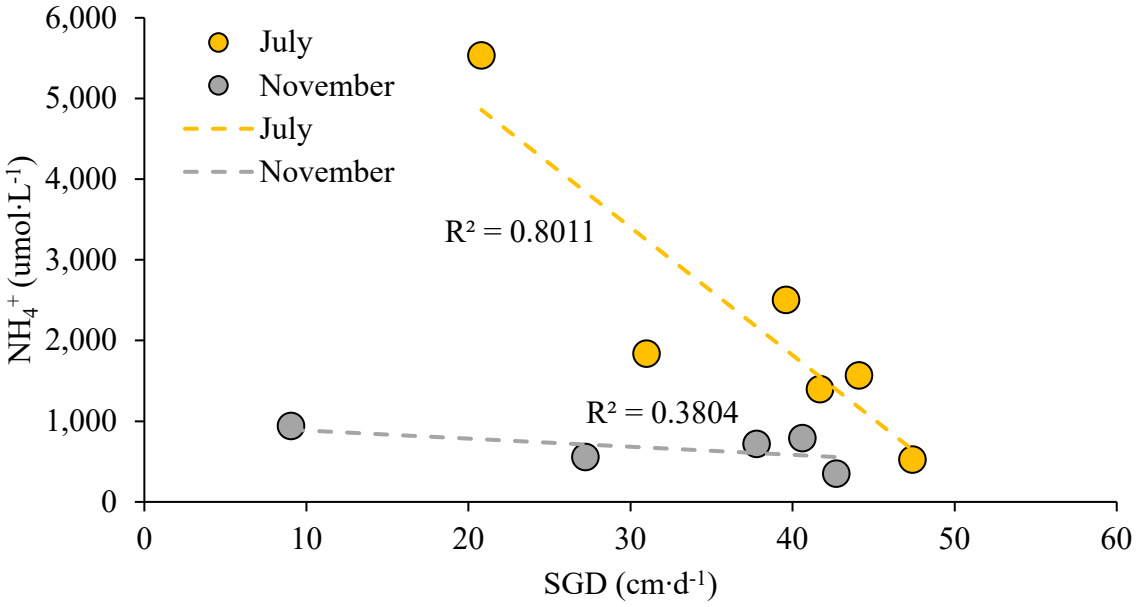

Figure 35: SGD rates, calculated using the mobile continuous ^{222}Rn method, versus porewater NH_4^+ concentration. The July event negative correlation is significant (R^2: -0.8; p-value: 0.01595). In November, the negative correlation is not statistically significant (R^2: -0.4; p-value of 0.2678).

Orthophosphate

The average flux of HPO_4^{2-} in Baffin Bay across all events was $7.1x10^4$ µmol·d^{-1} (n=11). The highest HPO_4^{2-} fluxes were measured at stations 2 and 3 ($1.8x10^4$ and $1.7x10^4$ µmol·d^{-1}, respectively) in July near the location where Cayo del Grullo meets Laguna Salada, while the lowest ($3.7x10^2$ µmol·d^{-1}) at station 8 in November. In July, the lowest HPO_4^{2-} flux occurred at station 8 (**Figure 2 and Figure 34A**). The highest measured HPO_4^{2-} concentrations for July and November occurred at stations 1, 2, and 3. Thus, higher HPO_4^{2-} fluxes measured at stations 2 and

3 in both months are the result of larger porewater concentrations and higher SGD rates (**Table 15**). On the other hand, at station 1, HPO_4^{2-} fluxes are lower due to lower measured SGD. Seasonal trends are similar to NH_4^+, with decreasing fluxes of HPO_4^{2-} from July to November.

Hydrogen Silicate

The average flux of $HSiO_3^-$ in Baffin Bay for July and November was $1.0x10^5$ μmol d^{-1} (n=11) with the highest ($2.4x10^5$ μmol·d^{-1}) measured at station 3 in July and the lowest ($3.2x10^4$ μmol·d^{-1}) at station 8 in November (**Figure 34**). In July, the largest $HSiO_3^-$ fluxes were measured at stations 2 and 3 ($2.1x10^5$ and $2.4x10^5$ μmol·d^{-1}, respectively) and the smallest at station 4 ($8.0 x10^4$ μmol·d^{-1}) (**Figure 34A**). In November, the highest flux of $HSiO_3^-$ was measured at station 6 ($7.3x10^4$ μmol·d^{-1}) and the lowest ($3.2x10^4$ μmol·d^{-1}) at station 8 (**Figure 34B**). The highest $HSiO_3^-$ measured each event occurred at stations 1, 2 and 3 with the July concentrations larger than the November. At station 8, $HSiO_3^-$ is also high but concentrations are higher in November than in July. Thus, the larger $HSiO_3^-$ flux at station 3 is the result of both, high $HSiO_3^-$ concentrations and SGD rates while at station 8, lower SGD rates in November lead to the lowest $HSiO_3^-$ flux for both seasons. As discussed in the SGD section, these may be the result of radon degassing and underestimated SGD rates.

DIN, TDN and DOC

Dissolved inorganic nitrogen (DIN) is comprised of nitrate plus nitrite and ammonium (DIN= $NO_3^- + NO_2^- + NH_4^+$). These forms of nitrogen are readily available to phytoplankton and often control the formation of blooms. In this study, in porewater, NH_4^+ makes up most of the DIN pool (**Table 16 and Figure 34**). Thus, DIN follows the same trends as NH_4^+ in terms of both concentrations and fluxes to the surface water.

Total dissolved nitrogen (TDN), which is comprised of DIN and dissolved organic nitrogen (DON), also follows similar trends to NH_4^+ with a few differences. The largest TDN flux was measured in July at station 1 ($6.7x10^5$ μmol·d^{-1}). Higher fluxes in July were also measured at stations 8 and 3 ($5.6x10^5$ and $4.0x10^5$ μmol·d^{-1}, respectively). The lowest overall TDN flux was measured in November at station 6 ($9.0x10^4$ μmol·d^{-1}). Contrary to DIN and NH_4^+, porewater TDN concentrations only slightly decreased from July to November (Table 16). As a result, the TDN flux between July and November did not vary as much ($3.6x10^5$ and $1.7x10^5$ μmol·d^{-1}, respectively) for the four stations that have been sampled during both events (3, 4, 6 and 8) (**Figure 2**). Including all stations with porewater TDN concentrations, November fluxes are about ½ smaller than in July.

It is important to note that since DIN is larger than TDN in most instances, TDN fluxes estimated herein may not be reflective of the actual field conditions. This is a common problem with porewater measurements with high NH_4^+/DIN and organic nitrogen levels. Using the catalytic oxidation at high temperature with a TOC-VCPH Shimadzu instrument (Stubbins and Dittmar, 2012), measurements of TDN may be affected by analytical issues as not all the NH_4^+ (in our case) and/or organic nitrogen may have been oxidized, thus, leading to erroneously low TDN. In this study, this is indicated by the resulting negative DON levels for most porewaters, especially in July, when NH_4^+/DIN are not only the highest for the study period, but the concentrations are at least one order of magnitude higher than in the rest of the estuaries in South Texas (Douglas et al., 2017; Murgulet et al., 2015). Because there is no reliable way to measure DON directly, it is usually calculated from measured TDN and DIN values (DON=TDN-DIN). In this study, DIN exceeded TDN in 11 porewater samples and was lower in six samples. Since all DON measurements in July have been tampered with by the analytic limitations, there are no

DON fluxes available. In November, three porewater samples are available. Based on this, DON fluxes are $8.8x10^5$ µmol·d^{-1} at station 1, $4.1x10^4$ µmol·d^{-1} at station 4 and $1.3x10^4$ µmol·d^{-1} at station 8 (**Figure 2 and Figure 34**). The largest two DON fluxes correspond to the largest two DOC fluxes, indicating that carbon and nitrogen in the organic form may be available at similar locations.

DOC Fluxes

The average flux of DOC in Baffin Bay for the July and November events was $2.3x10^5$ µmol·d^{-1} (n=11). The largest DOC flux ($3.5x10^5$ µmol·d^{-1}) was measured at station 2 (**Table 15; Figure 34**) in July. The lowest flux of DOC ($5.0x10^4$ µmol·d^{-1}) was measured in November, at station 8. The highest porewater DOC measured each event occurred at station 1, followed by station 4 (available data are for July and November). Porewater DOC concentrations are steady or slightly increasing from July to November, thus larger overall fluxes in November at most stations, except at 1, are the result of larger SGD rates. At station 6, the DOC concentration remained similar between July and November, but when combined with a relatively higher SGD rate, resulted in DOC fluxes approximately three times greater in July.

Comparison of Subsurface and Surface Fluxes of Solutes

The surface water inflows modeled by TWDB (2016) were used to estimate fluxes of nutrients to the bay from surface runoff in January, June and July (**Table 17**). These modeled surface inflows include surface runoff from the three creeks that discharge into Baffin Bay and any land runoff resulting from precipitation within each of the watersheds. The fluxes were determined as the product of modeled surface inflows and the solute concentrations collected from each respective creek, at locations close to the discharge mouth to the bay. It is assumed that the concentrations of solutes in the creeks remained the same for each surveyed month. The

average fluxes presented in this section are derived from the full months of January, July, and November and for all three creeks discharging into Baffin Bay.

The average input of NO_3^- was $2.9x10^8$ μmol·d^{-1}. The maximum and minimum fluxes were both estimated to occur from Los Olmos Creek in January ($17x10^8$ μmol·d^{-1}) and November ($0.18x10^8$ μmol·d^{-1}), respectively. The average input of NO_2^- was $0.11x10^8$ μmol·d^{-1} with a maximum of $0.26x10^8$ μmol·d^{-1} in January and a minimum of $0.0052x10^8$ μmol·d^{-1} in July, both from Los Olmos. The three-month average flux of NH_4^+ was $2.7x10^8$ μmol·d^{-1} and while the maximum of $17x10^8$ μmol·d^{-1} occurred from Los Olmos Creek in January, the minimum of $0.13x10^8$ μmol·d^{-1} was estimated from the San Fernando Creek in January and November. The resulting average DIN flux was $5.7x10^8$ μmol·d^{-1} with the maximum and minimum of $34x10^8$ and $0.4x10^8$ μmol d^{-1} in January and November, respectively, both from Los Olmos Creek. This is mainly related to higher freshwater inflows that, based on our field assessments, likely to be overestimated by the model.

The average HPO_4^{2-} flux was $2.0x10^8$ μmol·d^{-1} with a maximum of $4.3x10^8$ μmol·d^{-1} from Petronila Creek in January and a minimum of $0.043x10^8$ μmol·d^{-1} from Los Olmos in November. The average $HSiO_3^-$ flux was $95x10^8$ μmol·d^{-1} with a maximum of $270x10^8$ μmol·d^{-1} from Petronila Creek in January and a minimum of $1.3x10^8$ μmol·d^{-1} from Los Olmos Creek in November.

Average flux of DOC for the creeks was estimated to be $320x10^8$ μmol·d^{-1} with maximum and minimum inputs from San Fernando Creek in January ($2{,}100x10^8$ μmol·d^{-1}) and November ($11x10^8$ μmol·d^{-1}). The average TDN flux was $89x10^8$ μmol·d^{-1} with a maximum of $640x10^8$ μmol·d^{-1} from Los Olmos Creek in January and a minimum of $2.9x10^8$ μmol·d^{-1} from San Fernando Creek. The DON flux was similar to the TDN flux, with an average of $84x10^8$ μmol·d^{-1}

and a maximum of $610x10^8$ µmol·d^{-1} from Los Olmos Creek in January and a minimum of $1.7x10^8$ µmol·d^{-1} from San Fernando Creek in January and November.

Creek	Event	NO_3^-	NO_2^-	NH_4^+	HPO_4^{2-}	$HSiO_3^-$	DOC	TDN	DIN	DON
Los Olmos	Jan.	17.0	0.26	17	4.0	120.0	2100	640	34	610
	Jul.	0.3	0.005	0.33	0.08	2.3	42	13	0.7	12
	Nov.	0.2	0.003	0.18	0.04	1.3	23	6.9	0.4	6.6
San Fernando	Jan.	1.1	0.04	0.13	0.63	4.3	11	2.9	1.2	1.7
	Jul.	2.8	0.1	0.33	1.6	11	28	7.5	3.2	4.3
	Nov.	1.1	0.04	0.13	0.63	4.3	11	2.9	1.2	1.7
Petronila	Jan.	1.6	0.2	2.4	4.3	270.0	230	51	4.2	47
	Jul.	1.4	0.2	2.1	3.7	240.0	200	44	3.6	40
	Nov.	1.2	0.16	1.8	3.1	200.0	170	37	3.1	34
Total watershed	Jan.	19.7	0.5	19.5	8.9	394.3	2341	693.9	39.4	658.7
	Jul.	4.5	0.3	2.8	5.4	253.3	270	64.5	7.5	56.3
	Nov.	2.5	0.2	2.1	3.8	205.6	204	46.8	4.7	42.3

Table 16: Freshwater inflow fluxes (µmol·$d^{-1}x10^8$) of NO_3^-, NO_2^-, NH_4^+, HPO_4^{2-}, $HSiO_3^-$ for July and November derived as the product of creek water nutrient concentration multiplied by creek discharge into Baffin Bay from TWDB (2016).

Nutrient fluxes were also estimated using the USGS stream gage daily discharge data for the San Fernando and Los Olmos Creeks (the Petronila Creek is ungaged) (**Table 18**). The streamflow data used is from the Los Olmos stream gage (USGS, 2017b), the San Fernando stream gage (USGS, 2017a), and from the Tranquitas Creek, a tributary of the San Fernando that joins the San Fernando Creek south of the previously mentioned stream gage (USGS, 2018).

During the period of the study, the Los Olmos Creek stream gage measured zero discharge; therefore, it is assumed that there was no solute input from Los Olmos Creek. In addition, no streamflow discharge data are available for Petronila Creek, leaving only the San Fernando Creek for comparison of solute flux rates with those derived from the modeled inflow. The average flux rate of NO_3^- across all events for the San Fernando Creek is $8.8x10^8$ µmol d^{-1} with the lowest output estimated for July ($2.3x10^8$ µmol d^{-1}) and the highest in January ($10x10^8$ µmol d^{-1}). The input of NO_2^- was on average $0.36x10^8$ µmol d^{-1} with the highest estimated input in November ($0.57x10^8$ µmol d^{-1}) and the lowest in July ($0.09x10^8$ µmol d^{-1}). The average input

of NH_4^+ was approximately $1.1x10^8$ μmol d^{-1} with the highest input being in November ($1.7x10^8$ μmol d^{-1}) and the lowest in July ($0.27x10^8$ μmol d^{-1}). The resulting input of DIN from the San Fernando Creek ($\overline{x}$: $10.5x10^8$ μmol d^{-1}) is larger than that derived from the modeled inflows (1.9 $x10^8$ μmol d-1). The highest input from stream gage estimates is estimated to have occurred in November ($17x10^8$) and the lowest in January ($2.6x10^8$ μmol d^{-1}), while the estimates from the modeled inflows are the largest in January (**Table 17 and Table 18**).

The average HPO_4^{2-} flux was $5.3x10^8$ μmol d^{-1} with the highest estimated rate in November ($8.4x10^8$ μmol d^{-1}) and the lowest in July ($1.3x10^8$ μmol d^{-1}). The average $HSiO_3^-$ flux was $35.7x10^8$ μmol d^{-1}, with the highest estimated rate in November ($57x10^8$ μmol d^{-1}) and the lowest in July ($9.0x10^8$ μmol d^{-1}). The average flux of TDN from the San Fernando Creek was $24.4x10^8$ μmol d^{-1} with the highest rate in November ($39x10^8$ μmol d^{-1}) and the lowest in July ($6.1x10^8$ μmol d^{-1}). The average DON input was $41.5x10^8$ μmol d^{-1}, with an estimated maximum in November ($22x10^8$ μmol d^{-1}) and minimum in July ($3.5x10^8$ μmol d^{-1}). DOC fluxes were on average $94.3x10^8$ μmol d^{-1} with the highest rate in November ($150x10^8$ μmol d^{-1}) and the lowest in July ($23x10^8$ μmol d^{-1}).

Overall, the estimated solute fluxes using the two surface inflows for the San Fernando Creek are in the same order of magnitude and closely related. Differences are noted among the months when the minimum or maximum are expected. However, given the close agreement among the two different estimates (i.e. using the modeled inflow and the stream gage data), we believe that the modeled inflow estimates may be used as substitutes for the gaged streamflow. As most gages are in general located a considerable distance upstream from the discharge mouth to the bay, the estimated solute fluxes may be overestimated as we observe in this study for San Fernando Creek. However, large solute fluxes were estimated from the Los Olmos Creek using

the ungagged flow (modeled), while there was no measurable discharge at the gage. Thus, the estimates from the ungagged inflow rates may be overestimating the flux of solutes into the bay in times with no rain or observed streamflow discharge to the bay.

Creek	Month	NO_3^-	NO_2^-	NH_4^+	HPO_4^{2-}	$HSiO_3^-$	DOC	TDN	DIN	DON
Los Olmos	Jan.	0	0	0	0	0	0	0	0	0
	Jul.	0	0	0	0	0	0	0	0	0
	Nov.	0	0	0	0	0	0	0	0	0
San Fernando	Jan.	10	0.41	1.2	6.1	41	110	28	12	16
	Jul.	2.3	0.090	0.27	1.3	9.0	23	6.1	2.6	3.5
	Nov.	14	0.57	1.7	8.4	57	150	39	17	22
Petronila	Jan.	--	--	--	--	--	--	--	--	--
	Jul.	--	--	--	--	--	--	--	--	--
	Nov.	--	--	--	--	--	--	--	--	--

Table 17: Solute fluxes ($\mu mol \cdot d^{-1} x 10^8$) for July and November derived as the product of stream nutrient concentration by sampling stations multiplied by *streamflow discharge from USGS water gages.* No streamflow data are available for the Petronila Creek, denoted as "--".

Given that SGD was measured spatially, across the Baffin Bay system, we applied a bay-wide seasonal average SGD rate to determine the bay-wide flux rate of solutes (in $\mu mol \cdot d^{-1}$ per $2.19x10^8$ m^2 bay system area) (**Table 19, Figure 36**). This, together with the average solute concentration of porewater, measured each season, indicates that a DIN contribution from the subsurface of $1{,}533.5x10^{11}$ $\mu mol \cdot d^{-1}$ is expected in July, while an almost three times lower rate of $479X10^{11}$ $\mu mol \cdot d^{-1}$, may occur in November. Similarly, orthophosphate (HPO_4^{2-}) and hydrogen silicate ($HSiO_3^-$) are also larger bay-wide in July ($22x10^{11}$ and $268x10^{11}$ $\mu mol \cdot d^{-1}$, respectively) than in November ($5.5x10^{11}$ and $172x10^{11}$ $\mu mol \cdot d^{-1}$, respectively), but of lower magnitudes overall than DIN. Average bay-wide DOC fluxes from SGD are larger in November ($710x10^{11}$ $\mu mol \cdot d^{-1}$) than July ($563x10^{11}$ $\mu mol \cdot d^{-1}$).

To estimate the overall importance of SGD in the bay-wide nutrient budget, surface runoff inputs were estimated using the Texas Water Development Board's Water Data for Texas modeled coastal freshwater inflows for the sub-watersheds feeding into the Baffin Bay system.

Solute concentrations from the three creeks discharging into Baffin Bay were used as the representative concentrations for the surface inflow fluxes (**Table 19, Figure 36**). Assuming that the solute concentration is constant across the seasons, a DIN of $39.4x10^{11}$ $\mu mol \cdot d^{-1}$ is expected in January, $7.5X10^{11}$ $\mu mol \cdot d^{-1}$ in July and $4.7x10^{11}$ $\mu mol \cdot d^{-1}$ in November. Orthophosphate (HPO_4^{2-}) and hydrogen silicate ($HSiO_3^-$) are also larger in January with a flux rates of ($8.9x10^{11}$ and $394x10^{11}$ $\mu mol \cdot d^{-1}$) followed by July ($5.4x10^{11}$ and $253x10^{11}$ $\mu mol \cdot d^{-1}$) and November ($3.8x10^{11}$ and $206x10^{11}$ $\mu mol \cdot d^{-1}$). Average DOC fluxes from surface runoff are larger January ($2{,}341x10^{11}$ $\mu mol \cdot d^{-1}$), followed by July ($270x10^{11}$ $\mu mol \cdot d^{-1}$) and November ($204x10^{11}$ $\mu mol \cdot d^{-1}$).

A comparison of bay-wide solute fluxes (**Figure 36**) indicates that DIN inputs, mainly in the form of ammonium, are almost two orders of magnitude higher in the SGD component than the surface runoff. DOC inputs are also larger in the SGD component in July and November. Inorganic nitrogen in the form of nitrate is likely to enter Baffin Bay from surface inputs while SGD may have larger contributions of nitrite. Orthophosphate and silicate (in the form of hydrogen silicate ion) are very similar in magnitudes.

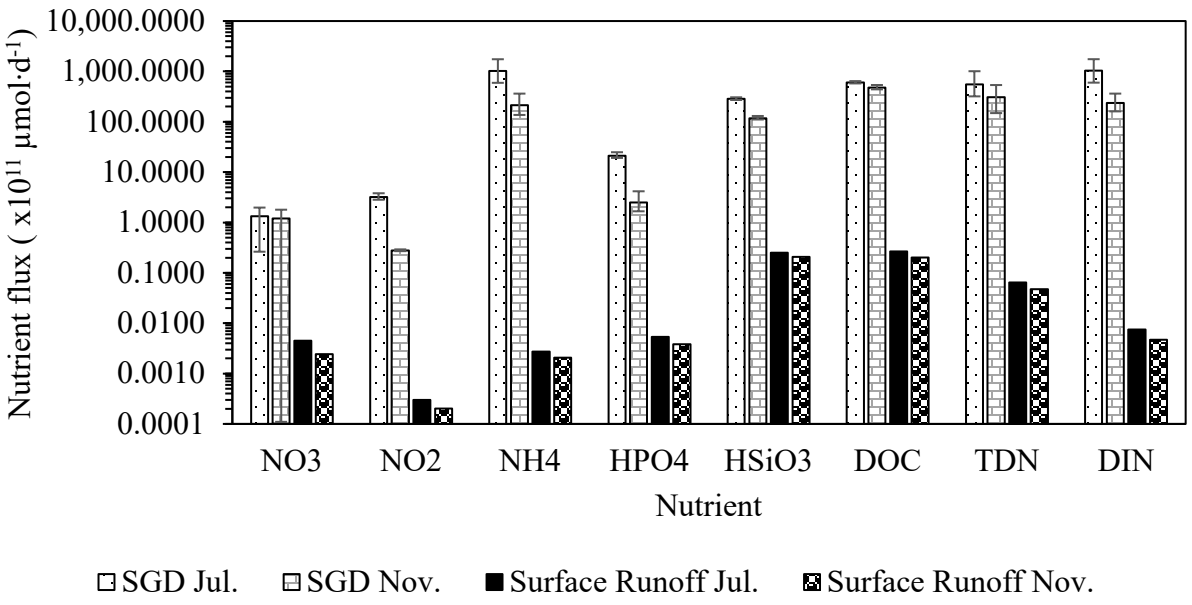

Figure 36: Comparison of solute fluxes derived from SGD and modeled surface runoff inflows. Error bars represent the maximum fluxes derived using the deep porewater nutrient concentration and the minimum fluxes determined using the shallow porewater depth range (**Tables 16, 19**).

Average solute flux	Event	Porewater depth	NO_3^-	NO_2^-	NH_4^+	HPO_4^{2-}	$HSiO_3^-$	DOC	TDN	DIN	DON
SGD flux: in ***µmol·d^{-1}x10^3 per 1 m^2 area***	July	Shallow	0.9	1.3	270.9	8.7	123.7	263.5	145.9	273.1	==
		Avg.	0.6	1.5	468.0	9.7	129.7	273.4	250.9	470.0	==
		Deep	0.1	1.7	796.5	11.3	139.7	293.1	460.8	798.3	==
	Nov.	Shallow	0.8	0.1	62.4	0.8	50.7	201.0	67.9	73.4	18.0
		Avg.	0.5	0.1	96.7	1.1	53.6	219.2	140.7	107.3	82.3
		Deep	0.0	0.1	165.4	1.9	59.5	245.3	244.9	165.5	146.6
SGD flux: in ***µmol·d^{-1}x10^{11}per bay area***	July	Shallow	1.98	2.83	593.2	19.1	270.9	577.2	319.6	598.0	==
		Avg.	1.33	3.20	1024.8	21.3	284.1	598.7	549.4	1029.4	==
		Deep	0.26	3.81	1744.3	24.8	306.0	641.9	1009.1	1748.3	==
	Nov.	Shallow	1.79	0.27	136.6	1.67	111.0	440.1	148.6	160.8	39.37
		Avg.	1.20	0.28	211.8	2.5	117.4	480.1	308.2	235.1	180.3
		Deep	0.0	0.29	362.2	4.16	130.3	537.1	536.3	362.5	321.2
Total watershed flux: in ***µmol·d^{-1}x10^8***	Jan.	---	19.7	0.5	19.5	8.9	394.3	2341	693.9	39.4	658.7
	Jul.	---	4.5	0.3	2.8	5.4	253.3	270	64.5	7.5	56.3
	Nov.	---	2.5	0.2	2.1	3.8	205.6	204	46.8	4.7	42.3

Table 18: Average solute fluxes for July and November derived from the bay-wide mobile continuous SGD estimates in µmol·d^{-1}x10^3 per 1 m^2 and in µmol·d^{-1}x10^{11} per bay area (2.19 x10^8

m^2) along with a total watershed flux (modeled) in $\mu mol \cdot d^{-1} x 10^8$. DON concentrations affected by analytical limitations of TDN measurements in porewater, are denoted by "==". SGD-derived fluxes per 1 m^2 and per bay area were determined using nutrient concentrations derived from average

SUMMARY

A key goal of this study is to understand the role of SGD and nutrient transport to Baffin Bay in order to improve environmental flow recommendations and nutrient criteria in Texas estuaries. SGD rates are expected to change across the hydroclimatic gradient in response to changes in precipitation rates, aquifer recharge rates, hydraulic gradients, and riverine inputs. Five of the seven bays along the Texas Gulf Coast have been classified as being potentially affected (≥67%) by increased salinization and decreases in water quality, productivity, sediment, and nutrient transport due to reductions in freshwater inflow. These adverse conditions have major impacts on the life cycles and success of many marine species, with potential repercussions throughout the food web. However, there is a lack of understanding of the role SGD plays in alleviating or contributing to these problems. Despite this, although, SGD has been recognized as an important component of the hydrologic and biogeochemical systems that link terrestrial waters to marine environments in many coastal areas. Due to the exceptionally high concentrations of nutrients and organic matter accumulated in aquifers, SGD may fuel bacterial respiration, leading to hypoxic conditions in estuaries.

Groundwater contribution for Baffin Bay estimated as part of this study is representative of mostly dry conditions during January, July, and November 2016. Groundwater discharge rates vary spatially and by season at different locations. However, the average of all SGD rates derived from continuous mobile ^{222}Rn surveys across the entire bay system exhibited some change between July (35.8 $cm \cdot d^{-1}$) and November (22.7 $cm \cdot d^{-1}$). SGD rates estimated from the ^{226}Ra inventory across the bay reveal very small changes from July (6.5 $cm \cdot d^{-1}$) to November (1.6 $cm \cdot d^{-1}$). Although not of same magnitude, these different estimates are in very close agreement, given the uncertainties associated with each measurement. ^{222}Rn estimates provide a

total SGD estimate, which includes both fresh (i.e. groundwater) and saline (i.e. recirculated seawater) inputs. The difference between the total (i.e. ^{222}Rn) and saline recirculated (i.e. ^{226}Ra) SGD estimates has been associated with the freshwater input in an unconfined sandy coastal aquifer. In our study, the two estimates may indicate that at least half of the SGD input may be due to seawater recirculation or saline groundwater input, with the two, fresh and saline inputs, on a similar order of magnitude.

Nutrient concentrations measured in the interstitial porewater vary spatially and temporally. In particular, ammonium concentrations were found to be largely elevated (by one or two orders of magnitude) when compared to other estuaries in South Texas, with the largest measured concentrations in porewater in July (5,531 $\mu mol \cdot L^{-1}$) and a minimum in January (538.6 $\mu mol \cdot L^{-1}$). In the Baffin Bay system, SGD-derived nutrient fluxes are not so much a function of changes in hydrologic conditions across seasons (i.e. changes in SGD rates) but more dependent on spatial and temporal nutrient concentrations in the porewater. To a small extent, nutrient fluxes are influenced by spatial and temporal changes in SGD rates. This study shows that average SGD-derived nutrient fluxes, in the form of dissolved inorganic nitrogen (DIN), per $1m^2$ area, are more than three times higher in July ($470x10^3$ $\mu mol \cdot d^{-1}$) than in November ($110 x10^3$ $\mu mol \cdot d^{-1}$). Similarly, orthophosphate (HPO_4^{2-}) and silicate ($HSiO_3^-$) are also larger in July ($9.72x10^3$ and $130x10^3$ $\mu mol \cdot d^{-1}$, respectively) than in November ($1.14x10^3$ and $53.6x10^3$ $\mu mol \cdot d^{-1}$, respectively), but with lower magnitudes overall than DIN. Average DOC fluxes from SGD are larger in July ($273x10^3$ $\mu mol \cdot d^{-1}$) than November ($219x10^3$ $\mu mol \cdot d^{-1}$), as a result of increased SGD in July.

Given that SGD was measured spatially across the entire Baffin Bay system, we applied a bay-wide seasonal average SGD rate to determine the bay-wide solute flux rate (per $2.19x10^8$ m^2

bay area). This, together with the average solute concentration of porewater measured each season, indicates that a DIN contribution from the subsurface of 1,029.4x10^{11} μmol·d^{-1} is expected in July, while an almost three times lower rate of 235.1x10^{11} μmol·d^{-1}, may occur in November. Similarly, orthophosphate (HPO_4^{2-}) and hydrogen silicate ($HSiO_3^-$) are also larger bay-wide in July (21.3x10^{11} and 284.1x10^{11} μmol·d^{-1}, respectively) than in November (2.5x10^{11} and 117.4x10^{11} μmol·d^{-1}, respectively), but of lower magnitudes overall than DIN. Average bay-wide DOC fluxes from SGD are smaller in November (480.1x10^{11} μmol·d^{-1}) than July (598.7x10^{11} μmol·d^{-1}).

To estimate the overall importance of SGD in the bay-wide nutrient budget, surface runoff inputs were estimated using the Texas Water Development Board's Water Data for Texas modeled coastal freshwater inflows for the sub-watersheds feeding into the Baffin Bay system. Solute concentrations from the three creeks discharging into Baffin Bay were used as the representative concentrations for the surface inflow fluxes. Assuming that the solute concentration is constant across the seasons, a DIN flux of 39.4x10^7 μmol·d^{-1} is expected in January, 75X10^7 μmol·d^{-1} in July and 47x10^7 μmol·d^{-1} in November. Orthophosphate (HPO_4^{2-}) and hydrogen silicate ($HSiO_3^-$) are also larger in January with a flux rates of (89x10^7 and 3948.9x10^7 μmol·d^{-1}) followed by July (54x10^7 and 2497.7x10^7 μmol·d^{-1}) and November (38x10^7 and 2065.8x10^7 μmol·d^{-1}). Average DOC fluxes from surface runoff are larger in January (2,3672x10^7 μmol·d^{-1}), followed by lower values in July (2671.9x10^7 μmol·d^{-1}) and November (2017.2x10^7 μmol·d^{-1}).

A comparison of bay-wide solute fluxes indicates that DIN inputs, mainly in the form of ammonium, are almost two orders of magnitude higher in the SGD component than the surface runoff. DOC inputs are also larger in the SGD component in July and November. Inorganic

nitrogen in the form of nitrate is likely to enter Baffin Bay from surface inputs while SGD may have larger contributions of nitrite. Orthophosphate and silicate (in the form of hydrogen silicate ion) are very similar in magnitudes. Therefore, the nutrient input associated with SGD, regardless of its nature (i.e. fresh or saline; groundwater or recirculated saline), is likely significant in this shallow bay system. Persistent winds are likely the dominant driver of seawater recirculation, while episodic rain events may enhance the fresher SGD input in this bay. Both scenarios can lead to diffusion of porewater solutes into the water column.

This project builds upon previous efforts to estimate the impacts of temporal and spatial variation of nutrient fluxes to Texas coastal embayments through additional measurements conducted in the Baffin Bay system. Results from the phase I and II of this effort (and ongoing projects) indicate that SGD rates in Nueces and Corpus Christi Bays increased considerably following spring rain events, while those in the Mission-Aransas Estuary and Upper Laguna Madre Estuary show an overall highly limited response to hydroclimatic conditions (i.e. lower SGD rates), in general. Overall, these results find SGD rates in the Nueces Estuary to be greater than those in the Mission-Aransas Estuary, the Upper Laguna Madre Estuary, and the Baffin Bay Estuary. Measured SGD-derived nutrient fluxes in the semi-arid South Texas estuaries are shown to be significant, with the largest magnitudes occurring between late summer and early fall, potentially enhancing the occurrence of algae blooms (i.e. Texas Brown Tide). In Baffin Bay, although the SGD rates are among the lowest, the daily nutrient fluxes are larger when compared to the rest of the bays as a result of much more elevated porewater nutrient concentrations. These initial studies are indicative of a strong SGD component that, although patchy, is likely contributing to the water column nutrient concentrations and microbial respiration, at least under the environmental conditions in which the sampling regime took place. Furthermore, due to the

diffuse and heterogeneous nature of SGD input and the spatial and temporal variability in groundwater end-member concentrations (caused by different hydraulic conditions), increased spatial and temporal monitoring of SGD rates along the hydroclimatic gradient of Texas are necessary to project input loads to these systems. This work is critically important for understanding nutrient dynamics in Texas estuaries and helps in setting nutrient criteria by Texas Commission on Environmental Quality (TCEQ) and the US Environmental Protection Agency (US EPA).

References Cited

Advanced Geosciences, I., (2017) SuperSting Marine Resistivity. Advanced Geosciences, Inc.

Alaniz, R.T., Goodwin, R.H. (1974) Recent sediments of a hypersaline estuarine bay: Gulf Coast Association of Geological Societies. Transactions 24, 308-313.

Ashworth, J.B., Hopkins, J., (1995) Major and minor aquifers of Texas, in: Board, T.W.D. (Ed.), p. 69.

Behrens, E.W. (1963) Buried Pleistocene river valleys in Aransas and Baffin bays, Texas. Publications of the Institute of Marine Science, University of Texas 9, 7-18.

Behrens, E.W. (1966) Surface salinities for Baffin Bay and Laguna Madre, Texas, April 1964-March 1966. Publications of the Institute of Marine Science, University of Texas 11, 168-179.

Bighash, P., Murgulet, D. (2015) Application of factor analysis and electrical resistivity to understand groundwater contributions to coastal embayments in semi-arid and hypersaline coastal settings. Science of The Total Environment 532, 688-701.

Boyd, P.W., Watson, A.J., Law, C.S., Abraham, E.R., Trull, T., Murdoch, R., Bakker, D.C., Bowie, A.R., Buesseler, K., Chang, H. (2000) A mesoscale phytoplankton bloom in the polar Southern Ocean stimulated by iron fertilization. Nature 407, 695-702.

Breier, J.A., Breier, C.F., Edmonds, H.N. (2010) Seasonal dynamics of dissolved Ra isotopes in the semi-arid bays of south Texas. Marine Chemistry 122, 39-50.

Breuer, J.P. (1957) An ecological survey of Baffin and Alazan Bays, Texas: Publ., Inst. Mar. Sci 4, 134-155.

Brock, D. (2001) Uncertainties in Individual Estuary N-Loading Assessments. Nitrogen Loading in Coastal Water Bodies: An Atmospheric Perspective, 171-185.

Brown, R.M., McClelland, N.I., Deininger, R.A., Tozer, R.G. (1970) A Water Quality Index - Do We Dare.

Burnett, W.C., Dulaiova, H. (2003) Estimating the dynamics of groundwater input into the coastal zone via continuous radon-222 measurements. Journal of Environmental Radioactivity 69, 21-35.

Burnett, W.C., Taniguchi, M., Oberdorfer, J. (2001) Measurement and significance of the direct discharge of groundwater into the coastal zone. Journal of Sea Research 46, 109-116.

Buskey, E.J., Liu, H., Collumb, C., Bersano, J.G.F. (2001) The Decline and Recovery of a Persistent Texas Brown Tide Algal Bloom in the Laguna Madre (Texas, USA). Estuaries 24, 337-346.

Buzas-Stephens, P., Livsey, D.N., Simms, A.R., Buzas, M.A. (2014) Estuarine foraminifera record Holocene stratigraphic changes and Holocene climate changes in ENSO and the North American monsoon: Baffin Bay, Texas. Palaeogeography, Palaeoclimatology, Palaeoecology 404, 44-56.

Cerdà-Domènech, M., Rodellas, V., Folch, A., Garcia-Orellana, J. (2017) Constraining the temporal variations of Ra isotopes and Rn in the groundwater end-member: Implications for derived SGD estimates. Science of the Total Environment 595, 849-857.

Chaillou, G., Couturier, M., Tommi-Morin, G., Rao, A.M. (2014) Total alkalinity and dissolved inorganic carbon production in groundwaters discharging through a sandy beach. Procedia Earth and Planetary Science 10, 88-99.

Charette, M.A., Buesseler, K.O., Andrews, J.E. (2001) Utility of radium isotopes for evaluating the input and transport of groundwater-derived nitrogen to a Cape Cod estuary. Limnology and Oceanography 46, 465-470.

Conley, D.J., Paerl, H.W., Howarth, R.W., Boesch, D.F., Seitzinger, S.P., Havens, K.E., Lancelot, C., Likens, G.E. (2009) Controlling Eutrophication: Nitrogen and Phosphorus. Science 323, 1014-1015.

Corbett, D.R., Burnett, W.C., Cable, P.H., Clark, S.B. (1998) A multiple approach to the determination of radon fluxes from sediments. Journal of Radioanalytical and Nuclear Chemistry 236, 247-252.

Corbett, D.R., Dillon, K., Burnett, W., Chanton, J. (2000) Estimating the groundwater contribution into Florida Bay via natural tracers, 222Rn and CH4. Limnology and Oceanography 45, 1546-1557.

Cyronak, T., Santos, I.R., Erler, D.V., Eyre, B.D. (2013) Groundwater and porewater as major sources of alkalinity to a fringing coral reef lagoon (Muri Lagoon, Cook Islands). Biogeosciences 10, 2467-2480.

Dalrymple, D.W., (1964) Recent Sedimentary Facies of Baffin Bay, Texas, Geology. Rice University, University Microfilms, Inc., Ann Arbor, Michigan.

de Baar, H.J., de Jong, J.T., Nolting, R.F., Timmermans, K.R., van Leeuwe, M.A., Bathmann, U., van der Loeff, M.R., Sildam, J. (1999) Low dissolved Fe and the absence of diatom blooms in remote Pacific waters of the Southern Ocean. Marine Chemistry 66, 1-34.

Dickson, A.G., Sabine, C.L., Christian, J.R. (2007) Guide to best practices for ocean CO2 measurements.

Dimova, N., Burnett, W., Horwitz, E., Lane-Smith, D. (2007) Automated measurement of 224Ra and 226Ra in water. Applied radiation and isotopes 65, 428-434.

Dimova, N.T., Burnett, W.C., Speer, K. (2011) A natural tracer investigation of the hydrological regime of Spring Creek Springs, the largest submarine spring system in Florida. Continental Shelf Research 31, 731-738.

Dimova, N.T., Swarzenski, P.W., Dulaiova, H., Glenn, C.R. (2012) Utilizing multichannel electrical resistivity methods to examine the dynamics of the fresh water–seawater interface in two Hawaiian groundwater systems. Journal of Geophysical Research: Oceans 117.

Dong, L.F., Sobey, M.N., Smith, C.J., Rusmana, I., Phillips, W., Stott, A., Osborn, A.M., Nedwell, D.B. (2011) Dissimilatory reduction of nitrate to ammonium, not denitrification or anammox, dominates benthic nitrate reduction in tropical estuaries. Limnology and Oceanography 56, 279-291.

Dortch, Q. (1990) The interaction between ammonium and nitrate uptake in phytoplankton. Marine Ecology Progress Series, 183-201.

Douglas, A., Murgulet, D., Wetz, M.S., Spalt, N., (2017) Evaluating Groundwater Inflow and Nutrient Transport to Texas Coastal Embayments Phase II. Texas General Land Office, Texas General Land Office.

Driese, S.G., Nordt, L.C., Lynn, W.C., Stiles, C.A., Mora, C.I., Wilding, L.P. (2005) Distinguishing climate in the soil record using chemical trends in a Vertisol climosequence from the Texas Coast Prairie, and application to interpreting Paleozoic paleosols in the Appalachian Basin, USA. Journal of Sedimentary Research 75, 339-349.

Dulaiova, H., Burnett, W.C., Chanton, J.P., Moore, W.S., Bokuniewicz, H.J., Charette, M.A., Sholkovitz, E. (2006) Assessment of groundwater discharges into West Neck Bay, New York, via natural tracers. Continental Shelf Research 26, 1971-1983.

Fetter, C.W. (2001) Applied Hydrogeology, Fourth Edition ed. Prentice-Hall, Inc., Upper Sadle River, New Jersey.

Fisk, H.N. (1959) Padre Island and the Laguna Madre flats, coastal south Texas. 2nd Coastal Geography Confer, 103-151.

Folk, R.L., Siedlecka, A. (1974) The “schizohaline” environment: its sedimentary and diagenetic fabrics as exemplified by Late Paleozoic rocks of Bear Island, Svalbard. Sedimentary Geology 11, 1-15.

Fowler, D., Coyle, M., Skiba, U., Sutton, M.A., Cape, J.N., Reis, S., Sheppard, L.J., Jenkins, A., Grizzetti, B., Galloway, J.N. (2013) The global nitrogen cycle in the twenty-first century. Phil. Trans. R. Soc. B 368, 20130164.

Garcia-Orellana, J., Rodellas, V., Casacuberta, N., Lopez-Castillo, E., Vilarrasa, M., Moreno, V., Garcia-Solsona, E., Masque, P. (2013) Submarine groundwater discharge: Natural radioactivity accumulation in a wetland ecosystem. Marine Chemistry 156, 61-72.

George, P.G., Mace, R., Petrossian, R., (2011) Aquifers of Texas: Texas Water Development Board Report 380, p. 182.

Giblin, A.E., Gaines, A.G. (1990) Nitrogen inputs to a marine embayment: the importance of groundwater. Biogeochemistry 10, 309-328.

Giblin, A.E., Weston, N.B., Banta, G.T., Tucker, J., Hopkinson, C.S. (2010) The Effects of Salinity on Nitrogen Losses from an Oligohaline Estuarine Sediment. Estuaries and Coasts 33, 1054-1068.

Glass, C., Silverstein, J. (1999) Denitrification of High-Nitrate, High-Salinity Wastewater. Water Resources Research 33, 223-229.

Heidelberg, J.F., Seshadri, R., Haveman, S.A., Hemme, C.L., Paulsen, I.T., Kolonay, J.F., Eisen, J.A., Ward, N., Methe, B., Brinkac, L.M. (2004) The genome sequence of the anaerobic, sulfate-reducing bacterium Desulfovibrio vulgaris Hildenborough. Nature biotechnology 22, 554.

Holmes, R.M., Peterson, B.J., Deegan, L.A., Hughes, J.E., Fry, B. (2000) Nitrogen biogeochemistry in the oligohaline zone of a New England estuary. Ecology 81, 416-432.

Hu, C., Muller-Karger, F.E., Swarzenski, P.W. (2006) Hurricanes, submarine groundwater discharge, and Florida's red tides. Geophysical Research Letters 33.

Jolly, I.D., McEwan, K.L., Holland, K.L. (2008) A review of groundwater-surface water interactions in arid/semi-arid wetlands and the consequences of salinity for wetland ecology. Ecohydrology 1, 43-58.

Kahn, S.M.M.N., Kumar, A.R. (2012) Interpretation of Groundwater Quality using Correlation and Linear Regression Analysis from Tiruchengode taluk, Namakkal district, Tamilnadu, India. Journal of Chemical and Pharmaceutical Research 4, 4514-4521.

Kattner, G. (1999) Storage of dissolved inorganic nutrients in seawater: poisoning with mercuric chloride. Marine Chemistry 67, 61-66.

Katz, B.G., Coplen, T.B., Bullen, T.D., Davis, J.H. (1997) Use of chemical and isotopic tracers to characterize the interactions between ground water and surface water in mantled karst. Groundwater 35, 1014-1028.

Kelly, R., Moran, S. (2002) Seasonal changes in groundwater input to a well-mixed estuary estimated using radium isotopes and implications for coastal nutrient budgets. Limnology and Oceanography 47, 1796-1807.

Khalil, M.K., Rifaat, A.E. (2013) Seasonal fluxes of phosphate across the sediment-water interface in Edku Lagoon, Egypt. Oceanologia 55, 219-233.

Khan, S., Kumar, A.R. (2012) Interpretation of Groundwater Quality using Correlation and Linear Regression Analysis from Tiruchengode taluk, Namakkal district, Tamilnadu, India. Journal of Chemical and Pharmaceutical Research 4, 4514-4521.

Kim, G., Burnett, W., Dulaiova, H., Swarzenski, P., Moore, W. (2001) Measurement of 224Ra and 226Ra activities in natural waters using a radon-in-air monitor. Environmental science & technology 35, 4680-4683.

Knee, K.L., Garcia-Solsona, E., Garcia-Orellana, J., Boehm, A.B., Paytan, A. (2011a) Using radium isotopes to characterize water ages and coastal mixing rates: A sensitivity analysis. Limnology and Oceanography: Methods 9, 380-395.

Knee, K.L., Garcia-Solsona, E., Garcia-Orellana, J., Boehm, A.B., Paytan, A. (2011b) Using radium isotopes to characterize water ages and coastal mixing rates: A sensitivity analysis. Limnology and Oceanography-Methods 9, 380-395.

Krest, J.M., Moore, W.S., Gardner, L.R., Morris, J.T. (2000) Marsh nutrient export supplied by groundwater discharge: Evidence from radium measurements. Global Biogeochemical Cycles 14, 167-176.

Kristensen, G.H., Jepsen, S. (1991) Biological Denitrification of Waste Water from Wet Lime–Gypsum Flue Gas Desulphurization Plants. Water Science and Technology 23, 691-700.

Kroeger, K.D., Swarzenski, P.W., Greenwood, W.J., Reich, C. (2007) Submarine groundwater discharge to Tampa Bay: Nutrient fluxes and biogeochemistry of the coastal aquifer. Marine Chemistry 104, 85-97.

Lambert, M.J., Burnett, W.C. (2003) Submarine groundwater discharge estimates at a Florida coastal site based on continuous radon measurements. Biogeochemistry 66, 55-73.

Lamontagne, S., La Salle, C.L.G., Hancock, G.J., Webster, I.T., Simmons, C.T., Love, A.J., James-Smith, J., Smith, A.J., Kämpf, J., Fallowfield, H.J. (2008) Radium and radon radioisotopes in regional groundwater, intertidal groundwater, and seawater in the Adelaide Coastal Waters Study area: implications for the evaluation of submarine groundwater discharge. Marine Chemistry 109, 318-336.

Lee, J.-M., Kim, G. (2006) A simple and rapid method for analyzing radon in coastal and ground waters using a radon-in-air monitor. Journal of environmental radioactivity 89, 219-228.

Lee, M.W., Collett, T.S., (2006) Gas hydrate and free gas saturations estimated from velocity logs on Hydrate Ridge, offshore Oregon, USA, in: Tréhu, A.M., Bohrmann, G., Torres, M.E., Colwell, F.S. (Eds.), Proceedings of the Ocean Drilling Program, Scientific Results, pp. 1-25.

Loáiciga, H.A. (2006) Modern-age buildup of CO2 and its effects on seawater acidity and salinity. Geophysical Research Letters 33.

Lohse, E.A., (1955) Dynamic geology of the modern coastal region, northwest Gulf of Mexico, in: Hough, J.L. (Ed.), Finding Ancient Shorelines: A Symposium with Discussions. Society of Economic Paleontologists and Mineralogists Special Publication, pp. 99-104.

Manheim, F.T., Krantz, D.E., Bratton, J.F. (2004) Studying ground water under Delmarva coastal bays using electrical resistivity. Groundwater 42, 1052-1068.

Martin, J.H., Coale, K., Johnson, K., Fitzwater, S., Gordon, R., Tanner, S., Hunter, C., Elrod, V., Nowicki, J., Coley, T. (1994) Testing the iron hypothesis in ecosystems of the equatorial Pacific Ocean. Nature 371, 123.

Matson, E.A. (1993) Nutrient flux through soils and aquifers to the coastal zone of Guam (Mariana Islands). Limnology and Oceanography 38, 361-371.

Matson, E.A., Brinson, M.M. (1985) Sulfate enrichments in estuarine waters of North Carolina. Estuaries and Coasts 8, 279-289.

Militello, A., (1998) Hydrodynamics of wind-dominated, shallow embayments. Florida Institute of Technology, Melbourne, FL, p. 232.

Millero, F.J. (1993) What is PSU? Oceanography 6, 67-67.

Millero, F.J., Feistel, R., Wright, D.G., McDougall, T.J. (2008) The composition of Standard Seawater and the definition of the Reference-Composition Salinity Scale. Deep Sea Research Part I: Oceanographic Research Papers 55, 50-72.

Mitsch, W.J., Gosselink, J.G. (2015) Wetlands. John Wiley & Sons, Inc., Hoboken, NJ.

Moore, W., (1996) Large groundwater inputs to coastal waters revealed by 226Ra enrichments.--p. 612-614. En: Nature (London)(United Kingdom).--Vol. 380, no. 6575 (1996).

Moore, W.S. (2006) Radium isotopes as tracers of submarine groundwater discharge in Sicily. Continental Shelf Research 26, 852-861.

Moore, W.S. (2010) The effect of submarine groundwater discharge on the ocean. Annual review of marine science 2, 59-88.

Murgulet, D., Murgulet, V., Spalt, N., Douglas, A., Hay, R.G. (2016) Impact of hydrological alterations on river-groundwater exchange and water quality in a semi-arid area: Nueces River, Texas. Sci Total Environ 572, 595-607.

Murgulet, D., Trevino, M., Douglas, A., Spalt, N., Hu, X., Murgulet, V. (2018) Temporal and spatial fluctuations of groundwater-derived alkalinity fluxes to a semiarid coastal embayment. Sci Total Environ 630, 1343-1359.

Murgulet, D., Wetz, M.S., Douglas, A., McBee, W., Spalt, N., Linares, K., (2015) Evaluating Groundwater Inflow and Nutrient Transport to Texas Coastal Embayments. Texas General Land Office, Corpus Christi, TX.

NAAS, K., (2017) Kingsville, TX - Global Summary of the Month, in: NOAA (Ed.). NOAA, https://www.ncdc.noaa.gov/cdo-web/datasets/GSOM/stations/GHCND:USC00414810/detail.

NBBEST, (2011) Environmental Flows Recommendations Report. Final Submission to the Environmental Flows Advisory Group, Nueces River and Corpus Christi and Baffin Bays Basin and Bay Area Stakeholders Committee, and Texas Commission on Environmental Quality. Nueces River and Corpus Christi and Baffin Bays Basin and Bay Expert Science Team.

Network, T.C.O.O., (2016) Historical Standard Meteorological Data - Station BABT2 - 8776604 - Baffin Bay, TX, in: Network, T.C.O.O. (Ed.). National Oceanic and Atmospheric Administration, National Data Buoy Center.

NOAA (National Oceanic and Atmospheric Administration), (2014) National Weather Service.

Nyquist, J.E., Freyer, P.A., Toran, L. (2008) Stream bottom resistivity tomography to map ground water discharge. Groundwater 46, 561-569.

Paerl, H.W. (1997) Coastal eutrophication and harmful algal blooms: Importance of atmospheric deposition and groundwater as "new" nitrogen and other nutrient sources. Limnology and Oceanography 42, 1154-1165.

Price, W.A. (1936) Reynosa problem of South Texas, and origin of caliche.

Prokopenko, M., Sigman, D., Berelson, W., Hammond, D., Barnett, B., Chong, L., Townsend-Small, A. (2011) Denitrification in anoxic sediments supported by biological nitrate transport. Geochimica et Cosmochimica Acta 75, 7180-7199.

RCRA SOP, (2009) Protocol for Groundwater/Surface Water Interface Sampling Using a Pore Water Sampler, in: Beneski, B., Bonenfant, E. (Eds.), Standard Operating Procedure Change Record. Department of Environmental Protection Bureau of Remediation and Waste Management RCRA Program.

Rebich, R.A., Houston, N.A., Mize, S.V., Pearson, D.K., Ging, P.B., Evan Hornig, C. (2011) Sources and Delivery of Nutrients to the Northwestern Gulf of Mexico from Streams in the South-Central United States. JAWRA Journal of the American Water Resources Association 47, 1061-1086.

Rusnak, G.A., (1960) Sediments of Laguna Madre, Texas, in: Shepard, F.P., Phleger, F.B., Van Andal, T.H. (Eds.), Recent Sediments, Northwest Gulf of Mexico. American Association of Petroleum Geologists, Tulsa OK, pp. 153-196.

Rysgaard, S., Thastum, P., Dalsgaard, T., Christensen, P.B., Sloth, N.P. (1999) Effects of salinity on NH4+ adsorption capacity, nitrification, and denitrification in Danish estuarine sediments. Estuaries 22, 21-30.

Samouëlian, A., Cousin, I., Tabbagh, A., Bruand, A., Richard, G. (2005) Electrical resistivity survey in soil science: a review. Soil and Tillage research 83, 173-193.

Santos, I.R., Cook, P.L., Rogers, L., Weys, J.d., Eyre, B.D. (2012) The "salt wedge pump": Convection-driven pore-water exchange as a source of dissolved organic and inorganic carbon and nitrogen to an estuary. Limnology and Oceanography 57, 1415-1426.

Schulz, H.D., Dahmke, A., Schinzel, U., Wallmann, K., Zabel, M. (1994) Early diagenetic processes, fluxes, and reaction rates in sediments of the South Atlantic. Geochimica et Cosmochimica Acta 58, 2041-2060.

Service), U.U.S.D.o.A.a.N.R.C., (2012) National Soil Survey Handbook, Title 430-VI.

Simms, A.R., Aryal, N., Miller, L., Yokoyama, Y. (2010) The incised valley of Baffin Bay, Texas: a tale of two climates. Sedimentology 57, 642-669.

Smith, C.G., Robbins, L.L., (2012) Surface-Water Radon-222 Distribution along the Western-Central Florida Shelf. U.S. Geological Survey, p. 26.

Smith, R.L., Howes, B.L., Duff, J.H. (1991) Denitrification in nitrate-contaminated groundwater: occurrence in steep vertical geochemical gradients. Geochimica et Cosmochimica Acta 55, 1815-1825.

Sun, Y., Torgersen, T. (1998) The effects of water content and Mn-fiber surface conditions on 224Ra measurement by 220Rn emanation. Marine Chemistry 62, 299-306.

Swarzenski, P. (2007) U/Th series radionuclides as coastal groundwater tracers. Chemical Reviews 107, 663-674.

Takahashi, T., Broecker, W.S., Bainbridge, A.E. (1981) The alkalinity and total carbon dioxide concentration in the world oceans. Carbon cycle modelling, SCOPE 16, 271-286.

TCEQ, (2012) Surface Water Quality Monitoring Procedures, Volume 1: Physical and Chemical Monitoring Methods, Austin, TX.

Testa, J.M., Charette, M.A., Sholkovitz, E.R., Allen, M.C., Rago, A., Herbold, C.W. (2002) Dissolved iron cycling in the subterranean estuary of a coastal bay: Waquoit Bay, Massachusetts. Biol Bull 203, 255-256.

TWDB, (2016) Hydrology for the Laguna Madre Estuary Watershed, in: Studies, C.f.W.S. (Ed.).

Uddameri, V., Singaraju, S., Hernandez, E.A. (2013) Temporal variability of freshwater and pore water recirculation components of submarine groundwater discharges at Baffin Bay, Texas. Environmental Earth Sciences 71, 2517-2533.

Urquidi-Gaume, M., Santos, I.R., Lechuga-Deveze, C. (2016) Submarine groundwater discharge as a source of dissolved nutrients to an arid coastal embayment (La Paz, Mexico). Environmental earth sciences 75, 1.

USGS, (2017a) USGS 08211900 San Fernando Ck at Alice, TX, in: Inquiries, U.T.W.S.C.W.-D. (Ed.). National Water Information System: Web Interface.

USGS, (2017b) USGS 08212400 Los Olmos Ck nr Falfurrias, TX, in: Center, U.T.W.S. (Ed.). National Water Information System: Web Interface.

USGS, (2018) USGS 08212300 Tranquitas Ck at Kingsville, TX, in: Inquiries, U.T.W.S.C.W.-D. (Ed.). National Water Information System: Web Interface.

Wang, D., Chen, Z., Wang, J., Xu, S., Yang, H., Chen, H., Yang, L., Hu, L. (2007) Summer-time denitrification and nitrous oxide exchange in the intertidal zone of the Yangtze Estuary. Estuarine, Coastal and Shelf Science 73, 43-53.

Wanninkhof, R. (1992) Relationship between wind speed and gas exchange over the ocean. Journal of Geophysical Research: Oceans 97, 7373-7382.

Waterstone, Parsons, (2003) Groundwater availability of the central Gulf Coast aquifer--Numerical simulations to 2050, Central Gulf Coast, Texas.

Wetz, M.S., (2015) Baffin Bay Volunteer Water Quality Monitoring Study: Synthesis of May 2013-July 2015 Data. Coastal Bend Bays & Estuaries Program, pp. 1-28.

Wetz, M.S., Cira, E.K., Sterba-Boatwright, B., Montagna, P.A., Palmer, T.A., Hayes, K.C. (2017) Exceptionally high organic nitrogen concentrations in a semi-arid South Texas estuary susceptible to brown tide blooms. Estuarine, Coastal and Shelf Science 188, 27-37.

Winn, C.D., Li, Y.-H., Mackenzie, F.T., Karl, D.M. (1998) Rising surface ocean dissolved inorganic carbon at the Hawaii Ocean Time-series site. Marine Chemistry 60, 33-47.

Wood, W.W., (1976) Guidelines for collection and field analysis of ground-water samples for selected unstable constituents. US Geological Survey.

WSDE, (2017) Nitrogen from Atmospheric Deposition. Washington State Department of Ecology.

Zimmerman, A.R., Benner, R. (1994) Denitrification, nutrient regeneration and carbon mineralization in sediments of Galveston Bay, Texas, USA. Marine Ecology Progress Series, 275-288.